Studies on Optimal Planning and Control Methods of Battery Energy Storage Systems in Distribution Network with Photovoltaics

太陽光発電が導入された配電系統における蓄電池の最適計画・制御手法に関する研究

February 2019

Satoru AKAGI

赤木　覚

Studies on Optimal Planning and Control Methods of Battery Energy Storage Systems in Distribution Network with Photovoltaics

太陽光発電が導入された配電系統における蓄電池の最適計画・制御手法に関する研究

February 2019

Waseda University
Graduate School of Advanced Science and Engineering,
Department of Advanced Science and Engineering,
Research on Electrical Engineering and Bioscience A

Satoru AKAGI
赤木　覚

Outline

Abbreviations

ANSWER	Active network simulator with energy resources.
AIR	Array-to-inverter ratio.
BESS	Battery energy storage system.
EEPS	Excess electricity purchasing scheme.
FIT	Feed-in tariff.
LSPV	Large-scale photovoltaic.
LDC	Line drop compensator.
LNG	Liquefied natural gas.
LiB	Lithium-ion battery.
LFC	Load frequency control.
MCP	Multipurpose control and planning.
OLTC	On-load tap changer.
PV	Photovoltaics.
PVPR	Photovoltaics penetration rate.
PI	Proportional–integral.
PSP	Pumped storage power.
RFB	Redox flow battery.
RES	Renewable energy source.
RPS	Renewable portfolio standard.
RPF	Reverse power flow.
SoC	State of charge.
STATCOM	Static synchronous compensator.
SVC	Static VAR compensator.
SVR	Step voltage regulator.
SPL	Substation power leveling.
SDB	Supply-demand balance.
SDI	Supply-demand imbalance.

Symbols

α_k	k-th primitive priority factor. With respect to α_i and α_j $(i < j)$, $n\alpha_j < \alpha_i$ holds for all natural numbers n.
d	Ordinal number of simulation date.
D	Amount of voltage violation.
$\boldsymbol{\mathcal{D}}$	$= \{1, \ldots, N^{\mathrm{date}}\}$. Set of simulation days.
ΔP	Fluctuation value of active power from BESS.
ΔV	Fluctuation value of inverter terminal voltage.
ε	Target value of power smoothing.
$\mathcal{E}$	The BESS energy.

F	Evaluation value of control performance.
$\boldsymbol{\gamma}^{\mathrm{OLTC}}$	Control parameter set for voltage control by OLTC.
$\boldsymbol{\gamma}^{\mathrm{set}}$	Control parameter set.
$\boldsymbol{\gamma}^{\mathrm{SPL}}$	Control parameter set for SPL by BESS.
$\boldsymbol{\gamma}^{\mathrm{SVC}}$	Control parameter set for voltage control by SVC.
$\dot{I}$	Complex vector of secondary current of target tap controller.
j	$=\sqrt{-1}$. Imaginary unit.
K	Gain of PI control.
n	Ordinal number of node.
N	Number of simulation days/nodes/inverters.
P	Value of active power.
$\underline{P}, \overline{P}$	Lower/Upper limit of active power; e.g., $\overline{P}^{\mathrm{DB_{BESS}}}$ indicates the upper limit of SPL.
$\mathcal{P}$	BESS power.
pf	Power factor limit.
Q	Value of reactive power.
θ	Power factor angle.
$\underline{R}, \overline{R}$	Rate limit of ramp down/ramp up for active/reactive power output.
$\mathcal{R}$	Power-to-energy ratio of BESS.
SoC	State of charge.
T	Number of simulation steps.
$\boldsymbol{\mathcal{T}}$	$=\{1, \dots, T\}$. Set of simulation steps.
TAP	Tap position of voltage regulator.
V	Voltage magnitude.
$\dot{V}$	Complex vector of secondary voltage of target transformer.
$\boldsymbol{v}$	$=\{\underline{V},\ \overline{V}\}$. Lower/upper limit of voltage value; e.g., $\overline{V}^{\mathrm{allw}}$ indicates the upper limit of allowable range for voltage control.
$V^{\mathrm{vio}}(\boldsymbol{\gamma})$	Voltage violation under parameter $\boldsymbol{\gamma}$.
$\boldsymbol{w_t}$	$=\{\underline{w}_t,\ \overline{w}_t\}$. Target range of power smoothing control by BESS at time slice t.
$\boldsymbol{z}$	$=\{R, X\}$. Simulated line resistance R and reactance X of LDC control.

Subscripts and superscripts

$\dot{}$a	Of attenuation gain of PI control.
.allw	Of allowable range.
.avail	Of available capacity.
.BESS	Of BESS.
.cmd	Of command value.
$\dot{}d$	Of the d-th simulation day.
.date	Of simulation days.
.down	Of tap-down operation.
.$\mathrm{DB_{cen}}$	Of dead band of the centralized control.

$.\mathrm{DB_{inv}}$	Of dead band of voltage control by an inverter.
$.\mathrm{DB_{LDC}}$	Of dead band of the LDC control.
$.\mathrm{DB_{SPL}}$	Of dead band of SPL by BESS.
$.\mathrm{DB_{SVC}}$	Of dead band of voltage control by an SVC.
$.\mathrm{flu}$	Of target value of BESS output/distribution voltage fluctuation.
$\dot{}\mathrm{i}$	Of integral gain of PI control.
$.\mathrm{inv}$	Of inverter output.
$.\mathrm{LiB}$	Of LiB.
$.\mathrm{LiB_{reqd}}$	Of the required capacity of LiB.
$.\mathrm{LiB_{unit}}$	Of the unit capacity of LiB.
$.\mathrm{lim_{pf}}$	Of limitation value of active power for power factor restriction.
$.\mathrm{lim_{SoC}}$	Of limitation value of active power for SoC adjustment.
$.\mathrm{LSPV}$	Of LSPV.
$.\mathrm{max}$	Of the maximum.
$.\mathrm{max_{SoC}}$	Of the maximum value of active power for SoC adjustment.
$.\mathrm{min}$	Of the minimum.
$\dot{}n$	Of the n-th node.
$.\mathrm{node}$	Of the number of nodes.
$.\mathrm{OLTC}$	Of the OLTC.
$\dot{}\mathrm{p}$	Of proportional gain of PI control.
$\dot{}\mathrm{P}$	Of active power.
$.\mathrm{pt}$	Of the voltage change per tap of OLTC/SVR.
$\dot{}\mathrm{Q}$	Of reactive power.
$.\mathrm{ref}$	Of the reference value.
$.\mathrm{RFB}$	Of RFB.
$.\mathrm{RPF}$	Of BESS output of RPF prevention.
$.\mathrm{RPF_{cmd}}$	Of the command value of RPF prevention.
$.\mathrm{RFB_{reqd}}$	Of the required capacity of RFB.
$.\mathrm{RFB_{unit}}$	Of the unit capacity of RFB.
$.\mathrm{sec}$	Of the secondary side of tap controller.
$.\mathrm{smo}$	Of the power smoothing control.
$.\mathrm{SoC}$	Of BESS output of SoC adjustment.
$.\mathrm{SoC_{cmd}}$	Of the command value of SoC adjustment.
$.\mathrm{SPL}$	Of the SPL.
$.\mathrm{SPL_{opt}}$	Of the optimal parameter of SPL.
$.\mathrm{sub}$	Of the substation.
$.\mathrm{SVC}$	Of the SVC.
$.\mathrm{SVR}$	Of the SVR.
$\dot{}t$	At time slice t.
$.\mathrm{term}$	Of the inverter terminal; V_t^{term} indicates the inverter terminal voltage at time slice t.
$.\mathrm{tgt}$	Of target value.

$.\mathrm{up}$	Of tap-up operation.
$.\mathrm{VC}$	Of the voltage control.
$.\mathrm{vio}_{\mathrm{allw}}$	Of the violation from the allowable range.
$.\mathrm{vio}_{\mathrm{DB}}$	Of the violation from the dead band.
$.\mathrm{VV}_{\mathrm{cmd}}$	Of the command value of volt-VAR function: e.g., $Q_t^{\mathrm{VV}_{\mathrm{cmd}}}$ indicates the command value of reactive power output by volt-VAR function at time slice t.
$.\mathrm{vv}_k$	Of control parameter of volt-VAR function. $k = \{1, \dots, 4\}$.
$.\mathrm{VW}_{\mathrm{cmd}}$	Of the command value of PV curtailment calculated by volt-watt function.
$.\mathrm{vw}_k$	Of control parameter of volt-watt function. $k = \{1, 2\}$.

Chapter 1 Introduction

1.1 Research background

1.1.1 Trend of renewable energy installation

Exploiting renewable energy sources (RESs), such as photovoltaic (PV) energy, wind power, geothermal power, hydroelectric power, and biomass energy, can enable a country to reduce its carbon footprint and improve its self-sufficiency ratio. In Japan, several programs for promoting RESs have been implemented as follows: the Renewable Portfolio Standard (RPS) from June 2002 to July 2012 [1-1], the Excess Electricity Purchasing Scheme (EEPS) from November 2009 to July 2012 [1-2], and the Feed-in Tariff (FIT) from July 2012 [1-3]. In particular, the FIT program has contributed toward increased use of RESs because the electric power companies are obliged to purchase electricity generated from RESs at a higher price compared to the electricity sales price. Excluding large-scale hydroelectric power generation, the average annual growth rate of the RES capacity was 14% under the RPS and EEPS programs from 2003 to 2012, while it increased to 26% under the FIT program from 2012 to 2017 [1-3]. The operating capacity of RESs at the end of March 2017 is shown in Fig. 1.1; the figure indicates that most of the RES installation is PV.

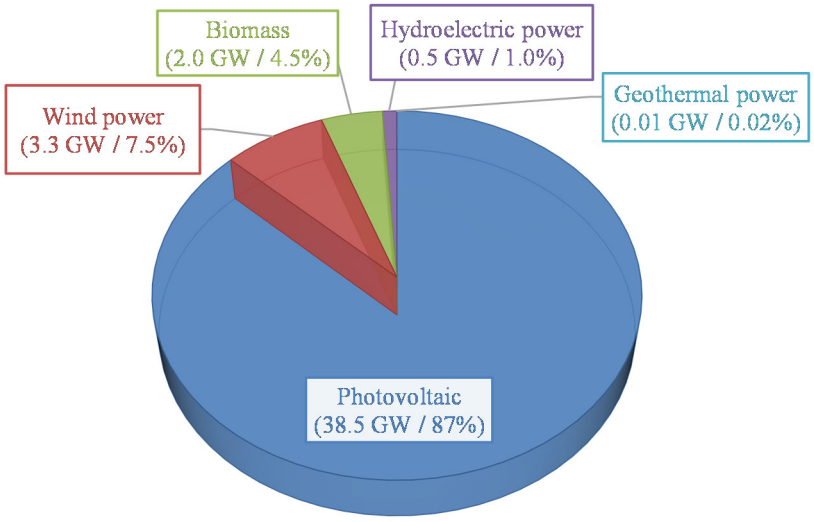

Fig. 1.1 RES installation at the end of March 2017
(Created based on [1-4]).

Regarding the operating PV capacity, the Ministry of Economy, Trade and Industry published statistical data, as shown in Fig. 1.2. From November 2012 to March 2014, the total capacity of operated PV is provided, and from April 2014 to March 2017, the operating capacity of different sizes of PVs is provided. The operating capacity of PVs less than 2 MW accounts for the majority of the total PV installation, as shown in the figure. The voltage classes of PV connections are listed in Table 1.1, which

shows that PVs with less than 2 MW are installed in distribution networks. Figure 1.2 and Table 1.1 indicates that most of the PVs are assumed to be installed in distribution networks. Rooftop PVs for households are generally connected to low-voltage distribution networks, and large-scale PVs (LSPVs) with megawatt-scale generation are connected to middle-voltage distribution networks.

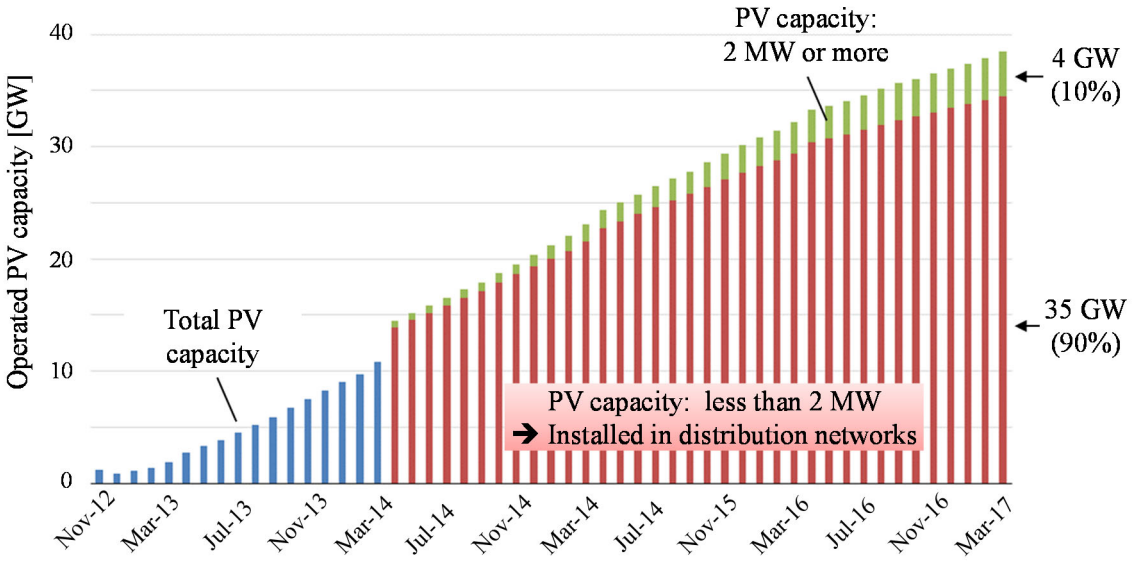

Fig. 1.2 Operated PV capacity
(Based on [1-4]).

Table 1.1 Voltage class and PV rated capacity
(Based on [1-5]).

	Low-voltage	Middle-voltage	High-voltage
PV rated capacity	Less than 50 kW	50 kW–2000 kW	More than 2000 kW
Voltage class	100 V–200 V	6.6 kV	33k V–66 kV
Network	Distribution network		Transmission network
Consumer	Household, Small-scale store	Small-scale factory, Building, LSPV	Large-scale factory

1.1.2 Issues in power network resulting from PV expansion

The popularization of PVs has enabled countries to reduce their carbon footprint and improve their self-sufficiency ratio. However, issues, such as (1) voltage rise/fluctuation, (2) reverse power flow (RPF) at substations, and (3) supply-demand imbalance (SDB), are causes for concern due to PV expansion. Such issues are assumed to emerge, but they do not necessarily occur in the order of (1)–(3) because these are independent phenomena. For instance, (3) SDB does not necessarily deteriorate even if RPF occurs at substations. In the current situation where the PV generation is less than the network demand, the main problem is the local voltage in distribution networks increases by the PV generation. Owing to further PV expansion, if the PV generation amount exceeds the network demand, issues such as RPF at a substation and supply-demand imbalance (SDI) may occur, as shown in Fig. 1.3.

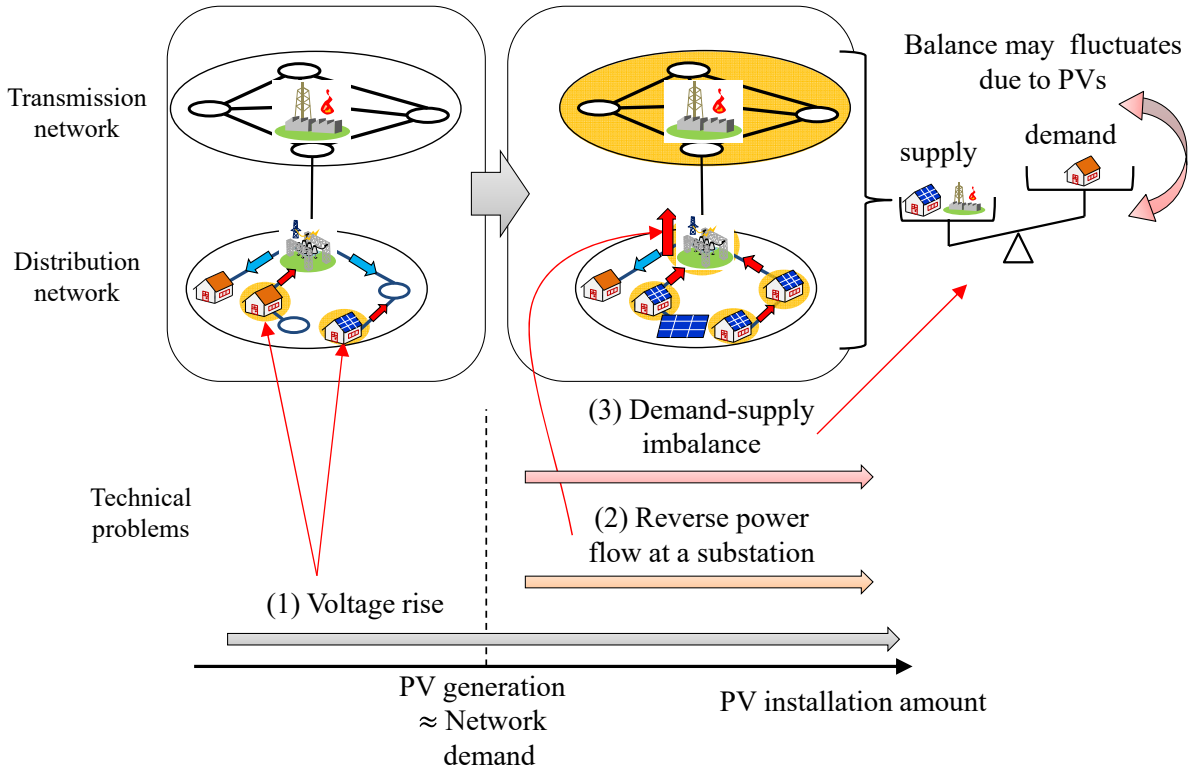

Fig. 1.3 Technical issues in power networks accompanying PV expansion.

(1) Voltage rise/fluctuation issue (the issue in distribution networks)

In Japan, the voltage in low-voltage distribution networks is maintained within 101 ± 6 V or 202 ± 20 V, which is regulated by Electricity Business Act Article 26 and Electricity Business Act Enforcement Regulations Article 45. A traditional distribution network is designed and operated assuming a forward power flow, which is a unidirectional power flow from a substation to customers [1-6]. The surplus power flows into distribution networks during the PV generation, and the power flow is directed from customers to a substation, which is called the RPF phenomenon. The RPF locally increases the distribution voltage and causes voltage violation from the allowable range, which is 101 ± 6 V, as shown in Fig. 1.4. Furthermore, the distribution voltage increase may cause PV curtailment. Japanese PV inverters are usually operated with a fixed power factor for voltage control, and PV generation is curtailed when the terminal voltage of the PV inverter reaches the upper limit [1-7]. In addition, the distribution voltage fluctuation due to the PV intermittency promotes many tap operations that accelerate the deterioration of the tap controllers.

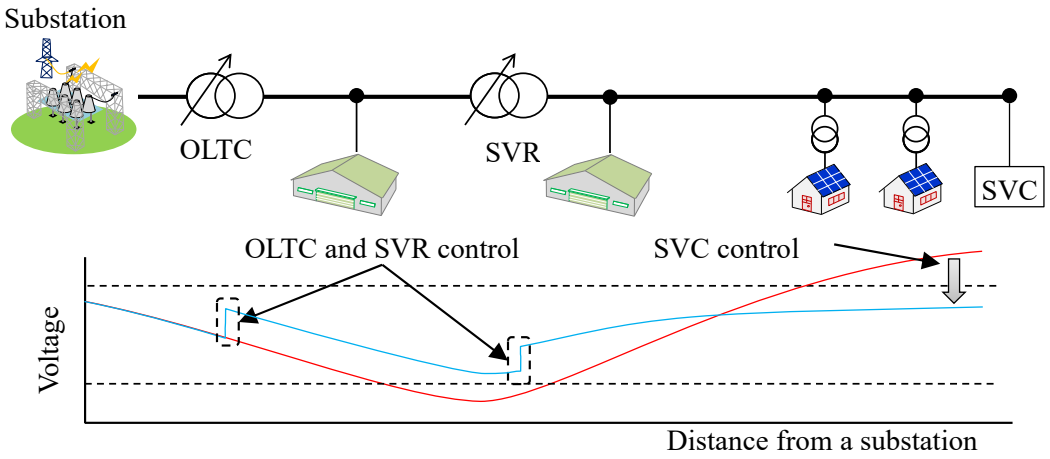

Fig. 1.4 Voltage rise issue.

(2) RPF at substations (the issue in distribution networks)

Traditionally, RPF at substations was uniformly prohibited for the following reasons: 1) Techniques for preventing islanding operation of distributed PVs during fault conditions in transmission networks had not been developed [1-8]. 2) The voltage control at the substation did not correspond to RPF [1-8]. The installation of LSPVs with megawatt-scale generation was restricted owing to the prohibition of RPF at substations, and demands for deregulation of RPF from LSPV generation producers grew. Thus, RPF was allowed for substations with appropriate countermeasures [1-9]. However, RPF at substations cannot be unlimited because the coordination of distributed RES and distribution network is a prerequisite.

(3) SDB (the issue in entire power networks)

The SDB is a critical indicator for transmission network operators, because if it deteriorates significantly, the frequency of the power networks will violate the allowable range, which may cause a blackout over a wide area. The SDB is maintained by adjusting the outputs of hydroelectric/thermal power plants according to the dynamic demand change. SDB control is considered to become severe along with PV expansion because the difference between supply and demand may change significantly depending on the weather conditions. However, hydroelectric/thermal power plants have a limited adjustable power range and power change rate, as listed in Tables 1.2 and 1.3, and there is a concern about the inability to prevent the SDI of a power network with a large amount of PVs [1-10]. Thus, improvement of the supply-demand adjustment capability is required to install a large amount of PVs without deteriorating the power quality.

Table 1.2 Specification of hydroelectric power plant

(From [1-11]).

	Run–of–river power plant	Pondage type power plant	Reservoir type power plant	Pumped storage hydropower plant	
				Power generation operation	Pumping operation
Governor–free operation	×	△	○	○	○
Load frequency control (LFC) ability	×	△	○	○	○
Power adjustment ability	—	○	○	○	○
Power adjustable range	—	50%–100%		○	70 %–100 %
Power change	—	about 1 minute			
Start/stop time		3–5 minutes / 1–2 minutes			5–10 minutes / 1–2 minutes
Main role	Base supply capacity	・Peak supply capacity ・regulated power supply		・Peak supply capacity ・regulated power supply ・ reserved capacity	・Pumping power ・regulated power supply

○: Very suitable / △: Suitable / ×: Not suitable

Table 1.3 Specification of thermal power plant

(From [1-11]).

Generator type		Steam power generation system						Combined cycle power generation			
		Drum–type boiler (350 MW class)			Once–through boiler (700 MW class)			1100 ℃ class (single-shaft 150 MW class)		1300 ℃ class (single-shaft 350 MW class)	
Fuel type		Oil	LNG	Coal	Oil	LNG	Coal	LNG		LNG	
Governor–free operation		○	○	○	○	○	○	○		○	
LFC ability		○	○	○	○	○	○	○		○	
Power adjustment ability		△	○	△	○	○	△	Single shaft ×	Multi shaft ○	Single shaft △	Multi shaft ○
Power adjustable range		30 %–100 %	20 %–100 %	30 %–100 %	15 %–100 %	15 %–100 %	30 %–100 %	80 %–100 %	20 %–100 %	50 %–100 %	20 %–100 %
Power change rate		3 %/min	3 %/min	1 %/min	5 %/min	5 %/min	5 %/min	7 %/min		10 %/min	
Start time	Weekly start stop	20–30 h			30–40 h			12 h			
	Daily Start Stop	3–5 h			5–10 h		—	1 h			

○: Very suitable / △: Suitable / ×: Not suitable

1.1.3 Countermeasures against power network issues due to PV expansion

This chapter presents an overview of the countermeasures against issues in distribution networks/entire power networks owing to a large amount of PV installation.

(1) Countermeasure against voltage rise/fluctuation issue

The distribution voltage is controlled on both the network-side and the demand-side. Currently, tap controllers, such as on-load tap changer (OLTC) and step voltage regulator (SVR), are mainly used for voltage control in distribution networks, and most of these tap controllers are operated assuming a conventional distribution network with no PVs. Thus, OLTC and SVR may not be able to regulate distribution voltage appropriately when a large amount of PVs are installed in distribution networks. To overcome this problem, advanced voltage control methods and next-generation voltage controllers have been developed to accelerate the installation of PVs. Table 1.4 summarizes the voltage controllers. The conventional voltage control methods of OTLC and SVR have been modified to be adaptable to PV expansion [1-6], [1-12]. Moreover, flexible AC transmission networks, such as static VAR compensator (SVC), static synchronous compensator (STATCOM), and battery energy storage systems (BESSs), have been developed.

On the demand-side, fixed power factor control is used for PV inverters connected to low-/middle-voltage distribution networks. The value of the fixed power factor is set as 95% for rooftop PVs [1-13] and generally 90% for LSPVs. In addition, smart inverters with multiple grid support/communication functions [1-14] have been proposed and studied in Europe, USA, and Japan. The control mode/parameters can be changed according to the request of the power network operator through the communication function. In Japan, studies have been conducted [1-15] to demonstrate the effectiveness and issues of smart inverters for actual operation.

Table 1.4 Characteristics of voltage control equipment.

	Equipment	Site	Control principle	Control time constant	Remarks
Network side	OLTC	Distribution substation	Tap operation	200 s	A criterion of replacement is 200,000 times
	SVR	Middle-voltage distribution network	Tap operation	45-180 s	About $30,000 limit is 200,000 times
	SVC		Reactive power control	100 ms	About $100,000
	STATCOM		Reactive power control	40 ms	About $150,000
Network /Demand side	BESS	Low-/middle-voltage distribution network	Active/reactive power control	From tens of milliseconds to several hundred millisecond	Features depends on the BESS type
	Smart inverter	Low-/middle-voltage distribution network	Active/reactive power control	From tens of milliseconds to several hundred milliseconds	Control mode/parameters can be updated by the communication function

Integrated control of the equipment on the network-side and demand-side is expected to be used as a countermeasure with high efficiency and reliability. However, it may take several years or decades for the integrated control preparation, such as establishment of the communication infrastructure and a control method. Therefore, countermeasures based on the network-side equipment are likely to be adopted to respond to rapid PV expansion. Regarding countermeasures on the network-side, there is a high possibility that countermeasures by conventional voltage controllers, such as OLTC, SVR, and SVC, will be implemented early from the viewpoints of cost reduction and effective utilization of existing facilities.

(2) Countermeasure against the RPF at substations

The upgrade of the OLTC control method is taken as a countermeasure against deterioration of the voltage control performance during the RPF at a substation. However, in the case when the operation is hindered by an increase in the RPF, further measures are required. BESS charging operation is also effective for RPF prevention, but it is not currently taken from the viewpoint of cost-effectiveness. Therefore, it is necessary to improve the added value of a BESS by using it together with other controls such as voltage control or power smoothing instead of using the BESS only for RPF measures.

(3) Countermeasure against SDI

As described in Section 1.1.2 (3), improvement in supply-demand adjustment capability will be required for a significant amount of PV installation, and the following countermeasures are considered: construction of new pumped storage power (PSP) plants, curtailment of PV generation, and utilization of BESSs. The usage situation and characteristics of these countermeasures are as follows.

For supply-demand adjustment, hydroelectric/thermal power plants are conventionally used, but these plants may not be able to appropriately maintain the SDB of a power network with a large amount of PVs owing to the limited adjustable power range and power change rate of the power plants. PSP plants are considered as an effective countermeasure for surplus power, but PSP plants cannot respond to significant PV expansion because the construction period is a decade or more. In addition, in Japan, the effect of PSP plant installation may not be significant because the number of suitable sites is limited.

PV curtailment is also a countermeasure against supply-demand adjustment. PV curtailment is not desirable as an additional countermeasure because frequent PV curtailment increases massive PV generation losses. In some demonstration examinations, PV curtailment is used for supply-demand control in micro-grids/islands where the supply-demand adjustment capability is limited. Recently, PV generation has also been curtailed in the jurisdiction of the Kyusyu Power Company [1-16].

To overcome these problems, BESSs have attracted considerable attention for the following reasons:

- Short construction period

  It generally takes a decade or more to build thermal power plants or PSP plants, whereas BESSs are constructed in a significantly shorter period. Thus, BESSs are expected to cope with the significant expansion of PVs in power networks.
- Flexible capacity design and installation site

  Compared to PSPs, BESSs can be designed in various sizes and their capacity can be increased as required. In addition, BESSs can be site in distributions networks, unlike the PSP plant.

  With this feature, BESSs are expected to contribute to distribution network management; for instance, BESSs can improve voltage control performance and defer the expansion of distribution network facilities owing to drastic PV increase, which cannot be handled by PSPs.

As an example of supply-demand adjustment by BESSs, the Hokkaido Electric Power Co., Inc. has met the requirement of alleviating output fluctuation of LSPVs/wind power generation using BESSs [1-17]. Specifically, concerning PV power generation equipment of 2000 kW or more, the rate of change in the total output of LSPV generation and BESS must be maintained at 1% or less per minute of the power generation rated output.

1.2 Research purpose

As mentioned above, many types of countermeasures are considered for technical issues: (1) voltage rise/fluctuation, (2) the RPF at a substation, and (3) SDI. (1) voltage rise/fluctuation and (2) the RPF at a substation have already occurred in some areas individually. While, in situations where more than two of (1) - (3) occur due to the PV expansion, it is expected that collective countermeasures by BESSs are more efficient than individual measures and are superior regarding operation and cost.

However, problems remain in improving the technical issues. Therefore, this thesis proposes the following schemes, and the effectiveness of the proposed schemes is evaluated through power flow calculation for distribution networks with high PV penetration rate (PVPR). Chapter 2 presents a planning scheme for upgrading the voltage controls. Chapters 3 and 4 describes a control method and planning scheme of BESS for multipurpose utilization. Chapter 5 concludes this thesis and explores directions for future work.

1.2.1 Planning scheme for upgrading voltage control methods

Upgrading the voltage control method and installing voltage controllers are necessary to mitigate voltage violations according to PV expansion. However, if ad hoc countermeasures are implemented, the countermeasure cost may increase sharply owing to excessive equipment enhancement and voltage violation may not be prevented owing to delays in adopting the countermeasures. Therefore, it is necessary to update the conventional voltage control method to a suitable method at an appropriate

timing according to PV expansion. In addition, determination of appropriate voltage control methods and voltage controllers is required because inappropriate countermeasure may cause voltage violation.

Chapter 2 presents the planning scheme to determine a suitable method, the type of voltage controllers, and the timing for upgrading the voltage controls according to PV expansion. The proposed scheme covers conventional voltage controllers, such as OLTC, SVR, and SVC (but not BESSs), reflecting the need for cost reduction of countermeasures of power companies. The proposed scheme starts with updating the OLTC control method from the conventional scalar line drop compensator (LDC) method to the vector LDC method or centralized control method; then, an SVR or SVC is installed. The control parameters/site of an SVR and SVC are optimized to maximize the PVPR. The suitable method, controller, and timing for upgrading the voltage type of the voltage controllers are demonstrated using a general distribution network with high PVPR.

1.2.2 Scheme for determination of control parameters and capacity of BESS for multipurpose utilization

Determination of optimal control parameters for stable control and suitable BESS capacity is vital for BESS utilization in distribution networks. Inappropriate control parameters may induce power-quality deterioration. For instance, rapid repetition of the BESS charge/discharge, called the hunting phenomenon, may cause voltage fluctuation and voltage violation, i.e., power-quality deterioration. The BESS capacity becomes excessive considering only the improvement in control performance. Therefore, it is necessary to determine the capacity considering the balance between control performance and BESS capacity.

Chapter 3 describes the scheme for determining the control parameters and BESS capacity. The BESS is used for voltage control and substation power leveling (SPL). Considering the OLTC operation, the proposed scheme determines optimal control parameters that prevent the BESS hunting phenomenon. The BESS capacity can be determined to reflect the BESS operator’s request by establishing the trade-off relationship between the control performance of SPL and BESS capacity. The effectiveness of the proposed scheme was confirmed through the power flow calculation using a distribution network model with high penetration of LSPVs.

1.2.3 Multipurpose control and planning scheme for BESS

BESSs are used for multiple purposes to increase the added value. However, multipurpose utilization with inappropriate control methods may deteriorate the control performance of BESSs. The interaction of BESS control may cause power-quality deterioration due to unstable BESS control. In addition, the BESS capacity required for operation varies with the BESS type even under the same control because the round-trip efficiency and capacity design are different for each BESS type, and the capacity and control effect of BESS depend on the sites in distribution networks. Thus, determination of suitable BESS site and type is critical for BESS utilization in distribution networks. In addition, BESSs are

generally assumed to be used for a long time (e.g., a decade or more), and the role and BESS capacity may change according to the PV expansion.

Chapter 4 presents the multipurpose control and planning (MCP) method of BESS corresponding to the LSPV expansion. This chapter is also targeted at distribution networks with a large amount of LSPVs, and BESSs are used for mitigating the RPF at a substation and power fluctuation of LSPVs. The proposed scheme includes the multipurpose control method and determines the suitable BESS site and type considering the LSPV expansion.

References

[1-1] The Agency for Natural Resources and Energy in the Ministry of Economy, Trade and Industry, "Website of RPS," (in Japanese). [Online]. Available: http://www.rps.go.jp/RPS/new-contents/top/main.html. [Accessed 7- Oct.-2018].

[1-2] The Agency for Natural Resources and Energy in the Ministry of Economy, Trade and Industry, "The Excess Electricity Purchasing Scheme for Photovoltaic Power," [Online]. Available: http://www.meti.go.jp/english/policy/energy_environment/renewable/photovoltaic.html. [Accessed 28- Nov.-2018].

[1-3] The Agency for Natural Resources and Energy in the Ministry of Economy, Trade and Industry, "The Guide Book of Feed-in Tariff for Renewable Energy," (in Japanese). [Online]. Available:www.enecho.meti.go.jp/category/saving_and_new/saiene/data/kaitori/2018_fit.pdf. [Accessed 7- Oct.-2018].

[1-4] The Agency for Natural Resources and Energy in the Ministry of Economy, Trade and Industry, "Website of Information Publication of Renewable Energy Installation Status," (in Japanese). [Online]. Available: http://www.enecho.meti.go.jp/category/saving_and_new/saiene/statistics/index.html. [Accessed 7- Oct.-2018].

[1-5] Japan Photovoltaic Energy Association, "Public/Industrial Photovoltaic Power Generation System Design and Point of PV Interconnection," (in Japanese). [Online]. Available: http://www.jpea.gr.jp/pdf/02semi210_04.pdf. [Accessed 7- Oct.-2018].

[1-6] S. Uemura, "Estimation and Measure by Comparing Voltage Regulation Method of Transformer for Distribution in Substation System with PV Large Penetration," (in Japanese), Report of Central Research Institute of Electric Power Industry, R14021, pp. 2-3, Mar. 2015.

[1-7] Hokkaido Electric Power Co., Inc., "Voltage Rise Mitigation Function of PV System," (in Japanese). [Online]. Available: http://www.hepco.co.jp/energy/recyclable_energy/fixedprice_purchase/voltage_rf.html. [Accessed 8-Oct.-2018].

[1-8] S. Uemura, M. Takahi, and K. Kawahara "Preventing Islanding by Distributed Power Generation at Transmission System Fault -Evaluation of Characteristic of Detecting Islanding by Power Conditioning Subsystem for Interconnecting Many Distributed Power Generations in Area with Rotated Type Distributed Power Generation," Report of Central Research Institute of Electric Power Industry, (in Japanese), R12020, p. 1, Mar. 2013

[1-9] Ministry of Economy, Trade and Industry, "Partial Revision of the Interpretation of Technical Standards of Electrical Equipment (Regulations Related to Reverse Power Flow of Distribution Substation Restriction)," (in Japanese). [Online]. Available: http://www.meti.go.jp/policy/safety_security/industrial_safety/oshirase/2013/05/250531-1.html. [Accessed 8-Oct.-2018].

[1-10] New Energy and Industrial Technology Development Organization, “NEDO Renewable Energy (2nd Edition),” (in Japanese). Chapter 9, Network Support Technology, Available: http://www.nedo.go.jp/library/ne_hakusyo_index.html. [Accessed 8-Oct.-2018]

[1-11] The Agency for Natural Resources and Energy in the Ministry of Economy, Trade and Industry, “The Way of Next-Generation Power Networks Considering After 2030,” (in Japanese). [Online.]. Available: http://www.meti.go.jp/committee/sougouenergy/denryoku_gas/ denryoku_gas/saiseikanou_jisedai/ 004_haifu.html

[1-12] Electric Technology Research Association, “Advancement of Distribution Automation System Technology,” (in Japanese), vol. 72, no.3, p. 63, Oct. 2016

[1-13] Japan Electrotechnical Standards and Codes Committee, “Grid Interconnection Code,” 2017 (in Japanese).

[1-14] B. Seal, “Common Functions for Smart Inverters 4th Edition,” The Electric Power Research Institute, Inc., 2016.

[1-15] New Energy and Industrial Technology Development Organization, “Development of Remote Output Control System for PV Systems,” (in Japanese). [Online]. Available: http://www.nedo.go.jp/english/index.html. [Accessed 5-Nov.-2018].

[1-16] The Electric Daily News (*The Denki Shimbun*), “PV Curtailment for Two Consecutive Weeks in Kyushu Electric Power Company Jurisdiction,” 23-Oct. 2018. [Browsed data: 23-Oct.2018]

[1-17] Hokkaido Electric Power Co., Inc., “Technical Requirements Relating to Measures to Mitigate Output Fluctuations of a Solar Power Generations,” (in Japanese). [Online]. http://www.hepco.co.jp/energy/recyclable_energy/fixedprice_purchase/pdf/solar_power_pv_ tec.pdf. [Accessed 5-Nov.-2018].

Chapter 2
Planning Scheme for Upgrading Voltage Control Methods

2.1 Introduction to this chapter

The use of PV systems is continually increasing in Japan. The capacity of installed PV systems reached approximately 38.5 GW (9.5 GW for households and 29.0 GW for non-households) by the end of March 2017 [1-4]. PV systems for households have been connected to the distribution networks. The Japanese government has set a goal of installing 28 GW PV systems by 2020 and 64 GW by 2030 [2-1]. It is assumed that the penetration of PV systems into distribution networks will continue to increase.

Studies on the hosting capacity of PV systems and novel voltage control methods have been conducted previously. Hosting capacity calculations are necessary in planning voltage control systems. In [2-2]-[2-8], hosting capacities under various situations were reported. 2-1Wang *et al*. [2-4] proposed an evaluation method for maximum hosting capacity (MHC) considering the optimal operation of OLTCs and SVCs. The authors discussed a method of determining the critical technical restrictions on MHC. Moreover, Jayasekara *et al*. [2-5] employed a BESS to increase the hosting capacity of distributed generation and proposed a number of voltage control methods. In their approaches, RPF from PV systems raises the distribution voltage at high PVPR.

Currently, distribution voltage is primarily controlled using tap changer transformers, such as the OLTC and SVRs. However, the conventional voltage control method for tap changers assumes only a load current without RPF. Thus, the tap changer may be unable to maintain the distribution voltage within an allowble range when the PV penetration is high [2-9]. Several methods have been proposed to resolve the voltage rise problem [2-9]–[2-20]. Yorino *et al*. [2-10] proposed a voltage control method for tap controllers in distribution networks with high PV penetration based on a multi-agent system. The results of numerical simulations showed that an increase in PV systems penetration causes frequent tap changing operations and distribution voltage violations with a conventional voltage control method. On the other hand, their proposed method realized optimal tap control by adding the function to the conventional tap controllers.

Another problem of using PV systems is that their output fluctuates significantly with respect to weather conditions, which may cause voltage violations in distribution networks. A tap changer cannot follow rapid voltage fluctuations on account of a working delay function that prevents life span deterioration [2-21]. To manage the fluctuating voltage, previous researchers have proposed control methods that use equipment that output reactive power (e.g., SVCs and shunt capacitors) [2-22]–[2-31]. In [2-22] for instance, a distribution static compensator was employed for voltage control to increase the PV hosting capacity of a distribution network. Using this method, the optimal PV hosting capacity was determined by maximizing the net present value.

As described in the foregoing, many studies have been conducted on hosting capacity and voltage control methods. In addition, selecting a suitable method and timing is important for upgrading the voltage control method to increase PV penetration in distribution networks without excessive capital investments or voltage violations due to transition delays. To date, however, few study has been reported on upgrading the voltage control method. Generally, upgrading the voltage control method is required along with increasing PV penetration. Thus, I propose a scheme to determine a suitable method, the type of voltage controllers and timing for upgrading the voltage control methods based on the limit of the PVPR. This limit was determined by numerical simulations and experiments using a distribution network model of a residential area. A numerical simulation was used to evaluate various simulation conditions, and experiments validated the simulation results. The proposed scheme may thus contribute toward the planning of voltage control in distribution networks and the increasing of distributed PVs.

The remainder of this chapter is organized as follows. Section 2.2 explains conventional and upgraded voltage control methods. Section 2.3 describes the upgrade process of voltage control methods and the selection of control parameters of the OLTC, SVR, and SVC. Sections 2.4 and 2.5 describe the simulation conditions and results of the numerical simulation and experiment, respectively. Section 2.6 concludes this chapter.

2.2 Voltage control methods

This section explains the conventional voltage control method of OLTC. In addition, two types of upgraded voltage control methods are described: upgrading the OLTC control method, and installing voltage control equipment, such as the SVR and SVC. As mentioned in Section 2.1, many voltage control methods using specific equipment have already been proposed. However, the OLTC, SVR, and SVC were selected as the voltage control equipment for the present study based on the results of a questionnaire provided to nearly all the Japanese power companies.

2.2.1 Scalar LDC method (conventional method of OLTC)

The scalar LDC method changes the tap position to maintain the calculated voltage of a reference point (reference voltage) within a dead band. The reference voltage V_t^{ref} is calculated as follows:

$$V_t^{\mathrm{ref}} = \left|\dot{V}_t^{\mathrm{sec}}\right| - \sqrt{3}\left|\dot{I}_t\right|\left(R^{\mathrm{OLTC}}\cos\theta + X^{\mathrm{OLTC}}\sin\theta\right), \tag{2.1}$$

where $\left|\dot{V}_t^{\mathrm{sec}}\right|$ is the absolute value of the secondary side voltage of the OLTC, $\left|\dot{I}_t\right|$ is the absolute value of the current passing through the OLTC, and R^{OLTC} and X^{OLTC} are the simulated line resistance and reactance with the set lag power factors, $\cos\theta = 0.98$ and $\sin\theta = 0.20$, respectively. The amount of voltage violation, D_t is integrated when the reference voltage violates the dead band and becomes zero when the reference voltage is within the dead band as follows:

$$D_t = \begin{cases} D_{t-1} + V_t^{\mathrm{ref}} - \overline{V}^{\mathrm{DB_{LDC}}} & , \text{if } \left(V_t^{\mathrm{ref}} > \overline{V}^{\mathrm{DB_{LDC}}}\right) \\ D_{t-1} + V_t^{\mathrm{ref}} - \underline{V}^{\mathrm{DB_{LDC}}} & , \text{if } \left(V_t^{\mathrm{ref}} < \underline{V}^{\mathrm{DB_{LDC}}}\right) \\ 0 & , \text{otherwise,} \end{cases} \tag{2.2}$$

where $\underline{V}^{\mathrm{DB_{LDC}}}/\overline{V}^{\mathrm{DB_{LDC}}}$ is the lower/upper limit of the dead band in the LDC method. The tap control is performed according to the following equation:

$$TAP_t = \begin{cases} -1 & , \text{if } \left(D_{t-1} > D^{\mathrm{down}}\right) \\ +1 & , \text{if } \left(D_{t-1} < D^{\mathrm{up}}\right) \\ 0 & , \text{otherwise,} \end{cases} \tag{2.3}$$

where D^{down} and D^{up} are voltage violations for tap-down and tap-up operations, and TAP_{t+1} is the change in the OLTC tap position. In addition, −1 denotes the tap-down operation, +1, the tap-up operation, and 0, non-operation.

2.2.2 Vector LDC method (upgraded method 1 of OLTC)

When the power factor changes dynamically due to the PV generation, the scalar LDC method cannot properly calculate the reference point voltage because of the fixed power factor. In contrast, the vector LDC method provides a more accurate calculation since the vector calculation considers dynamic changes in the power factor as follows:

$$V_t^{\mathrm{ref}} = \left|\dot{V}_t^{\mathrm{sec}} - \sqrt{3}\dot{I}_t \cdot \left(R^{\mathrm{OLTC}} + \mathrm{j}X^{\mathrm{OLTC}}\right)\right|, \tag{2.4}$$

where j is an imaginary unit. Voltage violation and tap operation are obtained using (2.2) and (2.3). The top of Fig. 2.1 shows the calculated reference voltage. The scalar LDC and vector LDC methods used to calculate the reference voltage are represented by (2.1) and (2.4), respectively. As shown in the bottom figure, the tap position of the OLTC changes when voltage violation D_t exceeds D^{down} or falls below D^{up}.

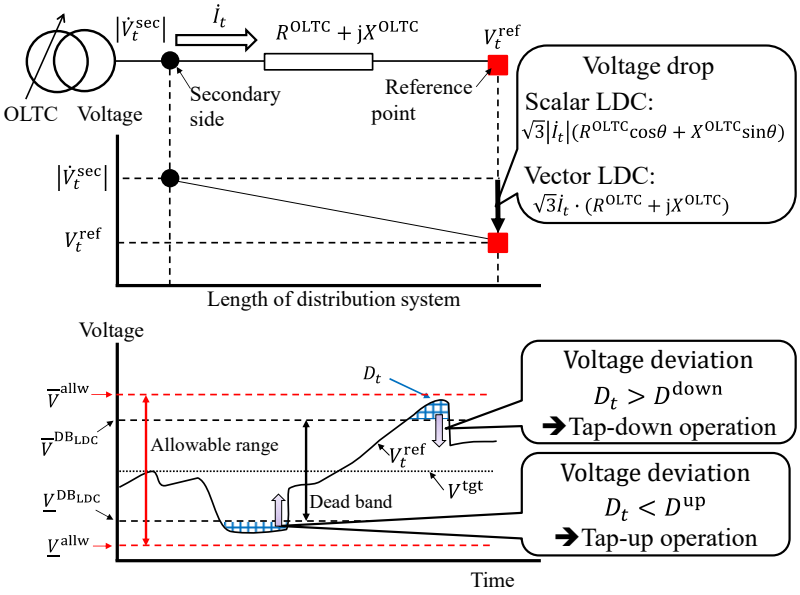

Fig. 2.1 Scalar and vector LDC method

2.2.3 Centralized control method (upgraded method 2 of OLTC and SVR)

The centralized control method manages the distribution voltage within an allowable range using the voltage measured at the switches with sensors. This method uses the maximum and minimum values of the measured voltages as the representative voltages. $V_t^{\max}$ and $V_t^{\min}$ are the maximum and minimum distribution voltages, respectively, measured at the switches with sensors, while $\overline{V}^{\mathrm{DB_{cen}}}$, and $\underline{V}^{\mathrm{DB_{cen}}}$ are the respective upper and lower limits of the dead band. V^{pt} is the voltage change per tap of the OLTC or SVR. The tap position is calculated as follows:

$$TAP_{t+1} = \begin{cases} -1 & ,\text{if}\left(V_t^{\max} > \overline{V}^{\mathrm{DB_{cen}}},\quad V_t^{\min} - V^{\mathrm{pt}} \geq \underline{V}^{\mathrm{DB_{cen}}}\right) \\ +1 & ,\text{if}\left(V_t^{\min} < \underline{V}^{\mathrm{DB_{LDC}}},\quad V_t^{\max} + V^{\mathrm{pt}} \leq \overline{V}^{\mathrm{DB_{cen}}}\right) \\ 0 & ,\text{otherwise.} \end{cases} \tag{2.5}$$

Figure 2.2 shows the tap operation using the maximum and minimum values of the measured voltage. The allowable voltage range is given by $\overline{V}^{\mathrm{allw}}$ and $\underline{V}^{\mathrm{allw}}$. The tap position changes when the representative voltage violates the dead band before the tap operation and when the voltages after the tap operation are within the dead band (left and middle of Fig. 2.2). The tap position does not change when voltages after the tap operation are outside the dead band or the distribution voltages are within the dead band (right part of Fig. 2.2).

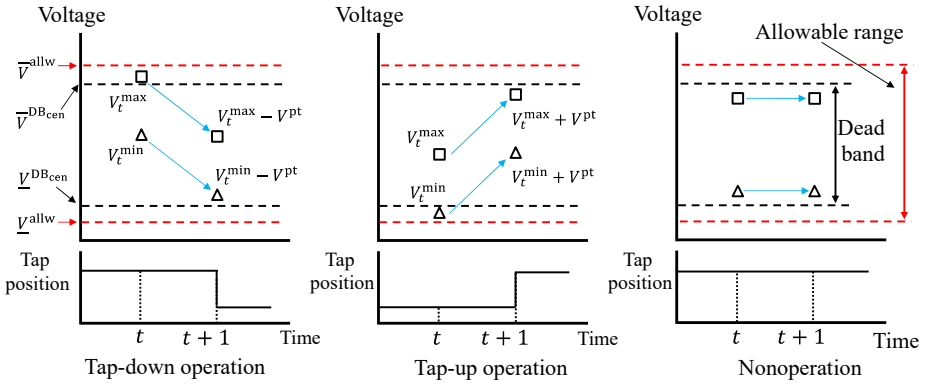

Fig. 2.2 Centralized voltage control method

2.2.4 Control method of SVC

The SVC outputs reactive power to maintain the monitored voltage at the interconnection point V_t^{SVC} to a distribution network within the dead band. The value of SVC terminal voltage violation from the dead band $V_t^{\mathrm{vio_{DB}}}$ is calculated via the following equation:

$$V_t^{\mathrm{vio_{DB}}} = \begin{cases} \overline{V}^{\mathrm{DB_{SVC}}} - V_t^{\mathrm{SVC}} & ,\mathrm{if}\left(V_t^{\mathrm{SVC}} > \overline{V}^{\mathrm{DB_{SVC}}}\right) \\ V_t^{\mathrm{SVC}} - \underline{V}^{\mathrm{DB_{SVC}}} & ,\mathrm{if}\left(V_t^{\mathrm{SVC}} < \underline{V}^{\mathrm{DB_{SVC}}}\right) \\ 0 & ,\mathrm{otherwise}. \end{cases} \tag{2.6}$$

The SVC outputs Q_t^{SVC} the reactive power based on proportional–integral (PI) [2-32] control according to the following equation:

$$Q_t^{\mathrm{SVC}} = \begin{cases} K_{\mathrm{p}} V_t^{\mathrm{vio_{DB}}} + K_{\mathrm{i}} \int V_t^{\mathrm{vio_{DB}}} \mathrm{d}t & ,\mathrm{if}\left(V_t^{\mathrm{vio_{DB}}} \neq 0\right) \\ Q_{t-1} - K_{\mathrm{a}} \int Q_{t-1}\, \mathrm{d}t & ,\mathrm{if}\left(V_t^{\mathrm{vio_{DB}}} = 0\right), \end{cases} \tag{2.7}$$

where $\{K_{\mathrm{p}}. K_{\mathrm{i}}, K_{\mathrm{a}}\}$ is the PI control parameters. When the voltage violates from the dead band ($V_t^{\mathrm{vio_{DB}}} \neq 0$), the reactive power output is calculated using the first condition of (2.7). Conversely, when the monitored voltage is within the dead band ($V_t^{\mathrm{vio_{DB}}} = 0$), the reactive power output is reduced based on the second condition of (2.7).

2.3 Upgrade of voltage control method and selection of control parameters

This section describes the upgrade policy for the voltage control method and the selection of control parameters for the scalar and vector LDC methods and PI control. The control parameters of each voltage control method are determined to maximize the PVPR.

2.3.1 Control parameters selection for OLTC

To obtain the control performance of the conventional voltage control method, the limit of the PVPR

is calculated using the scalar LDC method. The target voltage of the reference point, as well as the simulated line resistance, R^{OLTC}, and reactance, X^{OLTC}, comprise the control parameters for the LDC method. The control parameters for the scalar LDC method are determined using the load current with no PV systems.

As the first step of upgrading the voltage control method, the OLTC control method is changed from the scalar LDC to the vector LDC method. This is because the OLTC control method affects the entire distribution network, and upgrading to the vector LDC method does not require the introduction of new equipment. The control parameters of the vector LDC method are determined as follows. First, the control parameters are determined in a similar manner similar to the scalar LDC method. Second, when the voltage violates the allowable range in the scalar LDC method as the PVPR increases, the conventional control parameters are revised to prevent voltage violation. The control parameters of the LDC method are common for each validation day: three days with three types of PV profiles, and one day with no PV systems. The control parameters of the scalar and vector LDC methods are determined in such a way as to minimize the sum of voltage violations from the allowable range $V^{\mathrm{vio}_{\mathrm{allw}}}$ as calculated using the following equation:

$$V^{\mathrm{vio}_{\mathrm{allw}}}\left(\boldsymbol{\gamma}^{\mathrm{OLTC}}\right) = \sum_{d=1}^{N^{\mathrm{date}}} \sum_{t=1}^{T} \sum_{n=1}^{N^{\mathrm{node}}} V_{d,t,n}^{\mathrm{vio}_{\mathrm{allw}}}, \tag{2.8}$$

where $\boldsymbol{\gamma}^{\mathrm{OLTC}} = \left\{V^{\mathrm{tgt}}, R^{\mathrm{OLTC}}, X^{\mathrm{OLTC}}\right\}$ is the parameter set of the OLTC, N^{date} is the number of simulation dates, N^{node} is the total number of nodes, and T is the simulation time length. In addition, $V_{d,n,t}^{\mathrm{vio}_{\mathrm{allw}}}$, which is the voltage violation of each day, d, and node, n, which is calculated as follows:

$$V_{d,n,t}^{\mathrm{vio}_{\mathrm{allw}}} = \begin{cases} V_{d,n,t}\left(\boldsymbol{\gamma}^{\mathrm{OLTC}}\right) - \overline{V}^{\mathrm{allw}} & , \text{if } \left(V_{d,n,t} > \overline{V}^{\mathrm{allw}}\right) \\ \underline{V}^{\mathrm{allw}} - V_{d,n,t}\left(\boldsymbol{\gamma}^{\mathrm{OLTC}}\right) & , \text{if } \left(V_{d,n,t} < \underline{V}^{\mathrm{allw}}\right) \\ 0 & , \text{otherwise.} \end{cases} \tag{2.9}$$

When multiple control parameter sets minimize the summation of voltage violations, the last control parameter set is employed. The optimal value of $V^{\mathrm{vio}_{\mathrm{allw}}}$ is zero, which represents the case of no voltage violation.

2.3.2 Control parameter selection for SVR and SVC

The SVR or SVC is installed after the OLTC control method is upgraded to the centralized control method. The SVR and SVC control parameters are determined for the states in which voltage violation occurs with centralized control. The objective function for the SVC is given by (2.8), which is the same as that of the LDC method. However, the control parameter set of the SVC $\boldsymbol{\gamma}^{\mathrm{SVC}} = \left\{K_{\mathrm{p}},\ K_{\mathrm{i}},\ K_{\mathrm{a}}\right\}$ is used instead of $\boldsymbol{\gamma}^{\mathrm{OLTC}}$.

2.4 Simulation case studies

Numerical simulations were performed to evaluate the voltage control performance of each of the aforementioned methods based on the limit of the PVPR.

2.4.1 Simulation settings

The model of the distribution network consists of two residential feeders. The summed load of certain feeders was set for realistic OLTC operations as shown in Fig. 2.3. The configuration of feeders A and B were identical [2-33]; however, the PV systems were interconnected only with feeder A. The summed load profile was calculated by subtracting the loads of feeders A and B from the actual measured substation profile. The trunk line length of feeders A and B was 3.65 km with loads of 2,000 households, which were connected to nodes. The lag power factor of both feeders was 0.98, while the power factor of the PV system was one.

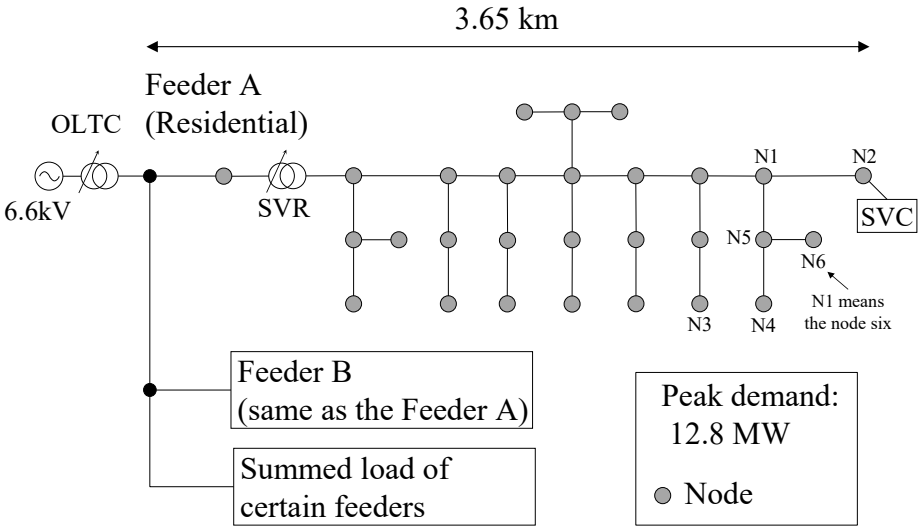

Fig. 2.3 Distribution network

Table 2.1 lists the number of voltage control equipment in each simulation case while Table 2.2 lists the numerical simulation settings. In case 1, only the OLTC was used for voltage control. In cases 2 and 3, the SVC or SVR was installed in addition to the OLTC. Each piece of equipment was installed at the site that maximized the limit of the PVPR. The SVC was installed at the end of the distribution trunk line (case 2), while the SVR was installed at the starting point. The dead band width of the LDC method was determined by consulting with specific power companies in Japan. For the centralized control method, the dead band was adjusted to minimize the tap change and prevent voltage violation. In this study, six types of PV profiles and two types of load profiles were assumed.

Table 2.1 Simulation cases and control method

Case number	Voltage control equipment		
	OLTC (Three methods)	SVC	SVR
Case 1 (only OLTC)	1	No installation	No installation
Case 2 (with SVC at end point)	1	1	No installation
Case 3 (with SVR at starting point)	1	No installation	1

Table 2.2 Settings of the numerical simulation

Content		Setting value
Simulation time step [s]		60
Rating voltage [V]		6600
Allowable voltage range [p.u.] [2-34]		0.981–1.019
Number of simulation dates (Two representative seasons have four days) (PV generation (three days) and no PV generation (1 day))		8
Total number of nodes (Feeders A and B have 28 nodes each)		56
Number of households in each feeder		2000
Peak values	Summed load [kW]	12789
	Load of household [kVA]	1
	PV system for household [kW]	2.77
OLTC	Rated capacity [MVA]	20
	Percent of reactance at the rated capacity [%]	15
	Voltage change per tap [p.u.] [2-35]	0.0091
	Dead band of the LDC method [p.u.] (Target voltage $\pm$ dead band width)	$V^{\mathrm{tgt}} \pm 0.01\, V^{\mathrm{tgt}}$
	Dead band of the centralized control method [p.u.]	0.982–1.018
SVR	Rated capacity [MVA]	10
	Percent of reactance at the rated capacity [%]	1.5
	Voltage change per tap [p.u.]	0.0151
	Dead band of the centralized control method [p.u.]	0.982–1.018
SVC	Maximum output [kvar]	600
	Dead band [p.u.]	0.990–1.010

Figure 2.4 shows the profiles of the low-voltage loads (top) and the summed load (bottom) with lagging reactive power. Figure 2.5 shows the output profiles of a PV system for a household on a sunny day and two types of cloudy days during two representative seasons. Same load and PV profiles were used for each household to simulate the most severe conditions. All PV and load profiles were actually measured on site, and the PV profiles of households were referenced from the work: “Demonstrative Research on Grid-interconnection of Clustered Photovoltaic Power Generation Systems,” which was

organized by the New Energy and Industrial Technology Development Organization [2-36]. The features of each PV profile were as follows. On a sunny day, the PV output was stable. On a type 1 cloudy day, the amount of output fluctuation was drastic, while on a type 2 cloudy day, the number of PV fluctuations was high.

To realize an ideal centralized control, switches with sensors were installed at nodes where the distribution voltage was maximum or minimum at each PVPR. Previously, the installation sites of switches with sensors were determined by calculating the power flow under a 100% PVPR. The voltage control performance of each method was evaluated based on the limit of the PVPR. The PVPR is defined as the ratio of the number of households with PV systems to the total number of households. The rate was specified as increasing in increments of 5% starting from zero. The 30-min averaged of each node voltage was used to determine voltage violation [2-37].

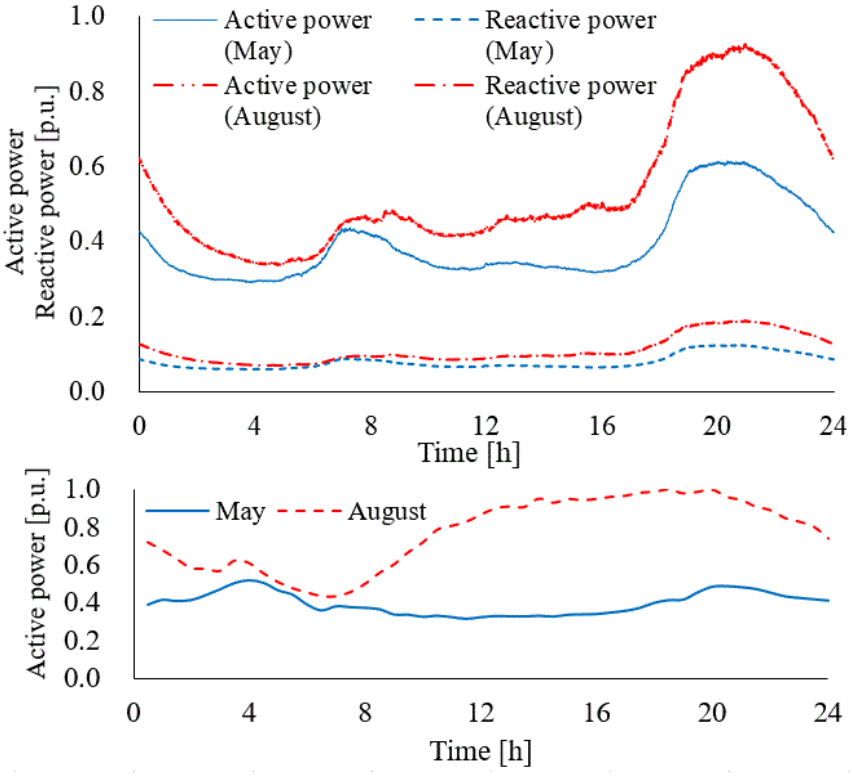

Fig. 2.4 Load profiles
Low-voltage load per household (top); summed load (bottom)

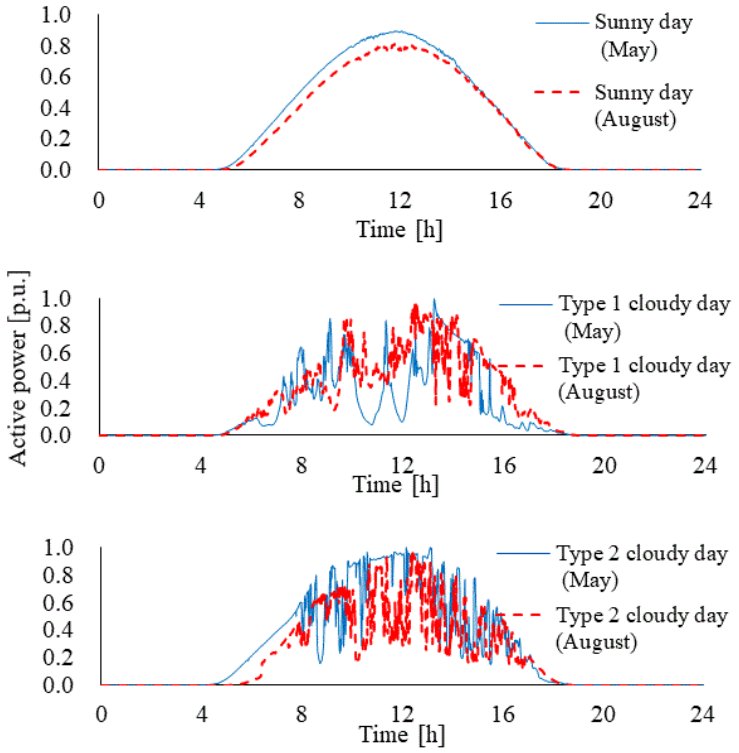

Fig. 2.5 PV profiles per household
sunny day (top), type 1 cloudy day (middle), type 2 cloudy day (bottom)

2.4.2 Analysis of distribution voltage control

Figure 2.6 shows the voltage profiles of all the nodes of the scalar LDC, vector LDC, and centralized control methods for case 1. In Fig. 2.6(a), the maximum distribution voltage is close to the upper limit of the allowable range. The OLTC tap position in the scalar LDC method during the day is 12. In Fig. 2.6(b), the distribution voltage is closer to the lower limit of the allowable range. The OLTC tap position of the vector LDC method is lower than that of the scalar LDC method because the control parameters of the vector LDC method were determined assuming PVPR, unlike the scalar LDC method. The control parameters are compared as follows. The simulated line resistance and reactance were almost the same in both LDC methods. The target voltage of the reference point was 6636.7 V in the scalar LDC method and 6618.5 V in the vector LDC method. For Figs. 2.6(b) and (c), the tap transitions of the vector LDC and centralized control methods are similar; therefore, the PVPRs of both methods are the same in case 1. The voltage control performances of the SVC and SVR, the voltage profiles, and the reactive power profiles for cases 2 and 3 were compared as shown in Fig. 2.7. The distribution voltage was managed by OLTC and SVR controls, as shown in Fig. 2.7(a). Figs. 2.7(b) and (c) indicate that the distribution voltage violates the allowable range in spite of the maximum reactive power output by the SVC.

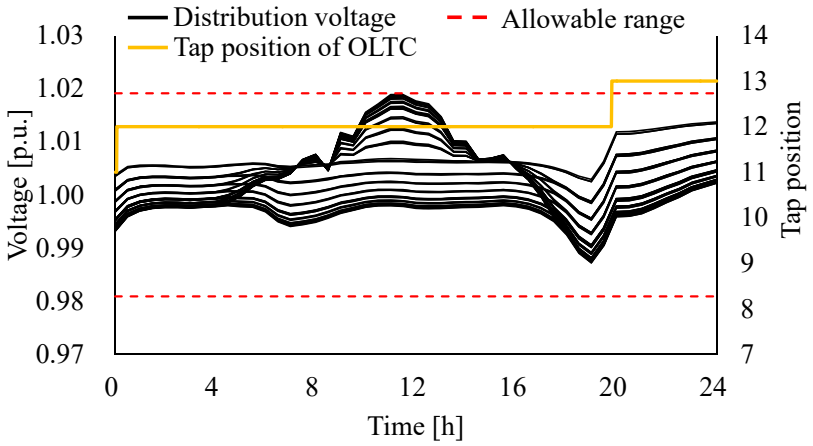

(a) Scalar LDC method.

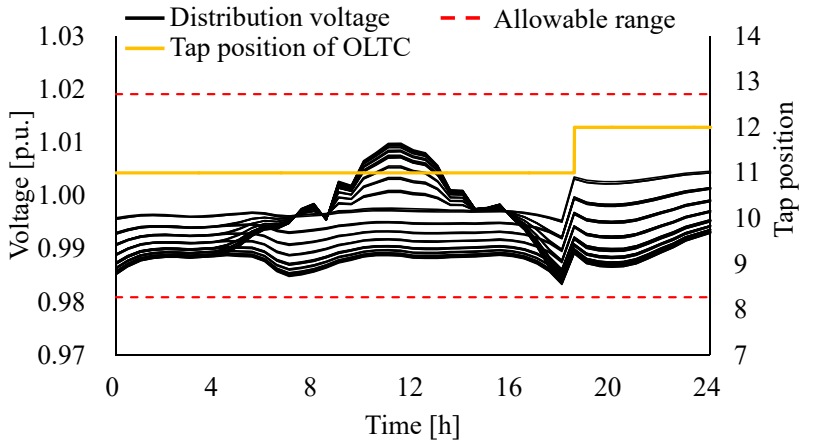

(b) Vector LDC method.

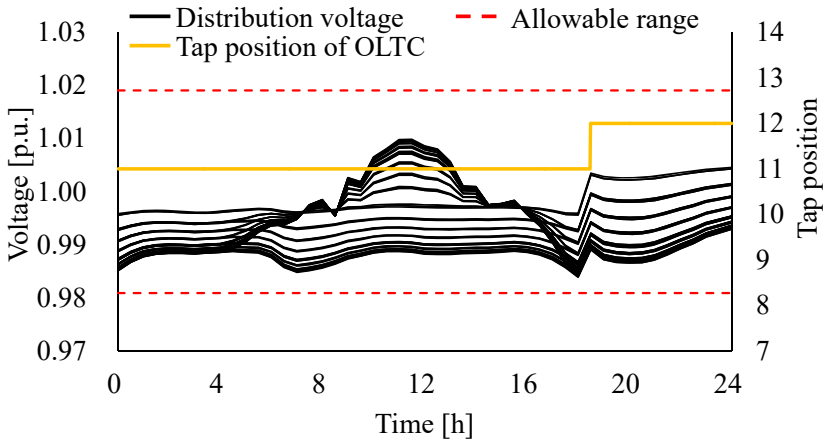

(c) Centralized control method

Fig. 2.6 Average voltage profiles
(Case 1, type 2 cloudy day, May, PV 40%) © IEEE 2018.

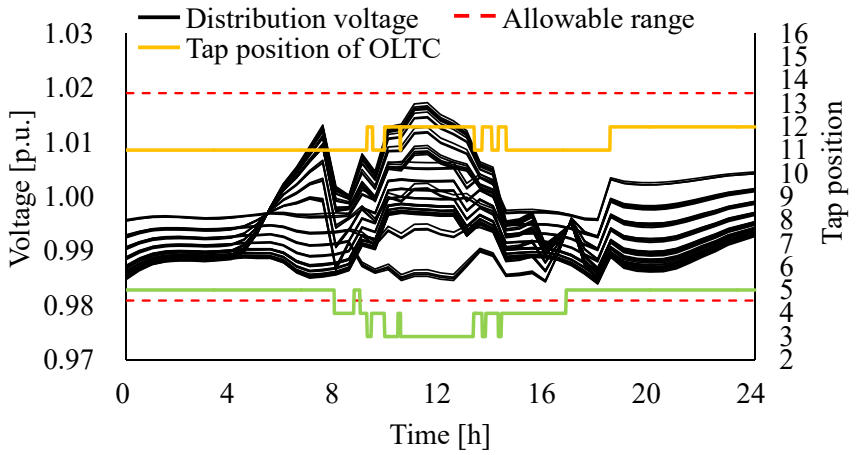

(a) Case 3.

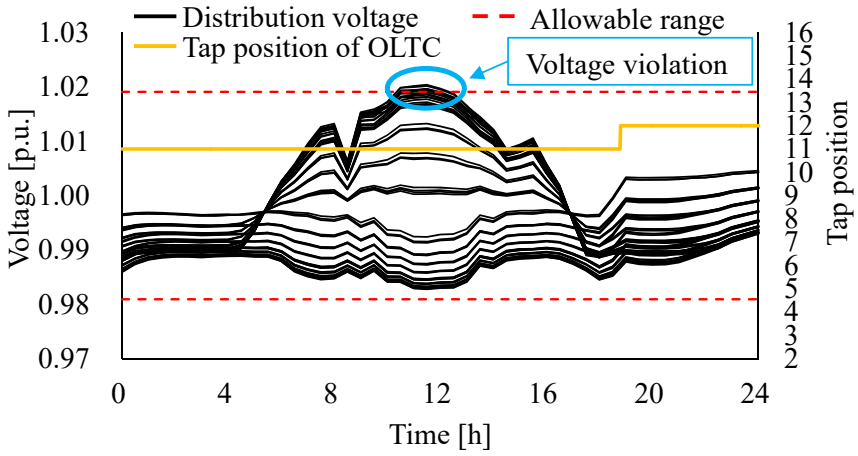

(b) Case 2.

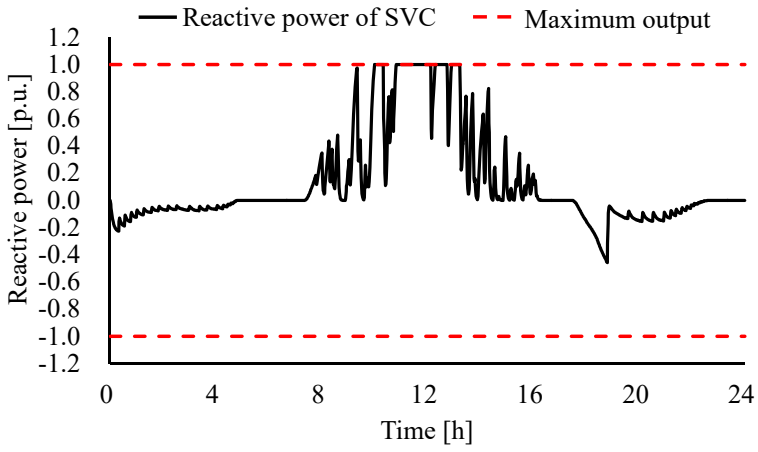

(c) Reactive power of SVC of (b)

Fig. 2.7 Average voltage profiles and reactive power profile
(Centralized control method, type 2 cloudy day, May, PV 100%) © IEEE 2018.

2.4.3 Limit of the PVPR with numerical simulation and experiment

By analyzing the distribution voltage control in each case, the PVPR was obtained. Figure 2.8 shows the common limit of the PVPR, which was the minimum installation rate achieved by any method in the six days of studies. The figure shows two additional findings.

First, except for Case 1 of the vector LDC and the centralized control methods, the limit of the PVPR increased as the voltage control method of the OLTC was upgraded. This was analyzed as follows. The PVPR obtained using the vector LDC method was higher than that obtained using the scalar LDC method by 15% because the control parameters of the vector LDC method were determined using the load current with PV systems.

Second, the limit of the PVPR increased from case 1 to case 3. Installing the SVR at the starting point of the distribution network increased the limit of the PVPR by 5% compared to installing the SVC at the end of the distribution network because the SVR controlled the whole distribution voltage, unlike the SVC.

The following conclusions can be drawn based on the results shown in Fig. 2.8 for the upgrade of the voltage control method. The OLTC control method with the scalar LDC method could manage a PVPR of up to 40%; after which, the OLTC control method should be upgraded to the vector LDC method, which requires no sensor installation, unlike the centralized control method. When the PVPR exceeded 55%, none of the OLTC control methods could prevent voltage violation, and SVC or SVR installation was necessary. As shown in Fig. 2.8, using the SVR increased the PVPR more than using the SVC. Thus, SVR installation was selected as the more suitable method.

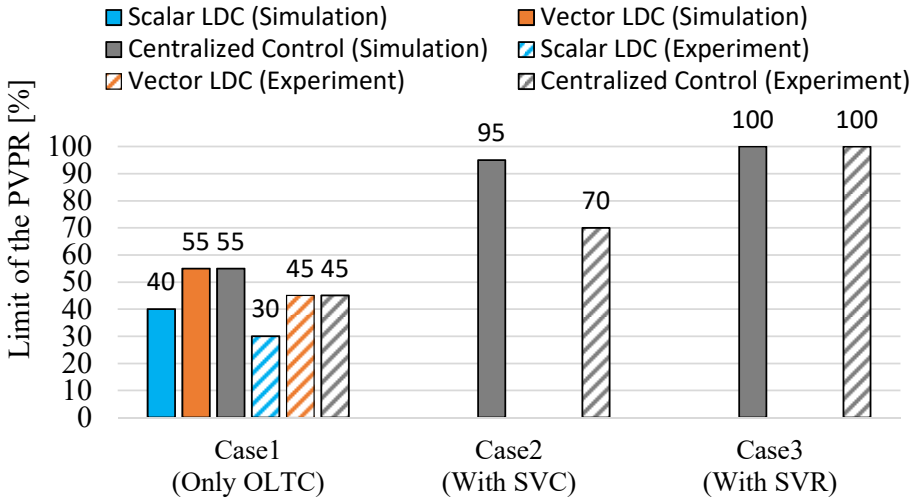

Fig. 2.8 Limit of the PVPR with the numerical simulation and experiment
(30-min averaged voltage was used to determine voltage violation) © IEEE 2018.

2.4.4 Comparison of SVR and SVC

The voltage control performances were compared in terms of the 30-min averaged voltage and the 60-s values used to check the instantaneous voltage violation (i.e., the step size of the used profiles). Figure 2.9 shows the instantaneous voltage profiles for the type 1 cloudy day in August. As shown in Fig. 2.9(a), the voltages at nodes one to six in Fig. 2.3 deviate above the upper limit twice. However, no distribution voltage violates below the lower limit. Figures 2.9(b) and (c) show that the instantaneous voltage is maintained within the allowable range with SVC control. Figure 2.10 shows the PVPR with centralized control in cases 2 and 3 for two types of cloudy days. The SVC increases the PVPR more than the SVR, because the former controls rapid voltage fluctuations, unlike the latter. This phenomenon is confirmed by Fig. 2.9. Based on the results of the numerical simulations, the SVR was more effective than the SVC in extending the PVPR while preventing 30-min averaged voltage violations. The SVC on the other hand, helped increase the PVPR while preventing instantaneous voltage violations.

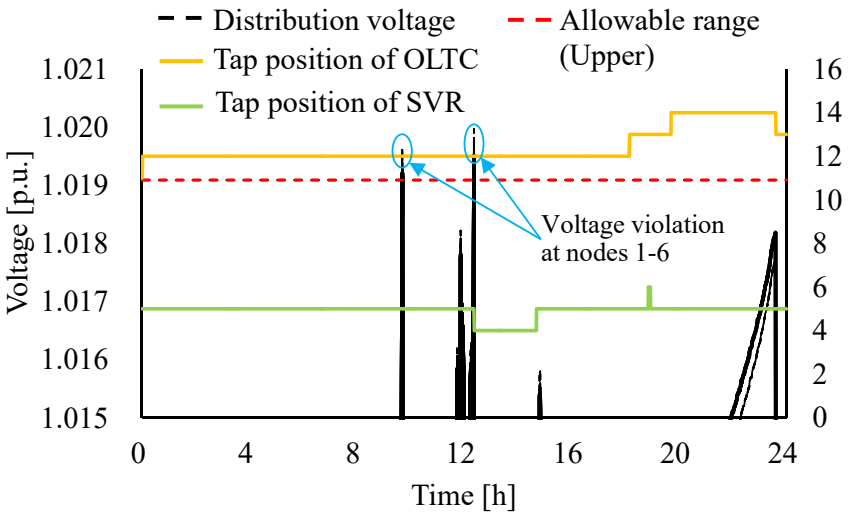

(a) Voltage profiles in case 3.

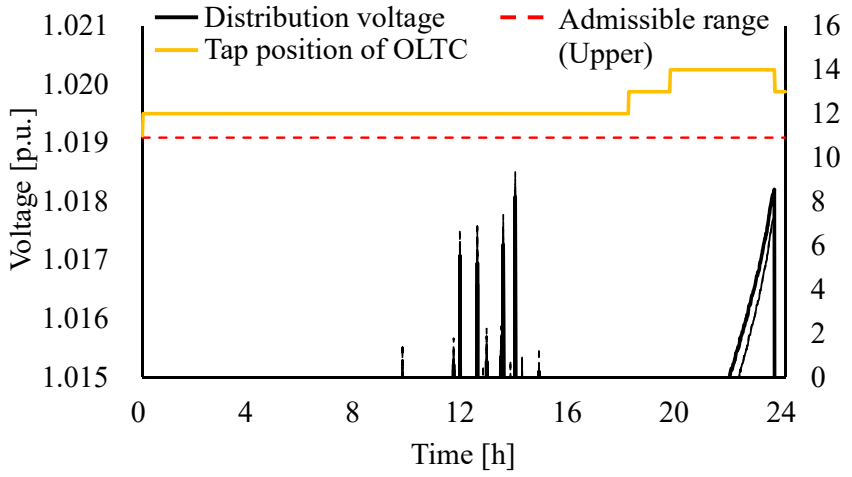

(b) Voltage profiles in case 2.

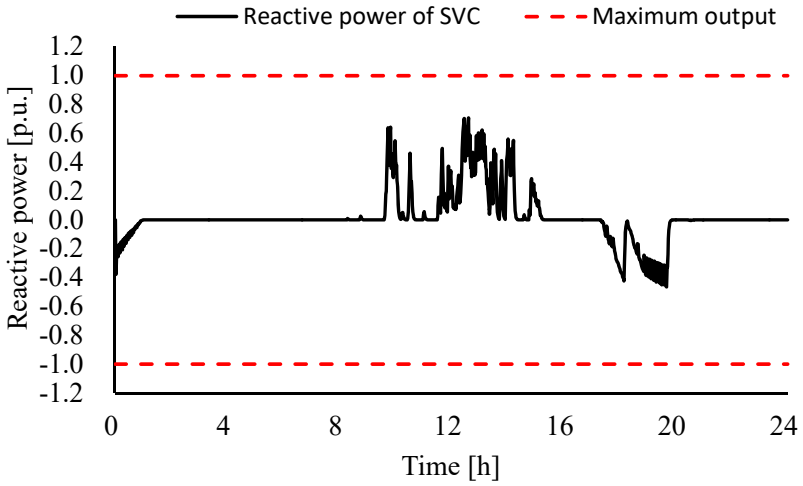

(c) Reactive power of SVC of (b).
Fig. 2.9 Instantaneous voltage and reactive power profiles
(Type 1 cloudy day, August, PV 65%) © IEEE 2018.

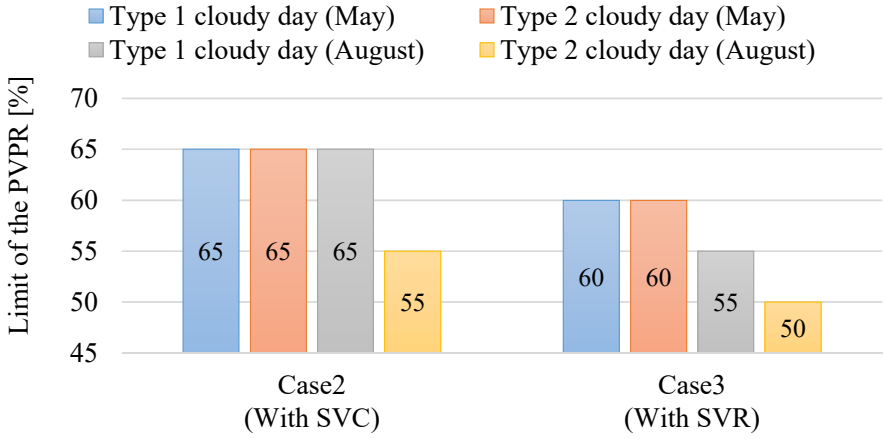

Fig. 2.10 Limit of the PVPR with the numerical simulation
(Instantaneous voltage was used to determine voltage violation) © IEEE 2018.

2.5 Experiment with test bed active network simulator with energy resources (ANSWER)

2.5.1 Experiment settings

ANSWER [2-38] was used to shape the experimental distribution network, which was a model of an actual 6.6-kV distribution network scaled down to 200-V. Figure 2.11 depicts ANSWER. The currents passing through each piece of equipment and the bus voltage were 1/25 and 1/33 of the actual 6.6-kV distribution network, respectively. The experimental distribution network was comprised of the power delivery device, the OLTC and SVR devices, ten distribution line devices, ten inverter devices that simulated the load, PV systems, and the SVC. The voltage values of each distribution line device and the feeder B were used for the centralized control method. Figure 2.12 shows the distribution network model of ANSWER. The distribution voltage of feeder B was calculated by the numerical simulation.

The experimental settings are as listed in Table 2.3. The control parameters of the OLTC, SVR, and SVC were determined as follows. A model of the distribution network was developed on a computer to optimize the control parameters of the ANSWER system. The line lengths were adjusted to match the most severe points of the distribution voltage, such as the maximum or minimum voltage in the experimental and modeled systems. The control parameters were then calculated as described in Section 2.3. When the distribution voltage deviated from the allowable range using the control parameters optimized on the computer, the control parameters were adjusted.

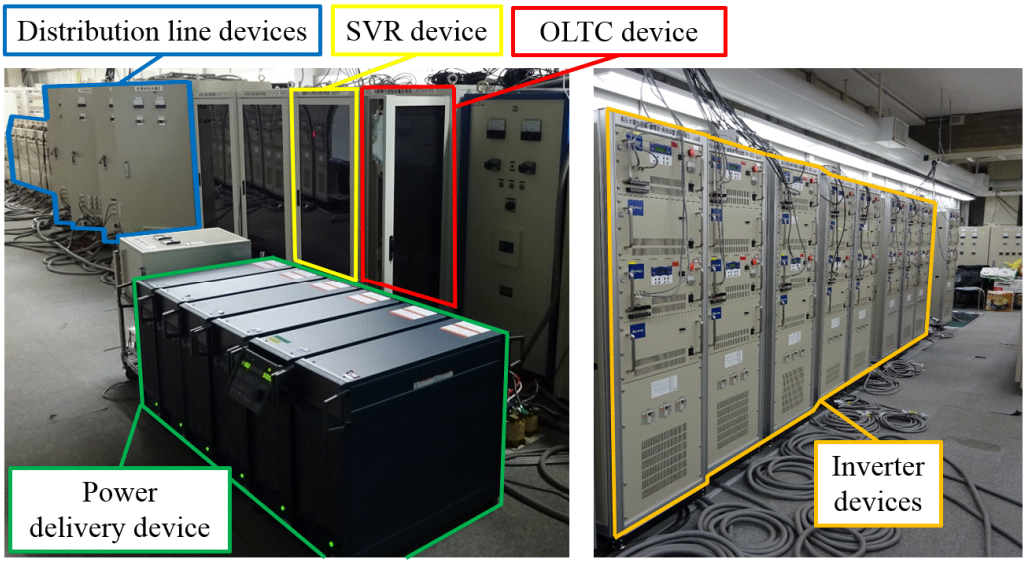

Fig. 2.11 ANSWER devices

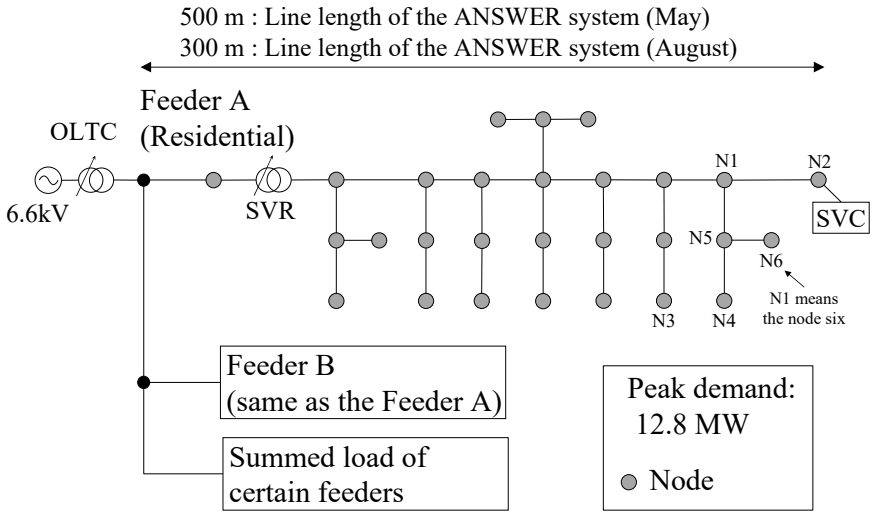

Fig. 2.12 Distribution network model of the ANSWER system

Table 2.3 Settings of the experiment

Content		Setting Value
Simulation time step [s]		60
Rated voltage [V]		200
Allowable voltage range [p.u.] [2-34]		0.981–1.019
Number of simulation dates (Two representative seasons have four days) (PV generation (three days) and no PV generation (one day))		8
Total number of nodes (Feeders A and B have nine nodes, respectively)		18
Peak values	Summed load [kW]	15.5
	Load of household [VA]	1.21
	PV system for household [W]	3.35
OLTC	Rated capacity [kVA]	20
	Voltage change per tap [p.u.] [2-35]	0.0091
	Dead band of the LDC method [p.u.] (Target voltage ± dead band width)	$V^{\mathrm{tgt}} \pm 0.01\, V^{\mathrm{tgt}}$
	Dead band of the centralized control method [p.u.]	0.982–1.018
SVR	Rated capacity [kVA]	20
	Voltage change per tap [p.u.]	0.0151
	Dead band of the centralized control method [p.u.]	0.982–1.018
SVC	Maximum output [kvar]	600
	Dead band [p.u.]	0.990–1.010

2.5.2 Comparison of numerical simulation and experiment results

To analyze the difference between the PVPR of the numerical simulation and those of the experiment, the distribution voltages were compared. Figure 2.13 shows the distribution voltage at the end of feeders A and B obtained in the numerical simulation and experiment for case 2 with the centralized control method and a PVPR of 50%. ANSWER is a 200-V distributions system. Thus, the distribution voltage of ANSWER was 33 times that of the numerical simulation. The trend of voltage profiles for the numerical simulation and ANSWER were consistent. The voltage difference reached 0.015 p.u. at the maximum. The difference in distribution voltage between the numerical simulation and the experiment may have decreased the limit of the PVPR of the experiment. However, the limit of the PVPR of the numerical simulation and experiment was the same as in case 3, as shown in Fig. 2.8. The SVR controlled the whole distribution voltage in feeder A, and therefore, the difference in distribution voltage in feeders A and B was reduced. Thus, the limit of the PVPR reached 100% in the numerical simulation and experiment.

Figure 2.14 shows the numerical simulation and experimental results for case 3. Both distribution voltage profiles were maintained within the allowable range. The operation of the OLTC and SVR in Figs. 2.14(a) and (b) were different since the voltage range of the numerical simulation was narrower than that of the experiment; therefore, the OLTC and SVR could frequently change the tap position in the numerical simulation.

The experimental results show the same trend as the numerical simulation in cases 1 and 2, as shown

in Fig. 2.8. The limit of the PVPR of experiment decreased from 10% to 25% compared to that of the numerical simulation. This decrease could be traceable to the differences in voltage distribution occasioned by the differences in the line impedances used in the numerical simulation and the experiment.

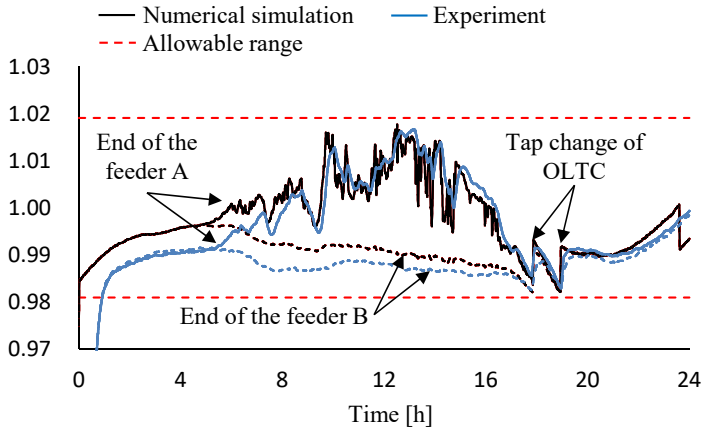

Fig. 2.13 Comparison of the distribution voltage of the numerical simulation with that of the experiment
(Case 1, type 1 cloudy day, August, PV 50%).

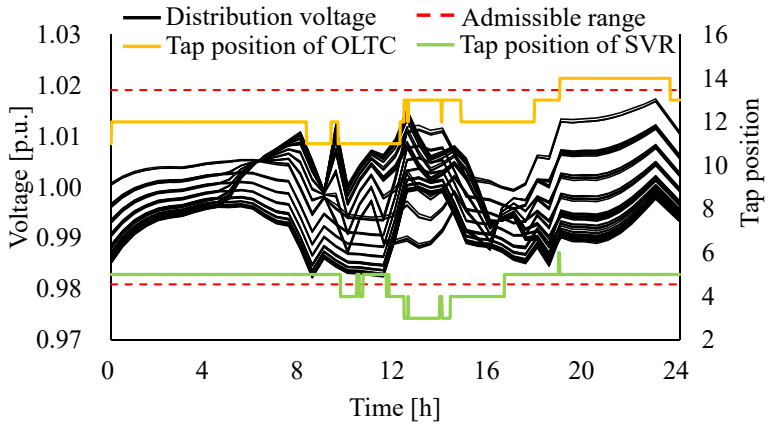

(a) Numerical simulation.

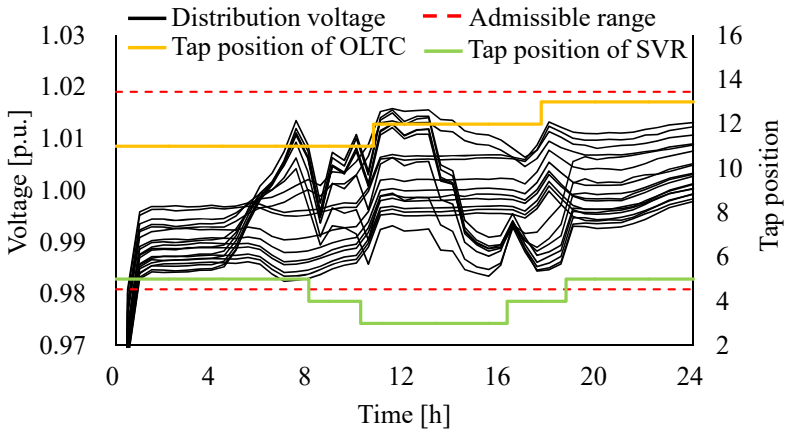

(b) Experimental results.

Fig. 2.14 Comparison of (a) numerical simulation and (b) experimental results of distribution voltage and tap operation
(Centralized control method, case 3, type 1 cloudy day, May, PV 100%)

2.6 Summary of this chapter

In this study, I devised a comprehensive scheme to determine a suitable method, type of voltage controllers, and timing for upgrading the voltage control method. The proposed scheme shows a suitable voltage control method and timing for upgrading the OLTC control method, and the additional installation of the SVC or SVR based on the limit of the PVPR. The limit of the PVPR with each voltage control method was calculated through numerical simulations and experiments with the ANSWER. The tendencies of the PVPR increase and distribution voltage profiles were consistent, validating the numerical simulation results. The results of numerical simulation indicate that the OLTC control method with the scalar LDC method could manage a PVPR of up to 40%, after which, the OLTC control method should be upgraded to the vector LDC method. The LDC method does not require sensor installation, unlike the centralized control method. When the PVPR exceeded 55%, none of the OLTC control methods could prevent voltage violation, and the installation of the SVR and SVC increased the rate to 95% and 100%, respectively. The results showed that the SVR increases the PVPR more than the SVC, while preventing violations of the 30-min averaged voltage. On the other hand, the SVC helped increase PV penetration while preventing instantaneous voltage violations. Thus, this work demonstrates the necessity of controlling the SVR and SVC to increase PV penetration while preventing instantaneous voltage violations. The proposed method was used in a distribution network consisting of two feeders.

References

[2-1] Ministry of Economy, Trade and Industry, "Long-Range Estimate of Energy Supply and Demand-Related," (in Japanese). [Online]. Available: http://www.enecho.meti.go.jp/committee/council/basic_policy_subcommittee/mitoshi/011/pdf/011_07.pdf

[2-2] M. Rylander, L. Rogers, and J. Smith, "Distribution Feeder Hosting Capacity: What Matters When Planning for DER?," The Electric Power Research Institute, Inc., Knoxville, TN, USA, Technical Results, Apr. 2015.

[2-3] M. Rylander, "Determining the Effectiveness of Feeder Clustering Techniques for Identifying Hosting Capacity for DER," The Electric Power Research Institute, Inc., Knoxville, TN, USA, Technical Results, Nov. 2015.

[2-4] S. Wang, S. Chen, L. Ge, and L. Wu "Distributed Generation Hosting Capacity Evaluation for Distribution Systems Considering the Robust Optimal Operation of OLTC and SVC," IEEE Trans. Sustain. Energy, vol. 7, no. 3, pp. 1111–1123, Jul. 2016.

[2-5] N. Jayasekara, M. A. S. Masoum, and P. J. Wolfs, "Optimal Operation of Distributed Energy Storage Systems to Improve Distribution Network Load and Generation Hosting Capability," *IEEE Trans. Sustain. Energy*, vol. 7, no. 1, pp. 250–261, Jan. 2016.

[2-6] F. Capitanescu, L. F. Ochoa, H. Margossian, and N. D. Hatziargyriou "Assessing the Potential of Network Reconfiguration to Improve Distributed Generation Hosting Capacity in Active Distribution Systems," *IEEE Trans. Power Syst.*, vol. 30, no. 1, pp. 346–356, Jan. 2015.

[2-7] S.-J. Huang, C.-W. Hsieh, and H.-H. Wan, "Confirming the Permissible Capacity of Distributed Generation for Grid-Connected Distribution Feeders," *IEEE Trans. Power Syst.*, vol. 30, no. 1, pp. 540–541, Jan. 2015.

[2-8] A. Navarro-Espinosa and L. F. Ochoa, "Increasing the PV Hosting Capacity of LV Networks: OLTC-Fitted Transformers vs. Reinforcements," in *Proc. IEEE PES ISGT 2015*, Washington, DC, USA, Feb. 2015.

[2-9] X. Liu, A. Aichhorn, L. Liu, and H. Li, "Coordinated Control of Distributed Energy Storage System with Tap Changer Transformers for Voltage Rise Mitigation Under High Photovoltaic Penetration," *IEEE Trans. Smart Grid.*, vol. 3, no. 2, pp. 897–906, Jun. 2012.

[2-10] N. Yorino, Y. Zoka, M. Watanabe, and T. Kurushima, "An Optimal Autonomous Decentralized Control Method for Voltage Control Devices by Using a Multi-Agent System," *IEEE Trans. Power Syst.*, vol. 30, no. 5, pp. 2225–2233, Sep. 2015.

[2-11] M. Kim, R. Hara, and H. Kita, "Design of the Optimal ULTC Parameters in Distribution System with Distributed Generations," *IEEE Trans. Power Syst.*, vol. 24, no. 1, pp. 297–305, Feb. 2009.

[2-12] M. E. Elkhatib, R. El Shatshat, and M. M. A. Salama, "Novel Coordinated Voltage Control for Smart Distribution Networks with DG," *IEEE Trans. Smart Grid*, vol. 2, no. 4, pp. 598–605, Dec. 2011.

[2-13] C. Gao and M. A. Redfern, "A Review of Voltage Control Techniques of Networks with Distributed Generations Using On-Load Tap Changer Transformers," in *45th International Universities' Power Engineering Conference*, Cardiff, UK, 2010, pp. 1-6.

[2-14] D. Ranamuka, A. P. Agalgaonkar, and K. M. Muttaqi, "Online Voltage Control in Distribution Systems with Multiple Voltage Regulating Devices," *IEEE Trans. Sustain. Energy*, vol. 5, no. 2, pp. 617–628, Apr. 2014.

[2-15] C. Gao and M. A. Redfern, "Advanced Voltage Control Strategy for On-Load Tap-Changer Transformers with Distributed Generations," in *46th International Universities' Power Engineering Conference*, Soest, Germany, 2011.

[2-16] T. Stetz, K. Diwold, M. Kraiczy, D. Geibel, S. Schmidt, and M. Braun, "Techno-Economic Assessment of Voltage Control Strategies in Low Voltage Grids*," IEEE Trans. Smart Grid,* vol. 5, no. 4, pp. 2125–2132, Jul. 2014.

[2-17] A. T. Procopiou, C. Long, and L. F. Ochoa, "On the Effects of Monitoring and Control Settings on Voltage Control in PV-Rich LV Networks," in *Proc. IEEE Power Energy. Soc. Gen. Meet.*, Denver, CO, USA, 2015, pp.1-5.

[2-18] C. Long, A. T. Procopiou, L. F. Ochoa, G. Bryson, and D. Randles,"Performance of OLTC-Based Control Strategies for LV Networks with Photovoltaics," in *Proc. IEEE Power Energy. Soc. Gen. Meet.*, Denver, CO, USA, 2015, pp.1-5.

[2-19] C. Long, and L. F. Ochoa, "Voltage Control of PV-Rich LV Networks: OLTC-Fitted Transformer and Capacitor Banks," *IEEE Trans. Power Syst.*, vol. 31, no. 5, pp. 4016–4025, Sep. 2016.

[2-20] K. M. Muttaqi, A. D. T. Le, M. Negnevitsky, and G. Ledwich, "A Coordinated Voltage Control Approach for Coordination of OLTC, Voltage Regulator, and DG to Regulate Voltage in a Distribution Feeder," *IEEE Trans. Ind. Appl.*, vol. 51, no. 2, pp. 1239–1248 Mar./Apr. 2015.

[2-21] J.-H. Choi and S.-I. Moon, "The Dead Band Control of LTC Transformer at Distribution Substation," *IEEE Trans. Power Syst.*, vol. 24, no. 1, pp. 319–326, Feb. 2009.

[2-22] C. Chen, C. Lin, W. Hsieh, C. Hsu, and T. Ku, "Enhancement of PV Penetration with DSTATCOM in Taipower Distribution System," *IEEE Trans. Power Syst.*, vol. 28, no. 2, pp. 1560–1567, May 2013.

[2-23] M. J. E. Alam, K. M. Muttaqi, and D. Sutanto, "A Multi-Mode Control Strategy for Var Support by Solar PV Inverters in Distribution Networks," *IEEE Trans. Power Syst.*, vol. 30, no. 3, pp. 1316–1326, May 2015.

[2-24] P. Jahangiri, and D. C. Aliprantis, "Distributed Volt/Var Control by PV Inverters," *IEEE Trans. Power Syst.*, vol. 28, no. 3, pp. 3429–3439, Aug. 2013.

[2-25] Z. Ziadi, M. Oshiro, T. Senjyu, A. Yona, N. Urasaki, T. Funabashi, and C. Kim, "Optimal Voltage Control Using Inverters Interfaced with PV Systems Considering Forecast Error in a Distribution System," *IEEE Sustain. Energy*, vol. 5, no. 2, pp. 682–690, Apr. 2014.

[2-26] M. Parniani and M. R. Iravani, "Voltage Control Stability and Dynamic Interaction Phenomena of Static VAR Compensators," *IEEE Trans. Power Syst.*, vol. 10, no. 3, pp. 1592–1597, Aug. 1995.

[2-27] T. Senjyu. Y, Miyazato, A. Yona, N. Urasaki, and T. Funabashi, "Optimal Distribution Voltage Control and Coordination with Distributed Generation," *IEEE Trans. Power Del.*, vol. 23, no. 2, pp. 1236–1242, Apr. 2008.

[2-28] F. A. Viawan, and D. Karlsson, "Voltage and Reactive Power Control in Systems with Synchronous Machine-Based Distributed Generation," *IEEE Trans. Power Del.*, vol. 23, no. 2, pp. 1079–1087, Apr. 2008.

[2-29] Y. P. Agalgaonkar, B. C. Pal, and R. A. Jabr, "Distribution Voltage Control Considering the Impact of PV Generation on Tap Changers and Autonomous Regulators," *IEEE Trans. Power Syst.*, vol. 29, no. 1, pp. 182–192, Jan. 2014.

[2-30] P. S. Sensarma, K. R. Padiyar, and V. Ramanarayanan, "Analysis and Performance Evaluation of a Distribution STATCOM for Compensating Voltage Fluctuations," *IEEE Trans. Power Del.*, vol. 16, no. 2, pp. 259–264, Apr. 2001.

[2-31] N. Daratha, B. Das, and J. Sharma, "Coordination Between OLTC and SVC for Voltage Regulation in Unbalanced Distribution System Distributed Generation," *IEEE Trans. Power Syst.*, vol. 29, no. 1, pp. 289–299, Jan. 2014.

[2-32] S. Kawasaki, N. Kurokawa, H. Taoka, and Y. Nakashima, "Cooperative Control by System Voltage Control Equipments in Consideration of Reducing Capacity of STATCOM," *IEEJ Trans. PE*, vol. 134, no. 5, pp. 378–385, Dec. 2013.

[2-33] Electric Technology Research Association, "Harmonic Failure Prevention Measures of the Distribution System," [*Denkikyoudoukenkyu*] vol. 37, no. 3, p. 102, Oct. 1981 (in Japanese).

[2-34] Y. Isozaki., S. Yoshizawa, Y. Fujimoto, H. Ishii, I. Ono, T. Onoda, and Y. Hayashi "Detection of Cyber Attacks Against Voltage Control in Distribution Power Grids with PVs," *IEEE Trans. Smart Grid.*, vol. 7, no. 4, pp. 1824–1835, Jul. 2016.

[2-35] The Institute of Electrical Engineering of Japan, Electrical Engineering Handbook (7th Edition), [*Denkikougakuhandobukku*], p. 1281, Sep., 2013 (in Japanese).

[2-36] New Energy and Industrial Technology Development Organization, "Empirical Research on Concentrated Interactive PV systems," (in Japanese). [Online]. Available: http://www.nedo.go.jp/activities/ZZ_00229.html. [Accessed 3-Nov.2018].

[2-37] Ministry of Economy, Trade and Industry, Electricity Business Act Enforcement Regulations, Article 45 Term 3, final revision date: Apr. 2015 (in Japanese).

[2-38] S. Yoshizawa, Y. Yamamoto, J. Yoshinaga, Y. Hayashi, S. Sasaki, T. Shigetou, and H. Nomura, "Voltage Control of Multiple Step Voltage Regulators by Renewing Control Parameters," Power Systems Computation Conference (PSCC), Wroclaw, Poland, 2014.

Chapter 3
Scheme for Determination of Control Parameters and Capacity of BESS for Multipurpose Utilization

3.1 Introduction to this chapter

The BESS utilization in distribution networks has attracted considerable attention, and studies have been conducted to improve the power quality and operation efficiency using BESSs. For instance, BESSs installed in distribution networks have been used for voltage control, peak load shaving, and network loss reduction in [3-1]–[3-9]. In [3-1], distributed BESSs installed in low-voltage distribution networks have been employed for voltage rise/drop issues. BESSs regulate the distribution voltage by charging/discharging during the peak PV generation period/peak demand period. A coordinated control method for voltage control and BESS state of charge (SoC) adjustment has been proposed. Simulation results have shown that the proposed method maintained the distribution voltage and SoC within a target range, indicating the effectiveness of the proposed method. Reihani *et al.* analyzed the effectiveness of BESS for peak load shaving and load curve smoothing in a real network on the island of Maui. The authors proposed two types of demand forecasting methods for BESS operation, and the advantages and disadvantages of the methods were discussed on the basis of numerical simulations with actual measured data. As described in Chapter 2, the distribution voltage rise becomes a problem along with the PV expansion. If the PV installation will continue, the PV generation will exceed the demand of the distribution networks, causing RPF at the distribution substations. The RPF adversely affects the voltage control of the substation, which may cause a distribution voltage violation. A BESS can be used for voltage rise mitigation by reactive power output and prevention of RPF at a substation by surplus power charging; thus, a BESS can handle both problems, and efficient countermeasures using a BESS are expected. Furthermore, a BESS can be used for peak load shaving, which provides it with added value. As described above, the BESS utilization are expected, and determination of optimal control parameters for stable control and suitable BESS capacity is vital. Inappropriate control parameters may induce power-quality deterioration, and the BESS capacity becomes excessive considering only the improvement of control performance. However, to my knowledge, few studies has proposed the determination scheme of control parameters and capacity of BESS for multipurpose utilization. Therefore, I propose a scheme for determining the optimal control parameters and BESS capacity. The control parameters were determined in the order of SPL and voltage control considering the mutual interaction of SPL and voltage control. The costs and benefits of BESS are related to the combined energy (kWh), power (kW) capacities, and control performance. Therefore, I focus on the relationships among these factors.

The reminder of this chapter is organized as follows. Section 3.2 explains control methods for SPL and voltage control. Section 3.3 describes the determination scheme of control parameters and BESS capacity. Section 3.4 describes the simulation conditions and results. Section 3.5 concludes this chapter.

3.2 Control methods for SPL and voltage control

This section describes control methods for SPL and voltage control. The distribution voltage is regulated by the OLTC tap operation and the reactive power control of the inverter and SPL is performed by the BESS charge/discharge operation. The LDC method is used for the OTLC tap operation. The BESS monitors the substation power flow P_t^{sub} and inverter terminal voltage V_t^{term} as shown in Fig. 3.1.

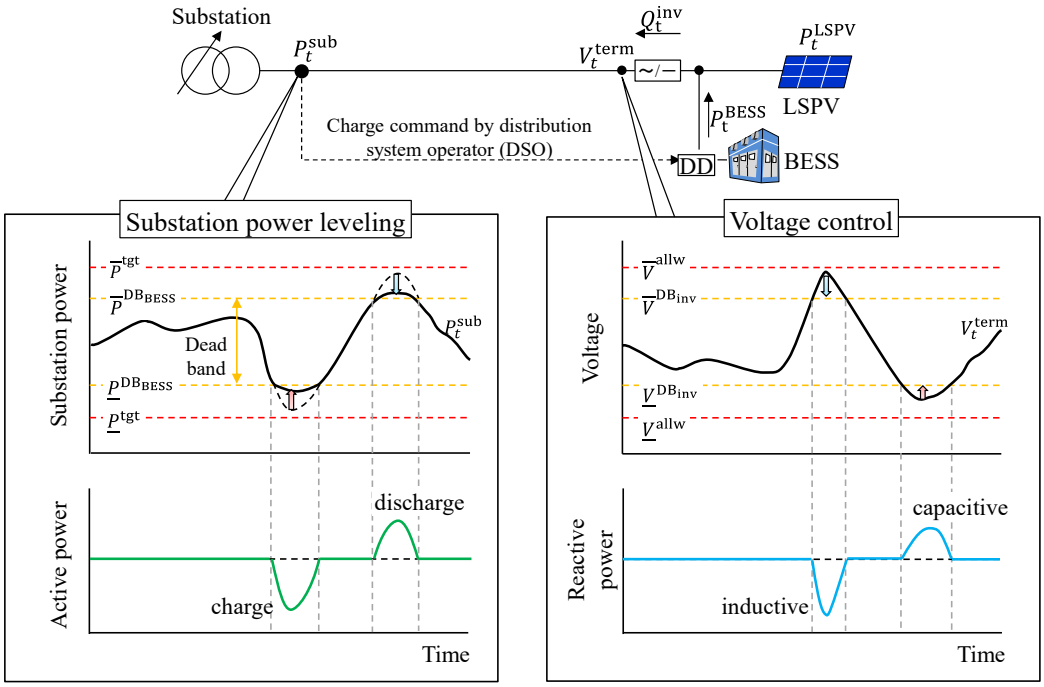

Fig. 3.1 Measurement data and BESS control.

3.2.1 Control method for SPL

The BESS charges/discharges to maintain the substation power flow within a target range for SPL. The reverse power is charged to prevent adverse effect on voltage control under a high LSPV penetration level. The command value of the active power output P_t^{cmd} is calculated by the PI control as follows:

$$P_t^{\mathrm{cmd}} = \begin{cases} K_{\mathrm{p}}^{\mathrm{SPL}} P_t^{\mathrm{sub}} + K_{\mathrm{i}}^{\mathrm{SPL}} \int P_t^{\mathrm{vio_{DB}}}\ \mathrm{d}t & ,\mathrm{if}\left(P_t^{\mathrm{vio_{DB}}} \neq 0\right) \\ P_{t-1}^{\mathrm{cmd}} - K_{\mathrm{a}}^{\mathrm{SPL}} \int P_{t-1}^{\mathrm{cmd}}\ \mathrm{d}t & ,\mathrm{if}\left(P_t^{\mathrm{vio_{DB}}} = 0\right), \end{cases} \tag{3.1}$$

where the value of power violation from the dead band $P_t^{\mathrm{vio_{DB}}}$ is given by

$$P_t^{\mathrm{vio_{DB}}} = \begin{cases} \overline{P}^{\mathrm{DB_{BESS}}} - P_t^{\mathrm{sub}} & ,\mathrm{if}\left(\overline{P}^{\mathrm{DB_{BESS}}} < P_t^{\mathrm{sub}}\right) \\ \underline{P}^{\mathrm{DB_{BESS}}} - P_t^{\mathrm{sub}} & ,\mathrm{if}\left(P_t^{\mathrm{sub}} < \underline{P}^{\mathrm{DB_{BESS}}}\right) \\ 0 & ,\mathrm{otherwise}. \end{cases} \tag{3.2}$$

In (3.1), P_t^{cmd} increases when $P_t^{\mathrm{vio_{DB}}}$ is not zero, but P_t^{cmd} decreases when $P_t^{\mathrm{vio_{DB}}}$ is zero, which indicates that substation power flow is within in the dead band. The PI control [2-32] is used for SPL, and three control parameters $\boldsymbol{\gamma}^{\mathrm{SPL}} = \{K_{\mathrm{p}}^{\mathrm{SPL}}, K_{\mathrm{i}}^{\mathrm{SPL}}, K_{\mathrm{a}}^{\mathrm{SPL}}\}$ are optimized to improve the SPL performance without causing the hunting phenomenon in the BESS charge/discharge. The BESS output P_t^{BESS} is subject to two restrictions: SoC and inverter capacity. The BESS output P_t^{BESS} is given by

$$P_t^{\mathrm{BESS}} = \begin{cases} \min\left(\underline{P}^{\mathrm{lim_{SoC}}}, P_t^{\mathrm{avail}}\right) & ,\mathrm{if}\left(P_t^{\mathrm{cmd}} < \min\left(\underline{P}^{\mathrm{lim_{SoC}}}, P_t^{\mathrm{avail}}\right)\right) \\ \max\left(\overline{P}^{\mathrm{lim_{SoC}}}, -P_t^{\mathrm{avail}}\right) & ,\mathrm{if}\left(\max\left(\overline{P}^{\mathrm{lim_{SoC}}}, -P_t^{\mathrm{avail}}\right) < P_t^{\mathrm{cmd}}\right) \\ P_{\mathrm{t}}^{\mathrm{cmd}} & ,\mathrm{otherwise}, \end{cases} \tag{3.3}$$

where $P_t^{\mathrm{avail}} = S^{\mathrm{inv}} - P_t^{\mathrm{LSPV}}$. The charge/discharge power is limited when the SoC is close to the lower/upper limit, and the BESS output is also limited such that the total power of the EBSS and LSPV generation does not exceed the inverter rated capacity S^{inv}. Figure 3.2 shows the block diagram of the SPL and voltage control.

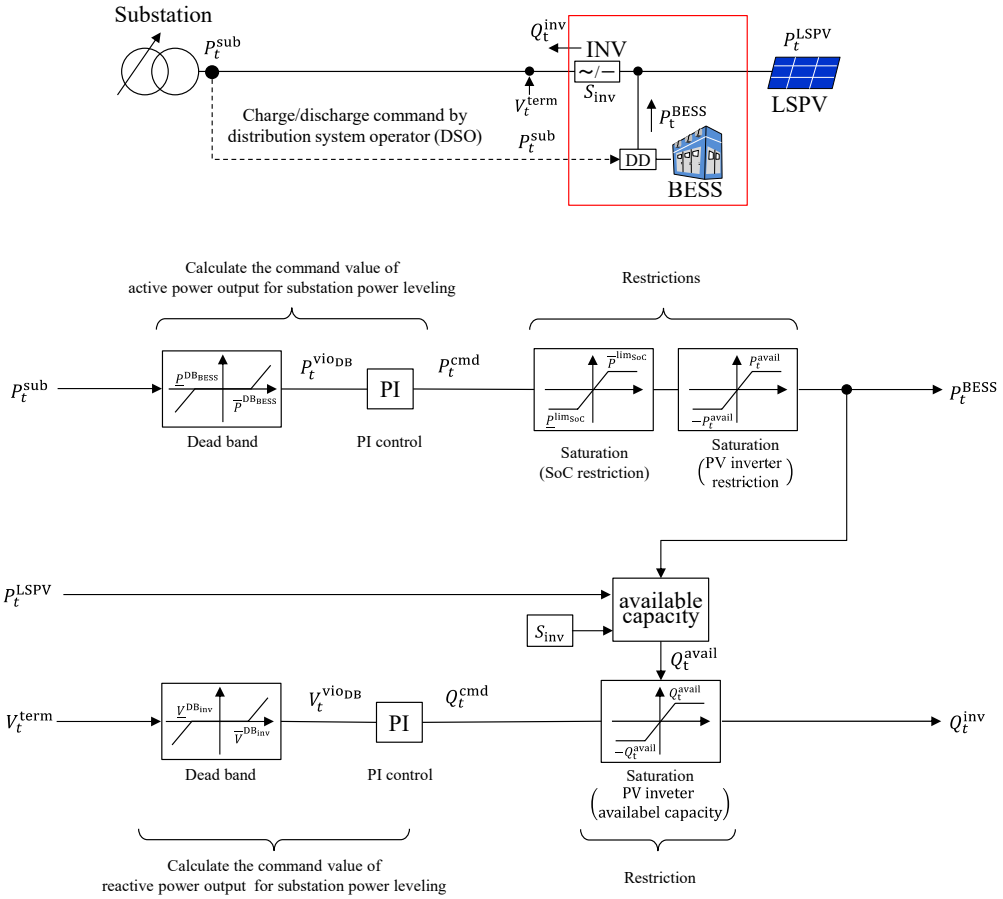

Fig. 3.2 Block diagram of SPL and voltage control.

A general evaluation index for SPL does not exist; therefore, the SPL violation F^{SPL} is used as an evaluation value of SPL, which is calculated by

$$F^{\mathrm{SPL}} = \sqrt{\sum_{t=1}^{T} \left(P_t^{\mathrm{vio_{allw}}}\right)^2}, \tag{3.4}$$

where the substation power violation from the allowable range $P_t^{\mathrm{vio_{allw}}}$ is given by

$$P_t^{\mathrm{vio_{allw}}} = \begin{cases} P_t^{\mathrm{sub}} - \overline{P}^{\mathrm{allw}} & , \mathrm{if}\ \left(\overline{P}^{\mathrm{allw}} < P_t^{\mathrm{sub}}\right) \\ \underline{P}^{\mathrm{allw}} - P_t^{\mathrm{sub}} & , \mathrm{if}\ \left(P_t^{\mathrm{sub}} < \underline{P}^{\mathrm{allw}}\right) \\ 0 & , \mathrm{otherwise}. \end{cases} \tag{3.5}$$

The evaluation index for SPL is defined as the square root of the amount of the substation power violation from the allowable range. By calculating the sum of squares of the power violation, a reduction is expected in the amount of instantaneous violation is expected.

3.2.2 Voltage control method

The inverter outputs inductive/capacitive reactive power to maintain the inverter terminal voltage $V_{\mathrm{t}}^{\mathrm{term}}$ within the allowable range as shown in Fig. 3.2. The command value of the reactive power output Q_t^{cmd} is calculated by the PI control as follows:

$$Q_t^{\mathrm{cmd}} = \begin{cases} K_{\mathrm{p}}^{\mathrm{VC}} V_t^{\mathrm{vio_{DB}}} + K_{\mathrm{i}}^{\mathrm{VC}} \int V_t^{\mathrm{vio_{DB}}}\ \mathrm{d}t & , \mathrm{if}\left(V_t^{\mathrm{vio_{DB}}} \neq 0\right) \\ Q_{t-1}^{\mathrm{cmd}} - K_{\mathrm{a}}^{\mathrm{VC}} \int Q_{t-1}^{\mathrm{cmd}}\ \mathrm{d}t & , \mathrm{if}\left(V_t^{\mathrm{vio_{DB}}} = 0\right), \end{cases} \tag{3.6}$$

where the value of inverter terminal voltage violation from the dead band $V_t^{\mathrm{vio_{DB}}}$ is given by

$$V_t^{\mathrm{vio_{DB}}} = \begin{cases} V_t^{\mathrm{term}} - \overline{V}^{\mathrm{DB_{inv}}} & , \mathrm{if}\ \left(\overline{V}^{\mathrm{DB_{inv}}} < V_t^{\mathrm{term}}\right) \\ \underline{V}^{\mathrm{DB_{inv}}} - V_t^{\mathrm{term}} & , \mathrm{if}\left(V_t^{\mathrm{term}} < \underline{V}^{\mathrm{DB_{inv}}}\right) \\ 0 & , \mathrm{otherwise}. \end{cases} \tag{3.7}$$

Three control parameters for voltage control $\boldsymbol{\gamma}^{\mathrm{VC}} = \left\{K_{\mathrm{p}}^{\mathrm{VC}}, K_{\mathrm{i}}^{\mathrm{VC}}, K_{\mathrm{a}}^{\mathrm{VC}}\right\}$ were optimized to minimize voltage violations while stabilizing the reactive power output of the inverter. The reactive power output is limited by the available capacity of the inverter to prioritize the active power output. The reactive power output of the inverter is calculated as follows:

$$Q_t^{\mathrm{inv}} = \begin{cases} Q_t^{\mathrm{avail}} & , \mathrm{if}\left(Q_t^{\mathrm{avail}} < Q_{\mathrm{t}}^{\mathrm{cmd}}\right) \\ -Q_t^{\mathrm{avail}} & , \mathrm{if}\left(Q_t^{\mathrm{cmd}} < -Q_t^{\mathrm{avail}}\right) \\ Q_t^{\mathrm{cmd}} & , \mathrm{otherwise}, \end{cases} \tag{3.8}$$

where available capacity for reactive power output Q_t^{avail} is given by

$$Q_t^{\mathrm{avail}} = \sqrt{(S^{\mathrm{inv}})^2 - \left(P_t^{\mathrm{LSPV}} + P_t^{\mathrm{BESS}}\right)^2}. \tag{3.9}$$

3.3 Scheme for determination of control parameters and BESS capacity

This section describes the method for determining the OLTC and BESS control parameters and BESS capacity. The distribution voltage was regulated by the OLTC and BESS, and the BESS was installed in addition to the OLTC. Thus, the control parameters were determined in the order of OTLC and BESS.

Figure 3.3 shows the determination procedure of the OLTC and BESS control parameters and BESS capacity. The control parameters of OLTC were determined to prevent voltage violation of the distribution network with no LSPVs following the traditional determination method of power companies. The BESS was used for SPL and voltage control, and three control parameters were determined for each control. The optimal control parameter set can be obtained using an exhaustive search method, but a simple method of determining the control parameters is expected in the actual operation. Focusing on each control, SPL was conducted by the BESS charge/discharge, which also affects the distribution voltage, whereas voltage control was performed by the reactive power output, which has negligible effect on the SPL. Therefore, in this chapter, the control parameters were determined in the order of SPL and voltage control. Large-scale BESS can improve the control performance of SPL and voltage control, but excess BESS capacity leads to low cost-effectiveness owing to its high cost. In practice, BESS owners, such as distribution network operators, determine the BESS capacity in consideration of the cost-effectiveness. Therefore, in this chapter, the BESS capacity is determined considering the balance between the SPL performance and the BESS capacity in relation to the cost-effectiveness. The minimum value among the BESS capacities that minimizes the SPL violation is calculated. The OTLC and BESS control parameters and BESS capacity are determined according to the following steps (step 1–step 6) as shown in Fig.3.3.

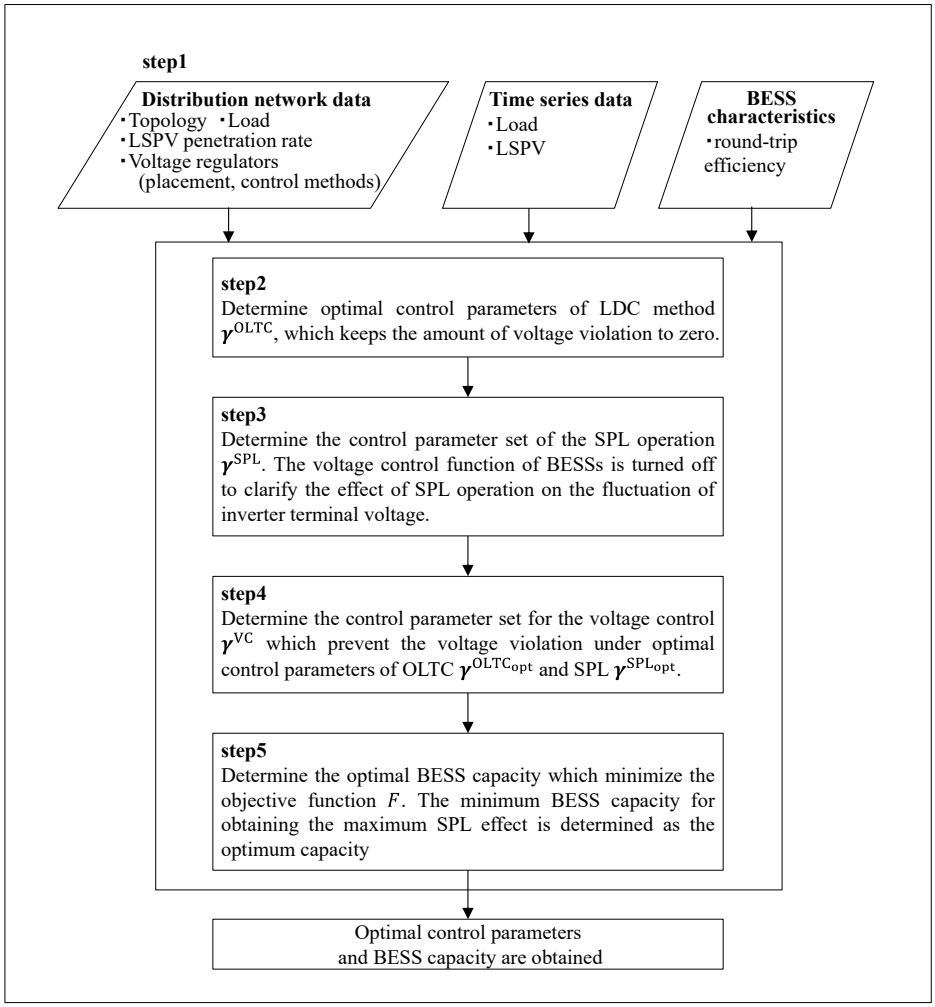

Fig. 3.3 Procedure for determination control parameters and BESS capacity.

step1) Distribution network data, time-series data, and BESS round-trip efficiency data are required as input data for the parameters and BESS capacity determination scheme.

step2) Determine the OLTC control parameters: dead band for LDC method $\boldsymbol{v}^{\mathrm{LDC_{DB}}} = \left\{ \underline{V}^{\mathrm{LDC_{DB}}}, \overline{V}^{\mathrm{LDC_{DB}}} \right\}$, and simulated line resistance and reactance $\boldsymbol{z}^{\mathrm{OLTC}} = \left\{ R^{\mathrm{OLTC}}, X^{\mathrm{OLTC}} \right\}$ which keep the amount of voltage violation F^{VC} to zero, by the following equation:

$$F^{\mathrm{VC}}\left(\boldsymbol{\gamma}^{\mathrm{OLTC}}\right) = \sum_{t}^{T} \sum_{n}^{N^{\mathrm{node}}} V_{t,n}^{\mathrm{vio_{allw}}}\left(\boldsymbol{\gamma}^{\mathrm{OLTC}}\right), \tag{3.10}$$

where T is the simulation time length, and N^{node} is the total number of nodes, and $\boldsymbol{\gamma}^{\mathrm{OLTC}} = \left\{ \boldsymbol{v}^{\mathrm{LDC_{DB}}}, \boldsymbol{z}^{\mathrm{OLTC}} \right\}$ is the control parameter set and $V_{t,n}^{\mathrm{vio_{allw}}}$ is expressed as follows:

$$V_{n,t}^{\mathrm{vio_{allw}}} = \begin{cases} V_{n,t}\left(\boldsymbol{\gamma}^{\mathrm{OLTC}}\right) - \overline{V}^{\mathrm{allw}} & , \text{if } \left(V_{n,t} > \overline{V}^{\mathrm{allw}}\right) \\ \underline{V}^{\mathrm{allw}} - V_{n,t}\left(\boldsymbol{\gamma}^{\mathrm{OLTC}}\right) & , \text{if } \left(V_{n,t} < \underline{V}^{\mathrm{allw}}\right) \\ 0 & , \text{otherwise.} \end{cases} \tag{3.11}$$

step3) Determine the control parameters of the SPL operation $\boldsymbol{\gamma}^{\mathrm{SPL}} = \{K_{\mathrm{p}}^{\mathrm{SPL}}, K_{\mathrm{i}}^{\mathrm{SPL}}, K_{\mathrm{a}}^{\mathrm{SPL}}\}$. In this step, the voltage control function of BESSs is turned off to clarify the effect of SPL operation on the fluctuation of inverter terminal voltage. The objective function is a minimization of the SPL violation F^{SPL}, and the constraint is to suppress the fluctuation of the BESS charge\discharge and inverter terminal voltage to less than the respective fluctuations during LSPV generation in cloudy weather, P^{flu} and V^{flu}, expressed as follows:

$$\begin{aligned} &\min\ F^{\mathrm{SPL}}(\boldsymbol{\gamma}^{\mathrm{SPL}}) = \sum_{t}^{T} P_{t}^{\mathrm{vio_{allw}}}(\boldsymbol{\gamma}^{\mathrm{SPL}}), \\ &s.t.\ \begin{cases} \max\{\Delta P_{d,t}(\boldsymbol{\gamma}^{\mathrm{SPL}})\} \le P^{\mathrm{flu}} & (\forall d \forall t) \\ \max\{\Delta V_{d,t}(\boldsymbol{\gamma}^{\mathrm{SPL}})\} \le V^{\mathrm{flu}} & (\forall d \forall t), \end{cases} \end{aligned} \tag{3.12}$$

where

$$\begin{aligned} \Delta P_{d,t}(\boldsymbol{\gamma}^{\mathrm{SPL}}) &= \left| P_{d,t}^{\mathrm{BESS}}(\boldsymbol{\gamma}^{\mathrm{SPL}}) - P_{d,t-1}^{\mathrm{BESS}}(\boldsymbol{\gamma}^{\mathrm{SPL}}) \right|, \\ \Delta V_{d,t}(\boldsymbol{\gamma}^{\mathrm{SPL}}) &= \left| V_{d,t}^{\mathrm{term}}(\boldsymbol{\gamma}^{\mathrm{SPL}}) - V_{d,t-1}^{\mathrm{term}}(\boldsymbol{\gamma}^{\mathrm{SPL}}) \right|. \end{aligned} \tag{3.13}$$

The constraint can prevent the hunting phenomenon which may cause voltage violation and substation power fluctuation. The fluctuation value of the substation power flow and inverter terminal voltage is calculated by (3.13).

step4) Determine the control parameters for the voltage control $\boldsymbol{\gamma}^{\mathrm{VC}} = \left[K_{\mathrm{p}}^{\mathrm{VC}}, K_{\mathrm{i}}^{\mathrm{VC}}, K_{\mathrm{a}}^{\mathrm{VC}}\right]$. In this step, the SPL function is active with optimal control parameters $\boldsymbol{\gamma}^{\mathrm{SPL_{opt}}}$ to determine the optimal control parameters for voltage control. The objective function is a minimization of inverter terminal voltage fluctuation, and the constraint is suppression of the BESS charge/discharge fluctuation and prevention of voltage violation in the entire distribution network, as expressed as follows:

$$\begin{aligned} &\min \max_{d \in \boldsymbol{\mathcal{D}},\, t \in \boldsymbol{\mathcal{T}}} \{\Delta V_{d,t}(\boldsymbol{\gamma}^{\mathrm{set}})\}, \\ &s.t.\ \begin{cases} \max\{\Delta P_{d,t}(\boldsymbol{\gamma}^{\mathrm{set}})\} \le P^{\mathrm{flu}} & (\forall d \forall t) \\ F^{\mathrm{VC}}(\boldsymbol{\gamma}^{\mathrm{set}}) = 0, \end{cases} \end{aligned} \tag{3.14}$$

where $\boldsymbol{\gamma}^{\mathrm{set}} = \{\boldsymbol{\gamma}^{\mathrm{OLTC_{opt}}},\ \boldsymbol{\gamma}^{\mathrm{SPL_{opt}}},\ \boldsymbol{\gamma}^{\mathrm{VC}}\}$.

step5) Determine the optimal BESS capacity which minimizes the objective function F. The minimum BESS capacity for obtaining the maximum SPL effect is determined as the optimum capacity, expressed as

$$\min F = \alpha_1 F^{\mathrm{SPL}} + \alpha_2 CAP. \tag{3.15}$$

where α is the primitive priority factor.

3.4 Simulation case studies

To verify the effectiveness of the proposed scheme, power flow calculations were performed on the basis of a 6.6-kV distribution network with an LSPV.

3.4.1 Simulation settings

Figure 3.4 shows the distribution network model [3-10]. A LSPV was connected to the end of the distribution line such that it represented the most difficult situation of voltage control. In addition, the BESS was connected to the LSPV. A communication line was established between the substation and the BESS to obtain active power information from the substation, and the BESS performed SPL with the obtained information. Figures 3.5 and 3.6 show the load profile [3-11] and PV profiles collected in a study by the New Energy and Industrial Technology Development Organization [3-12], respectively. In the simulation, the three characteristic types of PV profiles (sunny day, cloudy day type one, and cloudy day type two) were used. In terms of the PV profile features for each day, for a sunny day, the PV output was stable; for a cloudy day of type one, the amount of PV output change was drastic; and for a cloudy day of type two, the number of PV output changes was high. Table 3.1 lists the simulation conditions, including the distribution network conditions and the respective OLTC and BESS specifications.

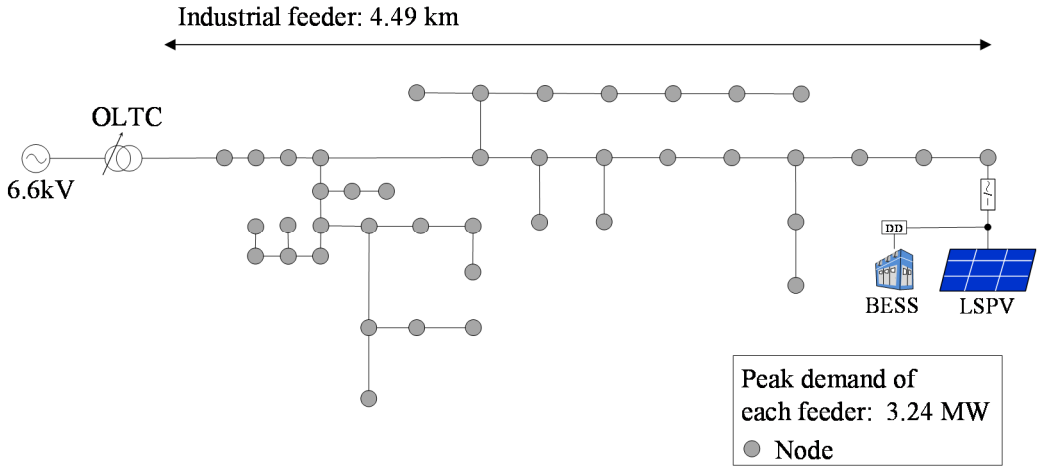

Fig. 3.4 Distribution network model.

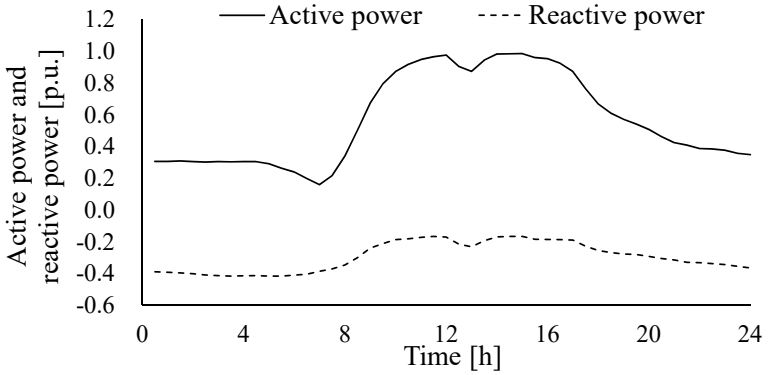

Fig. 3.5 Load profile.

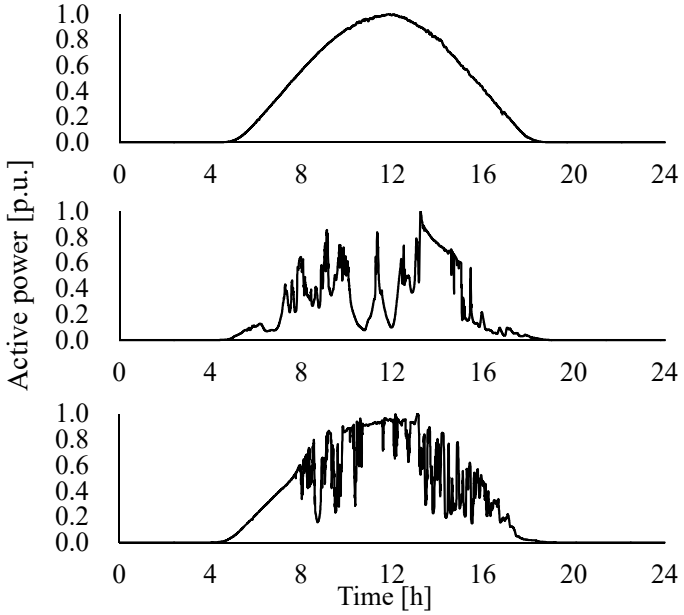

Fig. 3.6 PV profiles: sunny day (top)
Cloudy day of type one (middle), and cloudy day of type two (bottom).

Table 3.1 Simulation settings.

Content		Setting Value
Simulation time step [s]		10
Rated voltage [V]		6600
Allowable voltage range [p.u.] [2-34]		0.981–1.019
Number of simulation dates (PV generation (3 days))		3
Total number of nodes		42
Peak values	Summed load [kW]	3241
	LSPV [kW]	4794
OLTC	Rated capacity [MVA]	10
	Voltage change per tap [p.u.]	0.015
	Search range of control parameters Upper limit of the dead band [p.u.] Lower limit of the dead band [p.u.]	0.990 – 1.019 0.981 – 1.001 (0.00015 increment)
BESS	Target range of SPL [kW] (lower/upper)	0/500
	Dead band of SPL [kW] (lower/upper)	50/450
	Search range of control parameters voltage control: $K_{\mathrm{p}}^{\mathrm{VC}}[-]$, $K_{\mathrm{i}}^{\mathrm{VC}}[\mathrm{m}\cdot\mathrm{s}^{-1}]$, $K_{\mathrm{a}}^{\mathrm{VC}}[\mathrm{m}\cdot\mathrm{s}^{-1}]$ SPL: $K_{\mathrm{p}}^{\mathrm{SPL}}[-]$, $K_{\mathrm{i}}^{\mathrm{SPL}}[\mathrm{m}\cdot\mathrm{s}^{-1}]$, $K_{\mathrm{a}}^{\mathrm{SPL}}[\mathrm{m}\cdot\mathrm{s}^{-1}]$	1 – 30 (1 increment)

3.4.2 Optimal control parameters and BESS capacity

- Optimal control parameters of OLTC (step 2)

Figure 3.7 shows the optimal control parameters of the OLTC. The cell labeled "NaN" is outside the scope of the parameter search. The numbers in the colored cells denote the numbers of simulated line resistance R^{OLTC} and reactance X^{OLTC} combinations with no voltage violation. The total number of combinations is 121. Figure 3.7 shows the following: (1) More than half of the parameter set cannot prevent the distribution voltage violation. (2) The parameters with no voltage violation are dense, which may help to narrow the search range of control parameters. The lower/upper limits of the dead band of the LDC method $\left\{\underline{V}^{\mathrm{DB_{OLTC}}},\ \overline{V}^{\mathrm{DB_{OLTC}}}\right\}$ were determined as 6515V/6585V, respectively. Further, R^{OLTC} and X^{OLTC} were randomly determined in the 65 combinations.

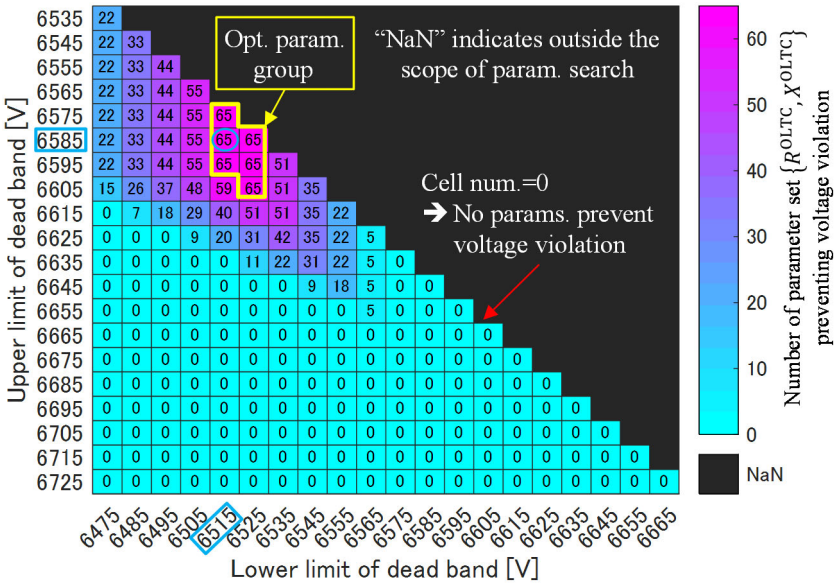

Fig. 3.7 Optimal OLTC control parameter set.

- Optimal SPL control parameter (step 3)

Figure 3.8 shows the total value of the SPL violation for three days under the optimal integral gain $K_{\mathrm{i}}^{\mathrm{SPL}} = 30$ for each PI control parameter set, $K_{\mathrm{p}}^{\mathrm{SPL}}$ and $K_{\mathrm{a}}^{\mathrm{SPL}}$, satisfying the fluctuation constraint of BESS. The SPL violation value rapidly increases as $K_{\mathrm{p}}^{\mathrm{SPL}}$ decreases, while the SPL violation value does not change significantly regardless of the $K_{\mathrm{a}}^{\mathrm{SPL}}$ change. A parameter set that minimizes the SPL violation was employed as an optimal parameter of SPL.

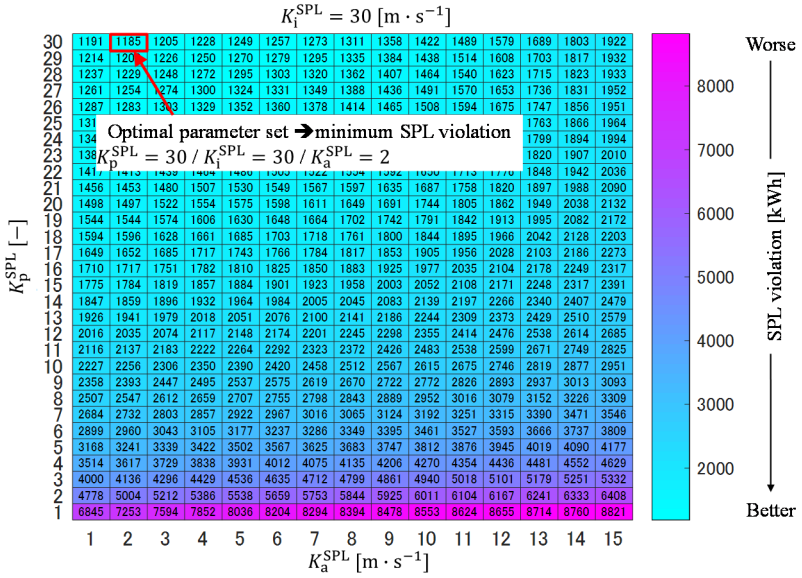

Fig. 3.8 SPL control parameter set and SPL violation.

- Optimal voltage control parameter (step 4)

Figure 3.9 shows the maximum value of the voltage fluctuation for three days under the optimal proportional gain $K_p^{VC} = 1$ for each PI control parameter set: K_i^{VC} and K_a^{VC}, satisfying the following constraints: the BESS charge/discharge fluctuation constraint, voltage fluctuation constraint, and no voltage violation. A parameter set that minimizes the inverter terminal voltage fluctuation was employed as an optimal parameter of voltage control. As an overall trend, most of the control parameter set exists in the rage where $K_i^{VC} \geq K_a^{VC}$. The reason for this is understood as follows: voltage fluctuation under the parameter set, which is $K_i^{VC} \geq K_a^{VC}$, below the target value V^{flu} because larger K_i^{VC} stabilizes the reactive power output change of the inverter. The optimal control parameters of the OLTC and BESS were determined in steps 2 – 4, which are listed in Table. 3.2

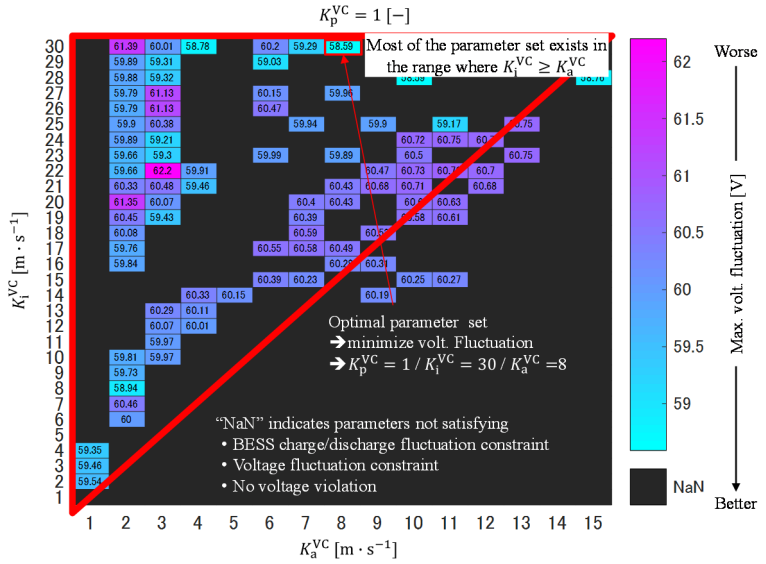

Fig. 3.9 Voltage control parameter set and inverter terminal voltage fluctuation.

Table 3.2 Optimal control parameters of OLTC and BESS.

Equipment	Control parameter	Value
OLTC	Dead band for LDC control	$\underline{V}^{\mathrm{DB_{OLTC}}} = 6515$ [V] / $\overline{V}^{\mathrm{DB_{LOTC}}} = 6585$ [V]
	Simulated line impedance of LDC method	$R^{\mathrm{OLTC}} = 0.03$ [Ω] / $X^{\mathrm{OLTC}} = 0.02$ [Ω]
BESS	PI control parameters for the SPL	$K_{\mathrm{p}}^{\mathrm{SPL}} = 30$ [m · s^{-1}] $K_{\mathrm{i}}^{\mathrm{SPL}} = 30$ [−] $K_{\mathrm{a}}^{\mathrm{SPL}} = 2$ [m · s^{-1}]
	PI control parameters for the voltage control	$K_{\mathrm{p}}^{\mathrm{VC}} = 1$ [m · s^{-1}] $K_{\mathrm{i}}^{\mathrm{VC}} = 30$ [−] $K_{\mathrm{a}}^{\mathrm{VC}} = 8$ [m · s^{-1}]

- Optimal BESS capacity (step5)

Figure 3.10 shows the relationship between the SPL violation values and the BESS capacities. The SPL violation decreases as the BESS capacity increases; in particular, the BESS energy has a more significant effect on the SPL violation. Figure 3.10 also indicates that the SPL violation is not significantly different when the BESS energy/power is more than 1150 kWh/1250 kW, which is denoted by an optimal parameter group. In the optimal parameter group, the optimal BESS capacity that minimizes the SPL violation and BESS cost was selected.

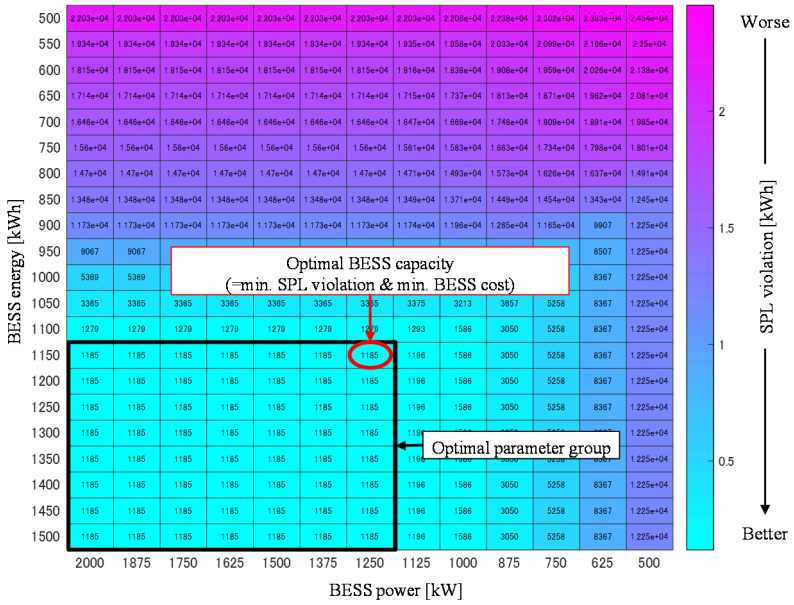

Fig. 3.10 Relationship between SPL violation values and BESS capacity.

3.4.3 Effectiveness of proposed scheme

The control performances with the optimal/conventional control parameter set were compared to confirm the effectiveness of the proposed scheme. The control parameter set which prevent the 30-min averaged voltage is selected as the conventional control parameter set. Figure 3.11 shows the (a)

distribution voltage, (b) substation active power, and (c) BESS active/reactive power outputs. In Fig. 3.11(a), the distribution voltage is maintained within an allowable range with the optimal control parameter (left side), while the amount of voltage violation reaches 17.7 [Vh] with the conventional control parameter (right side). Similarly, from Fig. 3.11(b), the optimal control parameter reduces the SPL violation by 73% from 3.95 [kWh] to 1.06 [kWh]. Figure 3.11(c) shows that the BESS output with the conventional control parameter is relatively small compared to the output with the optimal parameter, which leads to the difference in the voltage control and SPL control performance.

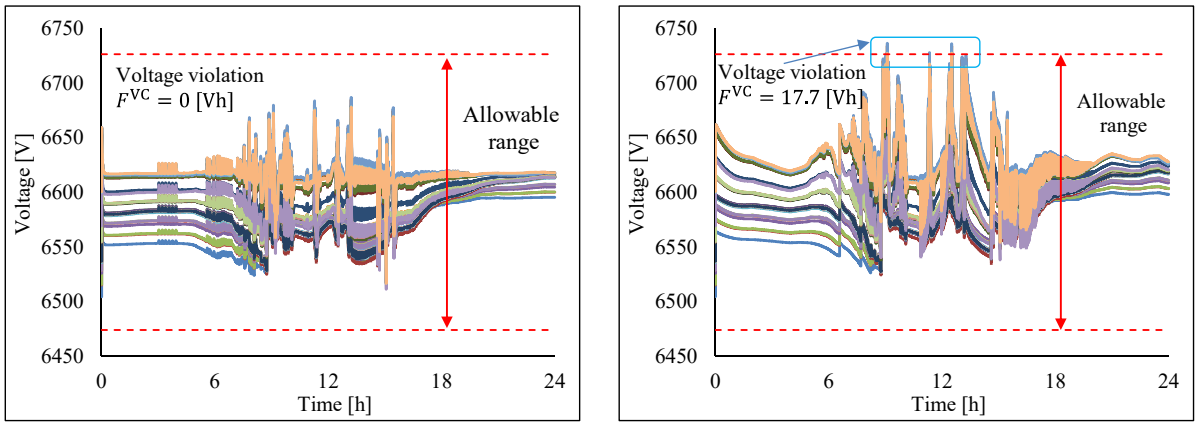

(a) Distribution voltage.

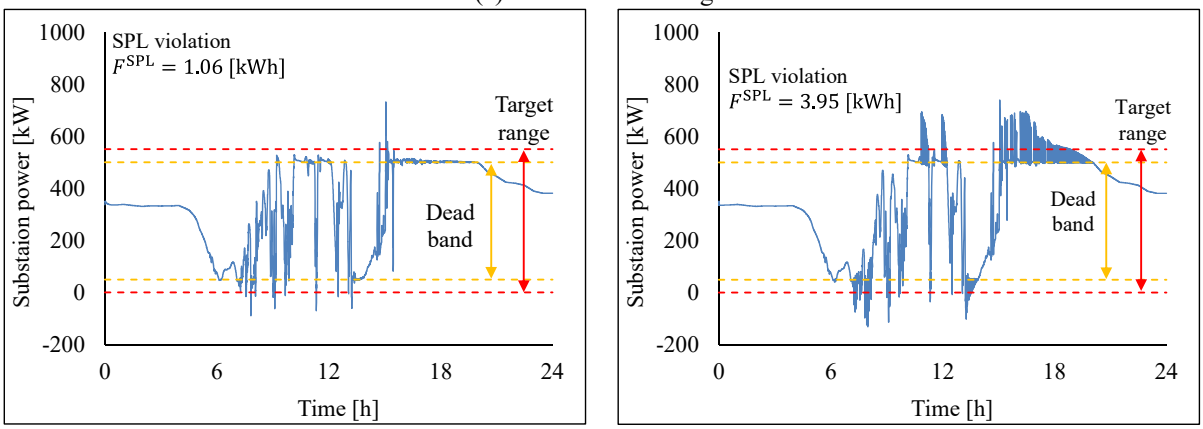

(b) Substation active power.

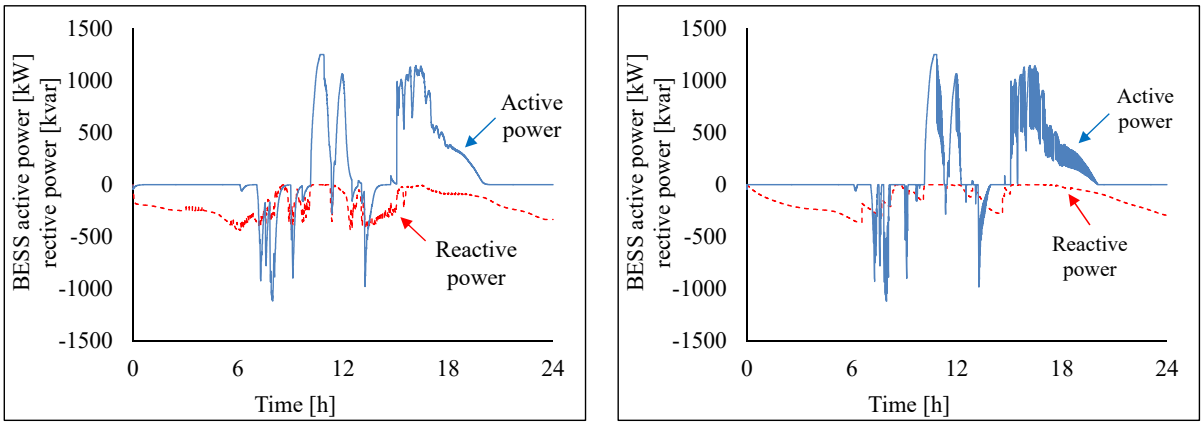

(c) BESS active/reactive power output.

Fig. 3.11 Comparison of optimal/conventional control parameter
(Left: with optimal parameter / right: with conventional parameter).

3.5 Summary of this chapter

In this chapter, I proposed a method to determine the optimal control parameters and BESS capacity in order to ensure effective control performance. To simplify the procedure of control parameter determination, the control parameters were determined in the order of SPL and voltage control considering the mutual interaction of SPL and voltage control. Simulations of three days were performed to obtain the proper capacity combination based on a quantitative evaluation of the control performance. The simulation results showed that the proposed scheme could determine the optimal control parameters for SPL and voltage control, which prevent voltage violation and minimize SPL violation. The optimal capacity combination for the simulated system was determined as follows: energy, 1150 kWh; power, 1250 kW which is about 30 % of the LSPV capacity. In addition, the following trends were confirmed. The SPL violation is influenced by the SPL proportional gain $K_{\mathrm{p}}^{\mathrm{SPL}}$ rather than the attenuation gain $K_{\mathrm{a}}^{\mathrm{SPL}}$. SPL violation is significantly influenced by the BESS energy. With regard to voltage control, a large value of $K_{\mathrm{i}}^{\mathrm{VC}}$ is preferred because larger $K_{\mathrm{i}}^{\mathrm{VC}}$ stabilizes the reactive power output and prevents the rapid fluctuation of distribution voltage.

References

[3-1] Y. Wang, K.T. Tan, X.Y. Peng, and P.L. So, "Coordinated Control of Distributed Energy Storage Systems for Voltage Regulation in Distribution Networks," *IEEE Trans. Power Delivery*, vol. 31, no. 3, pp. 1132–1141, June 2016.

[3-2] E. Reihani, M. Motalleb, R. Ghorbani, and L. S. Saoud, "Load Peak Shaving and Power Smoothing of a Distribution Grid with High Renewable Energy Penetration," *Renew. Energy*, vol. 86;, pp.1372–1379, Feb. 2016.

[3-3] A.F. Crossland, D.Jones, and N.S.Wade, "Planning the Location and Rating of Distributed Energy Storage in LV Networks Using a Genetic Algorithm with Simulated Annealing," *Electr. Power Energy Syst.*, vol. 59, pp. 103–110, July 2014.

[3-4] M. Nick, R. Cherkaoui, and M. Paolone, "Optimal Siting and Sizing of Distributed Energy Storage Systems via Alternating Direction Method of Multipliers," *Electr. Power Energy Syst.*, vol. 72, pp.33–39, Nov. 2015.

[3-5] E. Reihani, S. Sepasi, L. R. Roose, and M. Matsuura, "Energy Management at the Distribution Grid using a Battery Energy Storage System (BESS)," *Electr. Power Energy Syst.*, vol. 77, 337–344, May 2016.

[3-6] P. Balram, L.A. Tuan, O. Carlson, "Comparative Study of MPC Based Coordinated Voltage Control in LV Distribution Systems with Photovoltaic and Battery Storage," *Electr. Power Energy Syst.*, vol. 95, pp. 227–238, Feb. 2018.

[3-7] F. H. M Rafi, M. J. Hossain, and J. Lu, "Hierarchical Controls Selection Based on PV Penetration for Voltage Rise Mitigation in a LV Distribution Network," *Electr. Power Energy Syst.*, vol. 81,, 123–139, Oct. 2016.

[3-8] M. Motalleb, E. Reihani, and R. Ghobani "Optimal Placement and Sizing of the Storage Supporting Transmission and Distribution Networks," *Renew. Energy*,vol. 94,pp. 651–659, Aug. 2016.

[3-9] Q. Liao, B. Sun, Y. Liu, J. Sun, and G. Zhou, "A Techno-Economic Analysis on NaS Battery Energy Storage System Supporting Peak Shaving," *J. Energy Res.*, vol. 40, no. 2, pp. 241–247, Nov. 2015.

[3-10] R. Miyoshi, J. Yoshinaga, and Y. Hayashi, "Evaluation of Amount of Expansion in PV Introduction Limit by Fragmenting Pole Transformers and Increasing Diameter of Distribution Lines on Distribution Models in Consideration of Various District Divisions," *Proc. 27th Annual Conf. Power Energy Soc.*, IEE Japan, no. P21, 2013.

[3-11] Electric Technology Research Association, "Corresponding to the Issue of Power Factor in the Distribution System," [*Denkikyoudoukenkyu*], vol. 66, no. 1, p. 97, Jan. 2011 (in Japanese).

[3-12] [Online]. Available: http://www.nedo.go.jp/activities/ZZ_00229.html (in Japanese). [Accessed 8-Nov.-2018].

Chapter 4
Multipurpose Control and Planning Method for BESS

4.1 Introduction to this chapter

Large amount of PVs are installed in power networks. PVs have some environmental benefits such as low CO_2 emission and low fossil-fuel consumption. Conversely, a high PV penetration may cause power and frequency fluctuations and voltage-rise problems. A BESS is remarkable device that can solve these problems as it can mitigate the power-quality deterioration and thereby increase PV installation. Many researchers have reported control, sizing, and planning methods for BESSs [4-1]–[4-26]. References [4-1]–[4-5] have reported the optimal operation or optimal sizing of BESSs integrated with wind power (WP) or PV systems. In [4-1], a sizing scheme of the BESS for WP smoothing was presented. For smoothing WP generation and maintaining the state of health of the BESS, a variable-interval reference signal optimization approach and charge/discharge scheme based on fuzzy control were presented. The BESS capacity was determined separately according to a statistical model of the BESS output and an economic cost model. In [4-6]–[4-15], BESSs have been employed to regulate the frequency and voltage of a microgrid system. Miranda *et al*. proposed an optimization scheme for the operation and planning of the BESS in an islanding power network or microgrid [4-7]. The authors determined the suitable BESS capacity, site, and type for a real-world case study of a Portuguese island. The results provided an optimized BESS solution as well as operational and economic benefits. BESSs have been employed to enhance the power quality of distribution networks [2-5], [4-16]-[4-18] or transmission networks [4-19]-[4-26]. Yang *et al*. [4-16] utilized distributed BESSs installed in households for voltage control and peak load shaving, which have been achieved by centralized charging/discharging control. The suitable capacity of distributed BESSs was calculated based on a cost-benefit analysis considering the following factors: the BESS influence on voltage regulator operation, peak power generation and load shifting, and the BESS cost with its lifetime estimation. In [4-16], the authors proposed a tool for determining the optimal capacity and a day-ahead operation strategy of the BESS employed by a distribution network operator. The results showed that the optimal BESS integration could maximize operational cost benefits and improve distributed generation and load-hosting capacity in the distribution network. Recently, Japanese power utilities have faced problems of power fluctuations in distribution networks and RPF at substations due to a high LSPV penetration. The LSPVs in distribution networks will increase in the future, which may lead to more severe conditions and inhibit LSPV installation. The power smoothing of LSPVs is required by Hokkaido Electric Power Co., Inc. [1-17]. In addition, RPF prevention at substations is demanded by power companies because of its adverse effect on voltage control and the protection function for accident prevention. BESSs can achieve both power smoothing and RPF prevention, and the

multipurpose utilization of the BESS can contribute to cost effectiveness. Generally, BESSs in distribution networks are used over a decade or more. Therefore, the role and capacity of BESSs may differ with changes in the distribution network, such as the increase of LSPVs. Thus, BESSs are desired to be configured considering the increase of LSPVs. In addition, the charge/discharge control of BESSs may affect the operation of tap controllers and LSPV inverters, because of which the impact of BESS installation must be evaluated. However, few studies on BESS installation planning in distribution networks have been reported, and to my knowledge, no study has addressed an MCP scheme for BESSs in distribution networks or configured BESSs while considering its installation impact and the increase of LSPVs. Therefore, this chapter presents the MCP scheme and determines a suitable BESS site and type based on the BESS capacity and installation impact. The advantages of this method are summarized as follows. (1) Control of the MCP scheme: BESSs are employed for the smoothing of power flow at substations and LSPVs as well as for RPF prevention at substations. BESSs adjust the SoC to reduce the capacity. The control of the MCP scheme enables power smoothing and RFP prevention while maximally adjusting the SoC. The control of the MCP scheme prevents interactions between controls, which may cause the hunting phenomenon in the BESS output as well as BESS output shortage due to the simultaneous command of charge and discharge. (2) Planning of the MCP scheme: The planning method determines a suitable BESS site and type based on the required BESS capacity, number of tap operations of the OLTC and SVR, and LSPV curtailment considering the increase in LSPVs. The BESS capacity was calculated based on characteristics such as the power-to-energy ratio (P/E ratio) and round-trip efficiency. (3) Evaluation of impact of BESS installation on tap operation and LSPV curtailment: To evaluate the impact of BESS installation on tap operation and LSPV curtailment, the control schemes of tap controllers – OLTC, SVR [4-27], and LSPV inverters [1-14] were implemented. The control parameters of tap controllers and LSPV inverters were adjusted to prevent voltage violations and the control the hunting phenomenon.

The remainder of this chapter is organized as follows. Section 4.2 describes the MCP scheme. Section 4.3 describes the voltage control methods of OLTC, SVR, and LSPV inverters. Section 4.4 presents the simulation conditions and results. Section 4.5 concludes this chapter.

4.2 Overview of MCP scheme

This section provides an overview of the MCP scheme. Regarding the control of the MCP scheme, the power smoothing, RFP prevention, SoC adjustment, and multipurpose control method are described. Subsequently, the planning of the MCP scheme is explained. The planning of the MCP scheme determines a suitable BESS site and type considering the increase of LSPVs. Additionally, a BESS capacity calculation that reflects the P/E ratio and round-trip efficiency of the BESS is described.

4.2.1 Control of MCP scheme

Before the description of each BESS control, Fig. 4.1 shows measurement data and a control overview of the BESS at a substation/LSPV. In Fig. 4.1(a), the BESS is operated to mitigate the fluctuation of an LSPV generation (point B) and to prevent RPF at a substation (point A). In addition, the BESS charges the LSPV curtailment owing to voltage control and a high array-to-inverter ratio (AIR), which indicates that the LSPV generation is higher than the rated capacity of the LSPV inverter. The AIR was set to 1.66 [4-28]. In Fig. 4.1(b), the BESS mitigates the fluctuation of the substation power flow and RPF (point A).

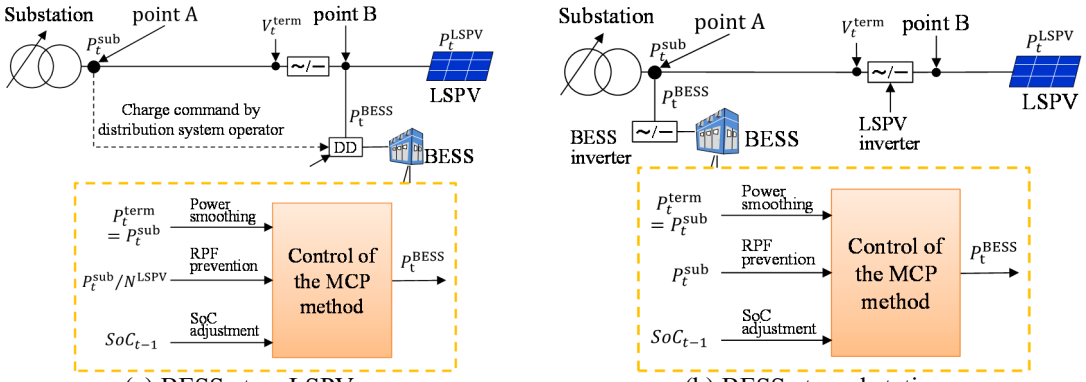

(a) BESS at an LSPV. (b) BESS at a substation.

Fig. 4.1 Measurement data and a control overview of the BESS.

- PV generation/substation power smoothing

The power flow of the substation and LSPV generation are smoothed to prevent a rapid power fluctuation. The BESS charges/discharges such that the maximum change in the terminal power per minute is maintained lower than the target range of power smoothing $\boldsymbol{w_t} = \{\underline{w_t},\ \overline{w_t}\}$ calculated as follows:

$$\begin{aligned} \overline{w_t} &= P_t^{\max} + \varepsilon, \\ \underline{w_t} &= P_t^{\max} - \varepsilon, \end{aligned} \tag{4.1}$$

where $P_t^{\max}$ and $P_t^{\min}$ are the maximum and minimum values of the terminal power in the last one minute, ε is the target value of power smoothing. Figure 4.2 shows the image of power smoothing operation.

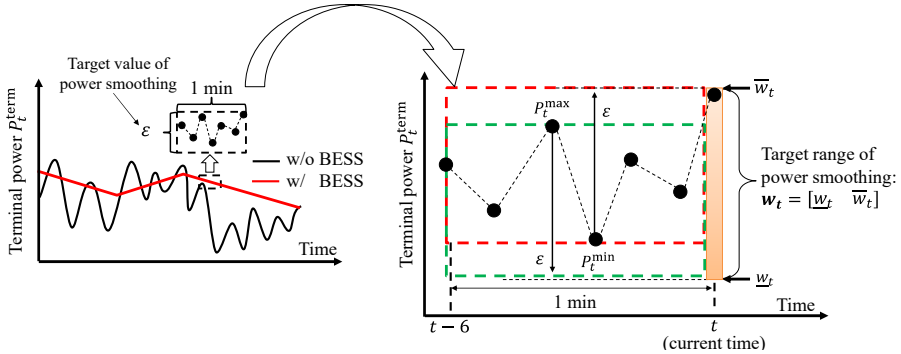

Fig. 4.2 Power smoothing operation.

- RPF prevention

The RPF at the substation is charged to prevent any adverse effect on voltage control and the protection function for accident prevention under a high LSPV penetration rate. The charging power for RFP prevention is calculated as follows:

$$P_t^{\mathrm{RPF_{cmd}}} = \begin{cases} P_t^{\mathrm{sub}} & ,\text{if } (P_t^{\mathrm{sub}} < 0) \\ 0 & ,\text{if } (P_t^{\mathrm{sub}} \geq 0). \end{cases} \tag{4.2}$$

- SoC adjustment

In addition to the power smoothing and RPF prevention, the BESS adjusts the SoC to reduce the energy for the operation. The BESS output for SoC adjustment is proportional to the difference between the target value of SoC $SoC^{\mathrm{tgt}}$and the value of SoC SoC_{t-1}, as expressed by the following equation:

$$P_t^{\mathrm{SoC_{cmd}}} = \frac{P^{\mathrm{max_{SoC}}}}{100} \cdot (SoC_{t-1} - SoC^{\mathrm{tgt}}). \tag{4.3}$$

Where $P^{\mathrm{max_{SoC}}}$ is the maximum value of active power for SoC adjustment.

- Control of the MCP Scheme

Figure 4.3 shows a flowchart of the control of the MCP scheme. Firstly, command values for RFP prevention $P_t^{\mathrm{RPF_{cmd}}}$ and SoC adjustment $P_t^{\mathrm{SoC_{cmd}}}$ are calculated using by (4.2) and (4.3).

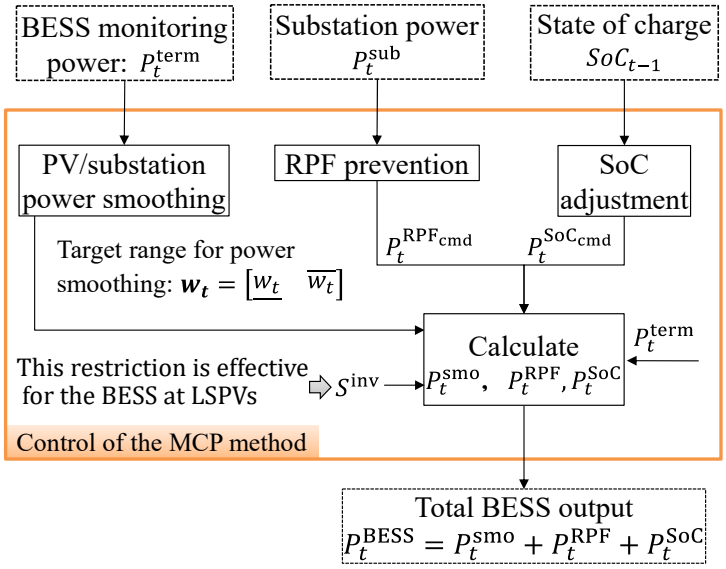

Fig. 4.3 Control of the MCP scheme.

Then, command values are adjusted to maintain the terminal power within two target ranges $(\boldsymbol{w_t}$ and $S^{\mathrm{inv}})$ as follows:

min

$$\alpha_1 \left| P_t^{\mathrm{RPF_{cmd}}} - P_t^{\mathrm{RPF}} \right| + \alpha_2 \left| P_t^{\mathrm{SoC_{cmd}}} - P_t^{\mathrm{SoC}} \right| + \alpha_3 |P_t^{\mathrm{smo}}|, \tag{4.4}$$

s.t.

$$\begin{gathered}\underline{w_t} \le P_t^{\mathrm{term}} + P_t^{\mathrm{BESS}} \le \overline{w}_t, \\ 0 \le P_t^{\mathrm{BESS}} + P_t^{\mathrm{sub}}, \\ \begin{cases} P_t^{\mathrm{smo}} \ge 0 \\ P_t^{\mathrm{RPF}} \ge 0 \\ P_t^{\mathrm{SoC}} \ge 0 \end{cases} \text{ or } \begin{cases} P_t^{\mathrm{smo}} \le 0 \\ P_t^{\mathrm{RPF}} \le 0 \\ P_t^{\mathrm{SoC}} \le 0, \end{cases} \\ -S^{\mathrm{inv}} \le P_t^{\mathrm{term}} + P_t^{\mathrm{BESS}} \le S^{\mathrm{inv}}. \end{gathered} \tag{4.5}$$

Finally, the total BESS output is calculated. The control of the MCP scheme does not charge/discharge for power smoothing when the terminal power is maintained within the target range $\boldsymbol{w_t}$ as a result of the BESS operation of the RPF prevention and SoC adjustment. The RPF prevention has priority over SoC adjustment. Thus, the BESS output is determined in the order of RPF prevention, SoC adjustment, and power smoothing, as expressed in (4.4). In (4.5), the control via the MCP scheme has four limiting constraints: 1) maintain the total value of terminal power and BESS output $P_t^{\mathrm{term}} + P_t^{\mathrm{BESS}}$ within the target range $\boldsymbol{w_t}$; 2) prevent RPF at the substation; 3) prevent the cancellation of power output for each control; and 4) maintain the total value of LSPV generation and BESS output within the LSPV inverter capacity, which is effective for BESSs at LSPVs.

4.2.2 Planning of MCP scheme

The MCP scheme determines the capacity for operation as well as suitable site and type of the BESS in the distribution network, as shown in Fig. 4.4. In the planning method, distribution-network data, time-series data, and BESS characteristics are prepared first (step 1). The distribution-network data includes topology, load capacity, and placement and control methods of voltage regulators. Subsequently, the BESS capacity and control performances of the BESS and voltage regulators are obtained (step 2). To guarantee the power smoothing performance regardless of the BESS site, the maximum value of substation power fluctuation in step 2 is employed as a target value of power smoothing, and the resulting capacity of the BESS at the substation is calculated (step 3). Steps 2 and 3 are executed with different BESS types: redox flow battery (RFB) and lithium-ion battery (LiB) (loop 1). Control parameters are renewed when the distribution voltage violates the allowable range from the viewpoint of reducing the update frequency of control parameters (loop 2). Generally, Japanese power companies use the 30-min averaged voltage to determine voltage violations [4-27]. The 5-min averaged value was used to consider the rapid voltage fluctuation due to LSPVs. This BESS capacity calculation is repeated for the number of installed LSPVs (loop 3), following which the suitable BESS site and type are determined based on the BESS capacity, number of tap operations, and LSPV curtailment (step 4).

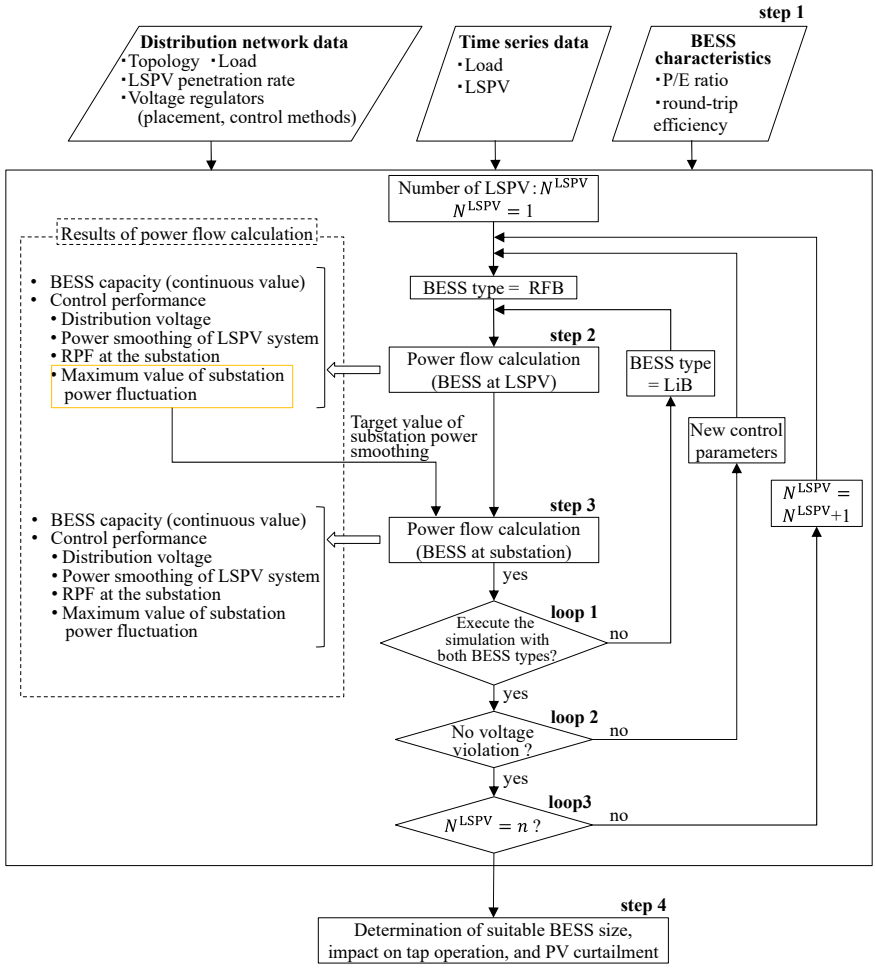

Fig. 4.4 Planning of MCP scheme.

4.2.3 BESS capacity calculation

The planning of the MCP scheme involves the calculation of the BESS capacity considering the P/E ratio and round-trip efficiency of each BESS type. Figure 4.5 shows the capacities of an RFB and LiB. The power and energy of the RFB can be designed separately [4-29]; for instance, the power can be increased in 125-kW increments [4-30], and the energy can be increased continuously. In contrast, the LiB was designed with a fixed P/E ratio, which was set to three. In this chapter, the power of the LiB was increased by 125 kW such that the conditions were aligned with those of the RFB. The energy of the LiB was assumed to be increased by 41.7 kWh, which is one-third of 125 kW. The round-trip efficiencies of the RFB and LiB are 0.75 and 0.8 [4-31], respectively. The gray area and green square indicate the possible ranges of RFB and LiB capacity, respectively. The simulation calculates the required BESS capacity for the operation, which is illustrated by cross marks.

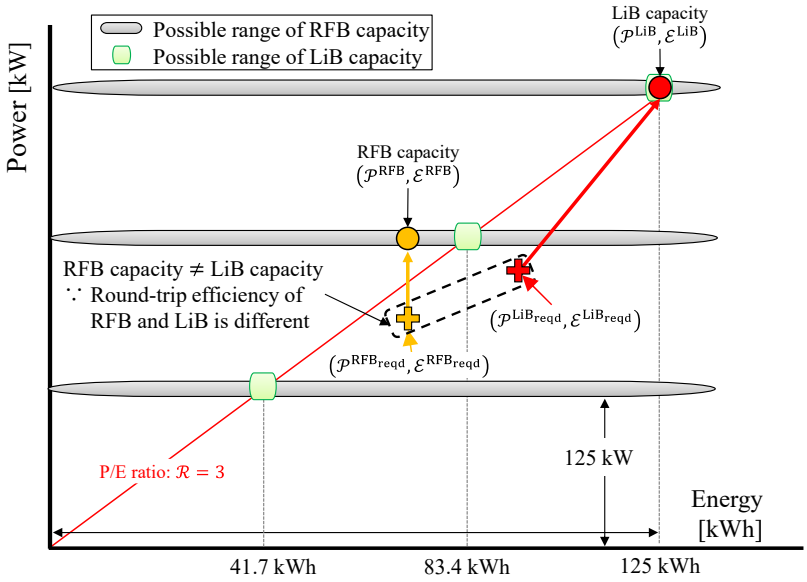

Fig. 4.5 Capacity design of RFB and LiB.

Subsequently, the capacities of RFB and LiB are calculated considering the P/E ratio, as expressed by the following equations:

$$\begin{cases} \mathcal{P}^{\mathrm{RFB}} = \mathcal{P}^{\mathrm{RFB_{unit}}} \cdot \mathrm{ceiling}\left(\dfrac{\mathcal{P}^{\mathrm{RFB_{reqd}}}}{\mathcal{P}^{\mathrm{RFB_{unit}}}}\right) \\ \mathcal{E}^{\mathrm{RFB}} = \mathcal{E}^{\mathrm{RFB_{reqd}}}, \end{cases} \tag{4.6}$$

$$\mathcal{E}^{\mathrm{LiB_{unit}}} = \frac{\mathcal{P}^{\mathrm{LiB}}_{\mathrm{unit}}}{\mathcal{R}},$$

$$\begin{cases} \mathcal{P}^{\mathrm{LiB}} = \mathcal{P}^{\mathrm{LiB_{unit}}} \cdot \mathrm{ceiling}\left(\dfrac{\mathcal{P}^{\mathrm{LiB_{reqd}}}}{\mathcal{P}^{\mathrm{LiB_{unit}}}}\right) \\ \mathcal{E}^{\mathrm{LiB}} = \mathcal{E}^{\mathrm{LiB_{unit}}} \cdot \mathrm{ceiling}\left(\dfrac{\mathcal{E}^{\mathrm{LiB_{reqd}}}}{\mathcal{E}^{\mathrm{LiB_{unit}}}}\right), \end{cases} \tag{4.7}$$

where $\mathcal{P}^{\mathrm{RFB}}$ / $\mathcal{P}^{\mathrm{LiB}}$ is the unit power of RFB/LiB, $\mathcal{E}^{\mathrm{LiB_{unit}}}$ is the unit energy of the LiB, $\mathcal{P}^{\mathrm{RFB_{reqd}}}/\mathcal{P}^{\mathrm{LiB_{reqd}}}$ is the required power of RFB/LiB, which is a continuous value calculated through numerical simulation, and $\mathcal{R}$ is the power-to-energy ratio of BESSs.

4.3 Voltage control method for LSPV inverters

The general voltage control method for tap controllers, called the LDC method, was used for OLTC and SVR as described in Chapter 2. LSPV inverters output the reactive power and curtail the LSPV generation following the volt-VAR-watt function, which is a smart inverter function proposed by EPRI [1-14]. When the terminal voltage of an LSPV inverter is outside the allowable range, LSPV inverters with the volt-VAR-watt function output reactive power first, following which the LSPV generation is curtailed such that the LSPV curtailment is minimized. The reactive power output and LSPV curtailment change dynamically according to the inverter terminal voltage V_t^{term}, as shown in Fig. 4.6.

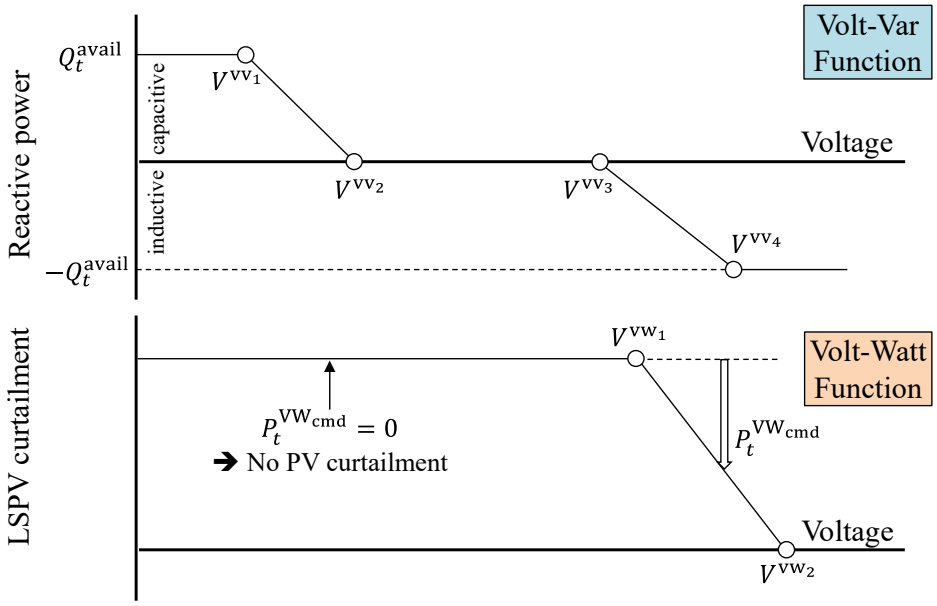

Fig. 4.6 Volt-VAR-watt function.

The command value of the volt-VAR function $Q_t^{\text{VV}_{\text{cmd}}}$ and LSPV curtailment $P_t^{\text{VW}_{\text{cmd}}}$ are calculated as follows:

$$Q_t^{\text{VV}_{\text{cmd}}} = \begin{cases} Q_t^{\text{avail}} & \text{, if } (V_t^{\text{term}} < V^{\text{vv}_1}) \\ \dfrac{V_t^{\text{term}} - V^{\text{vv}_2}}{V^{\text{vv}_1} - V^{\text{vv}_2}} \cdot Q_t^{\text{avail}} & \text{, if } (V^{\text{vv}_1} \le V_t^{\text{term}} < V^{\text{vv}_2}) \\ 0 & \text{, if } (V^{\text{vv}_2} \le V_t^{\text{term}} < V^{\text{vv}_3}) \\ -\dfrac{V_t^{\text{term}} - V^{\text{vv}_3}}{V^{\text{vv}_4} - V^{\text{vv}_3}} \cdot Q_t^{\text{avail}} & \text{, if } (V^{\text{vv}_3} \le V_t^{\text{term}} < V^{\text{vv}_4}) \\ -Q_t^{\text{avail}} & \text{, if } (V^{\text{vv}_4} \le V_t^{\text{term}}), \end{cases} \tag{4.8}$$

$$P_t^{\text{VW}_{\text{cmd}}} = \begin{cases} 0 & \text{, if } (V_t^{\text{term}} < V^{\text{vw}_1}) \\ \dfrac{V_t^{\text{term}} - V^{\text{vw}_2}}{V^{\text{vw}_1} - V^{\text{vw}_2}} \cdot P_t^{\text{LSPV}} & \text{, if } (V^{\text{vw}_1} \le V_t^{\text{term}} < V^{\text{vw}_2}) \\ P_t^{\text{LSPV}} & \text{, if } (V^{\text{vw}_2} \le V_t^{\text{term}}), \end{cases} \tag{4.9}$$

where Q_t^{avail} is the available capacity of reactive power output at time slice t, P_t^{LSPV} is the LSPV generation at time slice t, V_t^{term} is the inverter terminal voltage at time slice t, and $V^{\text{vv}_1} - V^{\text{vv}_4}/V^{\text{vw}_1} - V^{\text{vw}_2}$ are the control parameters of volt-VAR-watt function.

The change rates of reactive power output and LSPV curtailment are limited to prevent the hunting phenomenon, which may lead to voltage violations. In addition, the reactive power output is limited by restrictions on the available capacity Q_t^{avail} and power factor $Q_t^{\text{lim}_{\text{pf}}}$ as expressed by the following equation:

$$Q_t^{\text{avail}} = \sqrt{(S^{\text{inv}})^2 - \left(P_t^{\text{inv}}\right)^2}, \tag{4.10}$$

$$Q_t^{\lim_{pf}} = P_t^{LSPV} \sqrt{\frac{1}{(pf)^2} - 1}, \tag{4.11}$$

where S^{inv} is the rated capacity of the LSPV inverter, P_t^{inv} is the active power output of the BESS, and pf is the power factor limit. The power-factor restriction is regulated by Japanese grid code [1-13]. Therefore, LSPV inverters output the reactive power, which is not greater than the available capacity calculated in (4.10), while maintaining the power factor within 0.85 (leading) and 0.85 (lagging) in (4.11). Figure 4.7 shows the block diagram of the volt-VAR-watt function.

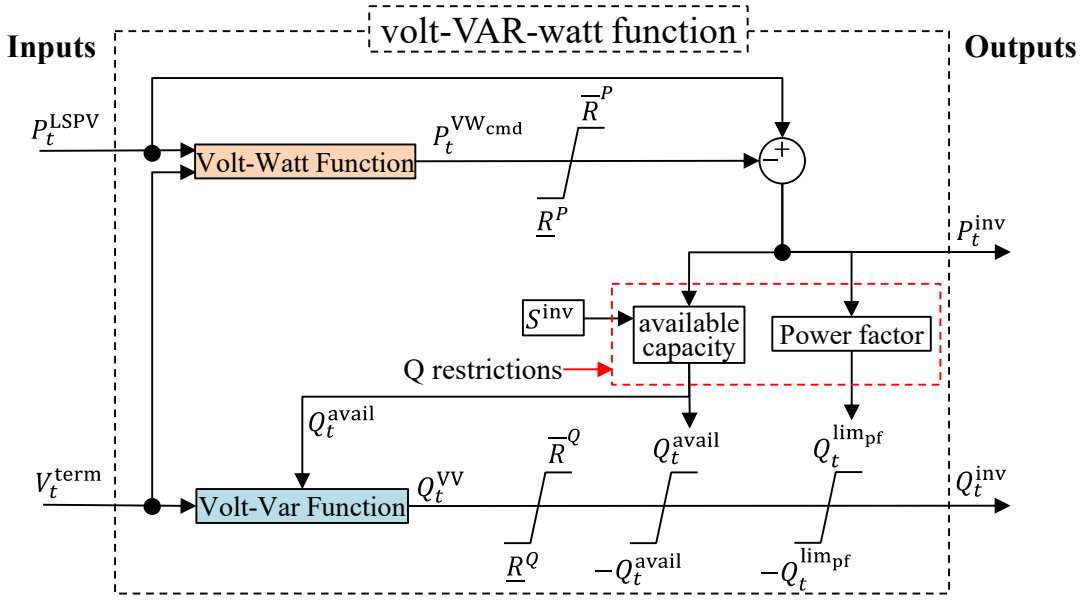

Fig. 4.7 Block diagram of the volt-VAR-watt function.

4.4 Simulation case studies

Case study simulations were executed to evaluate the effectiveness of the control of the MCP scheme and to determine the suitable BESS site and type considering the increase of LSPVs.

4.4.1 Simulation settings

The distribution network model consists of one industrial feeder (Feeder 1: F1) and two residential feeders (F2 and F3), as shown in Fig. 4.8. The trunk line lengths of F1, F2, and F3 are 4.49, 6.10, and 10.48 km, respectively. This distribution network model was constructed based on actual network information [4-32]. The peak demand of each feeder is approximately 2 MW, and the rated capacities of LSPVs are 2 MWac. The LSPV penetration rate is defined as the ratio of peak LSPV generation to peak demand (6.06 MW), and the penetration increase by 33.3% for each LSPV installation. Table 4.1 lists the settings of BESSs and LSPVs for two simulation cases. For the BESS planning according to the increase of LSPVs, control parameters of the OLTC, SVR, and LSPV inverters were adjusted to prevent distribution voltage violations. Table 4.2 lists the simulation settings: simulation time step,

details of the distribution network, and control parameters of the OLTC, SVR, and LSPV inverters. The actual measurement load and PV data were used for the simulation. The simulation was executed on 345 days, with the exception of 15 days for which the data of PV generation was missing, to consider the demand seasonality and various PV generation patterns. Examples of load and LSPV profiles are shown in Fig. 4.9.

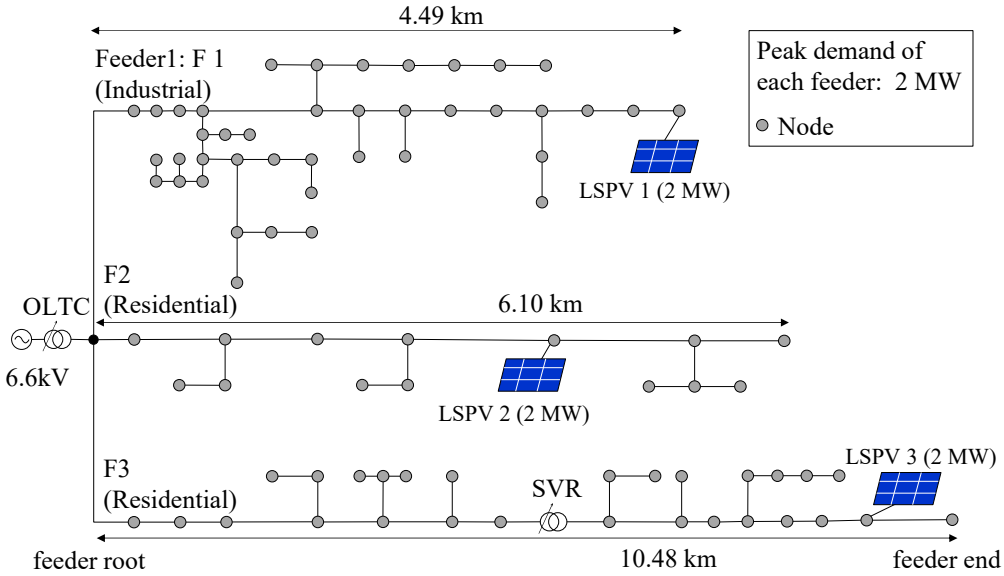

Fig. 4.8 Distribution network model

Table 4.1 Simulation cases and settings.

	BESS site	BESS type	Number of LSPVs
Case 1	LSPV	RFB LiB	1–3 Rated Capacity (2MWac/system)
Case 2	Substation		

Table 4.2 Simulation settings.

Content		Setting Value
Simulation time step [s]		10
Rated voltage [V]		6600
Allowable voltage range [p.u.] (the transformation ratio of pole transformer)		0.95 - 1.01 (6750/105) 0.93 – 0.99 (6600/105)
Number of simulation dates (N_{date}) (Except the missing values from annual data)		345 days 2007/1/1 – 2007/12/31
Peak values	Total load of three feeders [MW]	6.06
	LSPV [MWdc] LSPV [MWac]	3.32 2.00
OLTC	Rated capacity [MVA]	20
	Voltage change per tap [p.u.] [2-35]	0.0151
	Simulated line impedance of the LDC method [Ω]	$R^{\mathrm{OLTC}} = 0.01$ $X^{\mathrm{OLTC}} = 0.01$
	Dead band of the LDC method [p.u.] Case 1 (BESS at LSPV) Case 2 (BESS at substation)	Case1: 0.967 – 0.986 Case2: 0.970 – 0.985
SVR	Rated capacity [MVA]	10

	Voltage change per tap [p.u.]	0.015
	Simulated line impedance of the LDC method [Ω]	$R^{SVR} = 0$ / $X^{SVR} = 0$
	Dead band of the LDC method [p.u.]	0.975 – 0.995
LSPV Inverter	Control parameters of the volt-VAR-watt function $V^{vv1} - V^{vw2}$ [p.u.] ΔP^{max}, ΔP^{min} [kW/m] ΔQ^{max}, ΔQ^{min} [kvar/m]	$V^{vv1} = 0.939$ $V^{vv2} = 0.955$ $V^{vv3} = 0.978$ $V^{vv4} = 0.986$ $V^{vw1} = 0.983$ $V^{vw2} = 0.990$ $\Delta P^{max} = 300$ $\Delta P^{min} = -15$ $\Delta Q^{max} = 300$ $\Delta P^{min} = -15$
BESS	Target value of power smoothing [kW/m] Case 1 (BESS at LSPV) Case 2 (BESS at substation)	Case1: $\varepsilon = 20$ Case2: $\varepsilon = 57$ (LSPV×1) $\varepsilon = 100$ (LSPV×2) $\varepsilon = 106$ (LSPV×3)
	Round-trip efficiency [%] [4-31]	RFB: 75 / LiB: 80
	Increments of the BESS capacity [4-30] RFB: (power[kW] / energy[kWh]) LiB: (power[kW] / energy[kWh])	RFB: (125/continuous) LiB: (125/41.7)
	Cost [4-31] RFB: (power [$/kW] / energy[$/kWh]) LiB: (power [$/kW])	RFB: (775 / 215) LiB: (510)

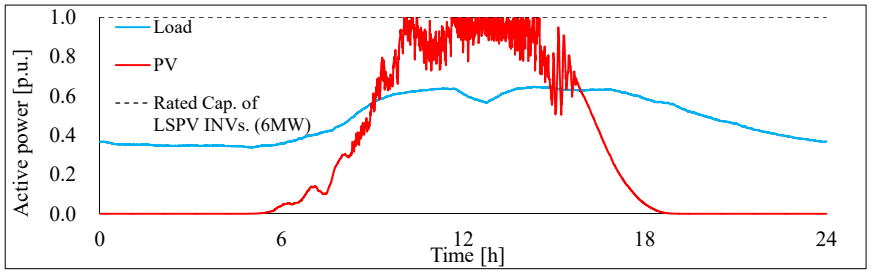

(a) Light load period (2007/5/7)

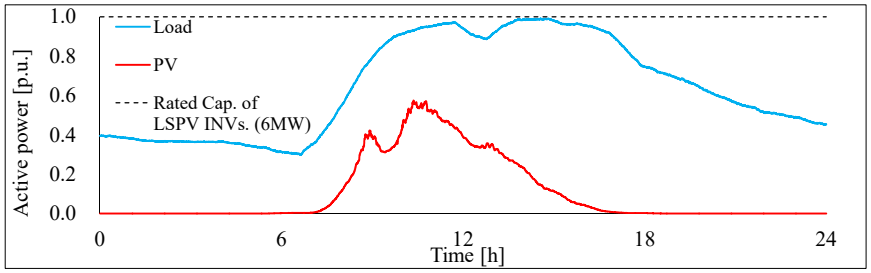

(b) Heavy load period (2007/12/25)
Fig. 4.9 Load and LSPV profiles.

4.4.2 Effectiveness of control of MCP scheme

The substation power flow and the maximum value of power fluctuation per minute, which is the evaluated value of power smoothing, are analyzed to evaluate the effectiveness of the control of the MCP scheme. In addition, the power output and energy transient of the BESS are analyzed to understand the BESS operation. Figure 4.10 shows the power flow of the substation (top) and the maximum value

of power fluctuation per minute (bottom) with and without the BESS control. In period A, the substation power fluctuation is smoothed (top), and the fluctuation value is maintained lower than the target value of power smoothing by the BESS operation (bottom). In period B, RPF at the substation is prevented (top), and no power fluctuation is observed because the RPF prevention maintains the substation power flow at zero. As mentioned above, the BESS mitigates the power fluctuation and prevents RPF, which indicates that the proposed control method is adequate for multipurpose utilization. Figure 4.11 shows the active power and the remaining capacity of the BESS at the substation. In period B, the BESS changes its charging power frequently to achieve RPF prevention. The remaining capacity of the BESS the BESS increases in response to the BESS charging operation. In period C, the BESS discharges to bring its energy close to the target value, which is optimized for minimizing the BESS capacity during the operation for 345 days. The BESS output for SoC adjustment is limited to 2 MW at maximum to prevent rapid power fluctuation.

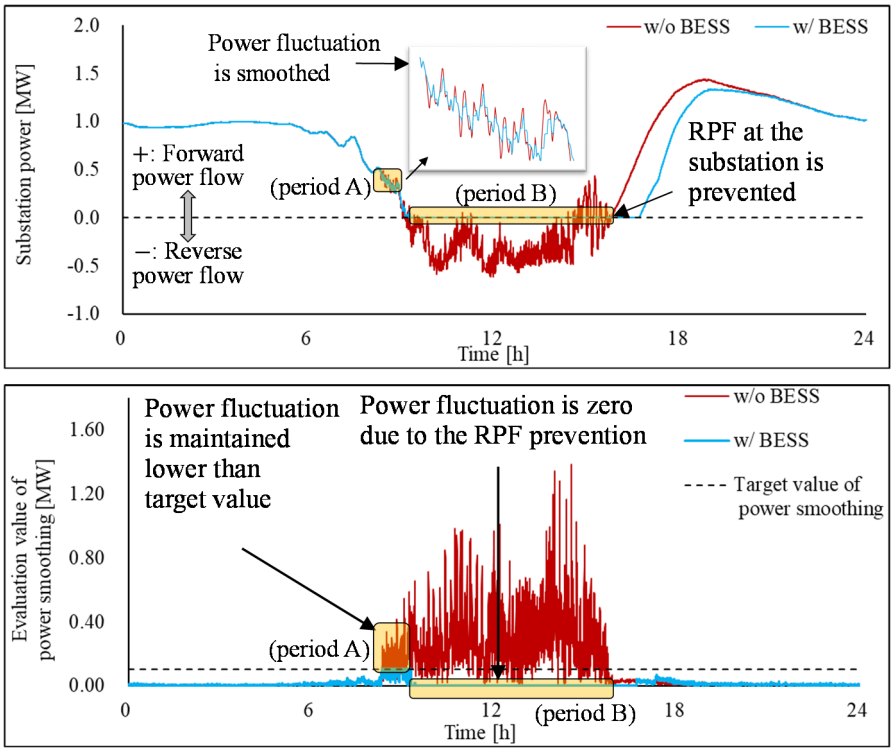

Fig. 4.10 Substation power flow and the evaluation value of power smoothing (2007/5/7).

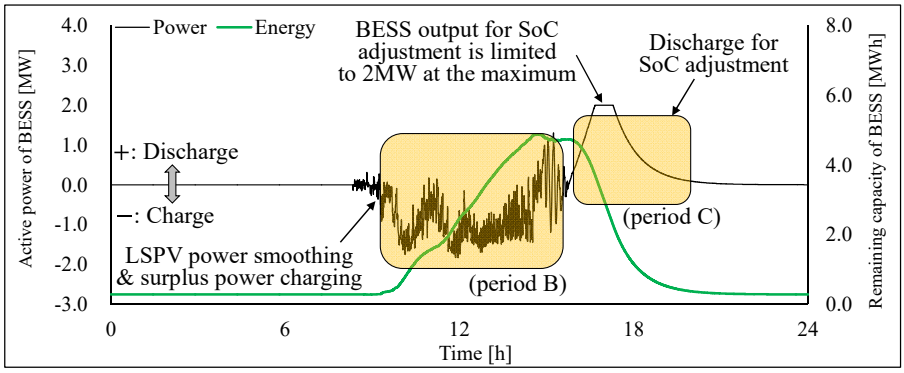

Fig. 4.11 Active power and remaining capacity of the BESS at the substation (2007/5/7).

4.4.3 Suitable BESS type considering increase in LSPVs

Figure 4.12 shows the RFB and LiB capacities in each case. In Case 1 with two and three LSPVs, each color (blue, yellow, and green) shows the capacity of the BESS at LSPVs. The BESS energy and power of Case 1 are greater than that of Case 2 regardless of the number of LSPV installations and BESS type, which indicates that the substation is the suitable site for reducing the BESS capacity. The suitable BESS type was not determined based on the BESS capacity, because the unit prices of these BESSs are different. Thus, the BESS cost was compared to determine the suitable BESS type.

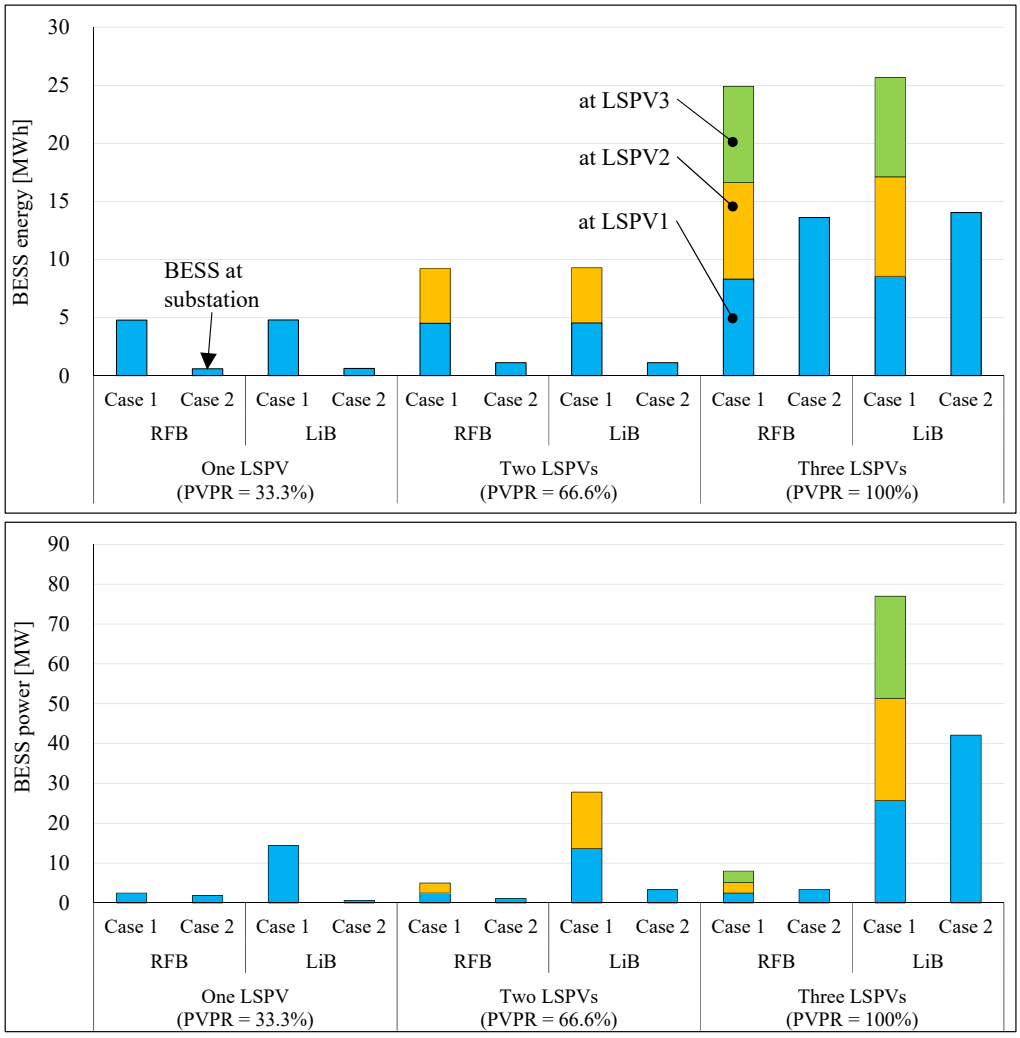

Fig. 4.12 Capacities of RFB and LiB.

Figure 4.13 shows the initial and O&M cost of the BESS, indicating the following points. The LiB is cheaper than the RFB by 79% and 73% with one and two LSPVs, respectively. In contrast, the RFB is cheaper than the LiB by 39% when three LSPVs are installed.

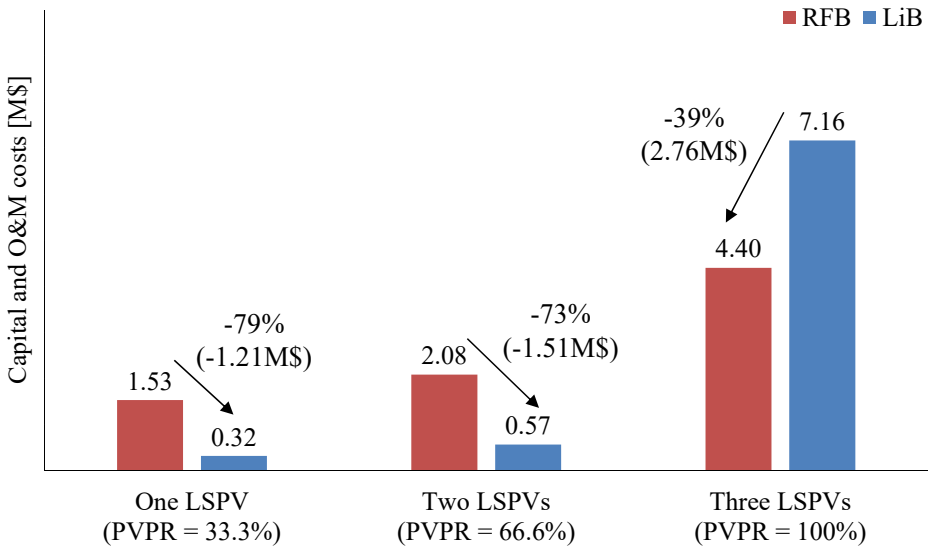

Fig. 4.13 Initial and O&M cost of the BESS at the substation.

The result was analyzed as follows. When one or two LSPVs are installed, RPF rarely occurs at the substation because the demand is higher than the LSPVs' generation in most days. Thus, the BESS operated mainly for smoothing, which requires a high power, and the LiB, which has the higher P/E ratio, was selected as the BESS type. Conversely, when three LSPVs were installed, RPF frequently occurred in light load periods, and a large energy was required for the BESS operation. Thus, the RFB, the energy cost of which is lower, was selected as the BESS type.

4.4.4 Impact of BESS site on tap operation and LSPV curtailment

The impact of BESS installation on tap operation and LSPV curtailment was not significantly different with respect to the BESS type. Figure 4.14 shows the number of OLTC and SVR tap operations with RFB. The OLTC tap operations are almost the same regardless of the BESS site because the power flow at the substation was not significantly different owing to the same strategy of RPF prevention at the substation. In contrast, the BESSs at LSPVs contribute to reducing the SVR tap operations significantly when three LSPVs are installed. LSPV3 was placed at the feeder end of SVR, as shown in Fig. 4.8. In Case 2, the BESS at the substation could not smooth the LSPV3 generation, and the intermittency of the LSPV3 generation increased the SVR tap operations. In Case 1, the power smoothing operation of the BESS at LSPV3 mitigates the power fluctuation of the SVR terminal point, which reduced the SVR tap operations by 48%.

Figure 4.15 shows the percentage of the total energy of LSPV curtailment to the total energy of LSPV generation. Yellow and blue lines indicate the LSPV curtailment percentage by the high AIR and voltage control, respectively. In Case 2, the LSPV curtailment percentage reaches just under 8% owing to the high AIR of 1.66. In Case1, the BESSs at LSPVs charged the LSPV generation, which exceeded the LSPV inverter capacity. The LSPV curtailment percentage is dynamically reduced to less than 0.5%, which is negligible. The results indicate that siting BESSs at LSPVs is suitable for

reducing LSPV curtailment. In addition, the LSPV curtailment for voltage control is less than 0.5% in both cases, which indicates that the volt-VAR-watt function curtailed little LSPV generation and control parameters were adequate.

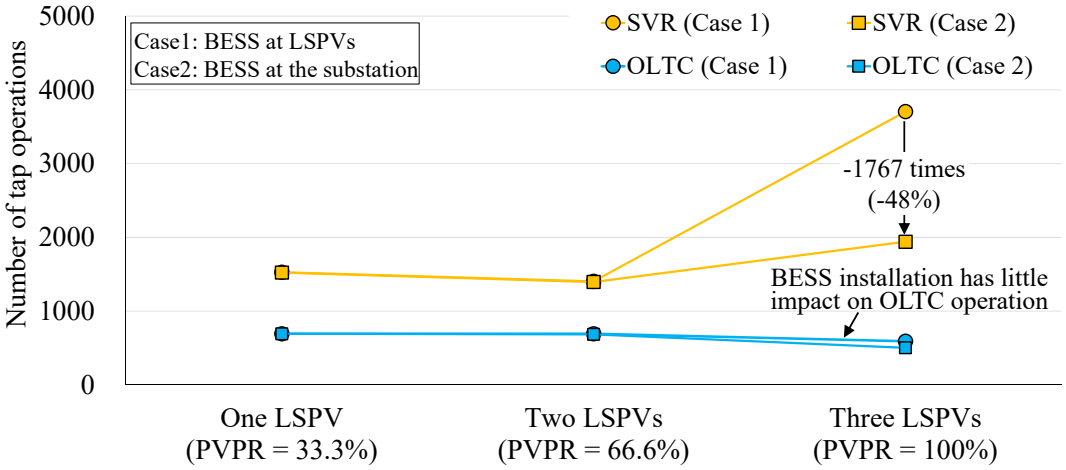

Fig. 4.14 Number of tap operations of the OLTC and SVR.

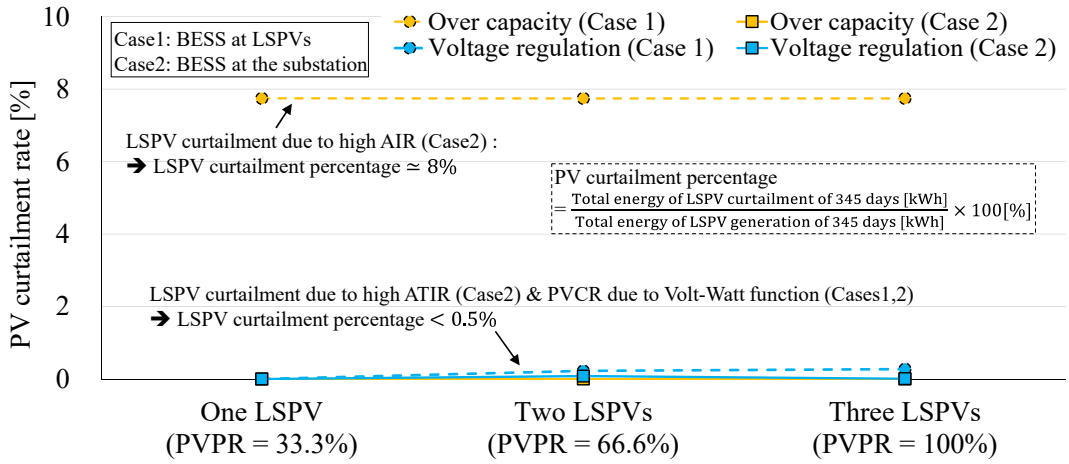

Fig. 4.15 Percentage of LSPV curtailment.

The reference voltage and SVR tap operation with three LSPVs were analyzed to understand the significant difference in SVR tap operations. Figure 4.16 depicts the reference voltages and tap operations of the SVR when the SVR tap operations of both cases were most different. In Case 1, the fluctuation of the reference voltage is mitigated as a result of power smoothing control, and the reference voltage tends to be maintained within the dead band, which reduces SVR tap operations. In contrast, the BESS at the substation cannot smooth the power fluctuation of the SVR, which caused frequent tap changes.

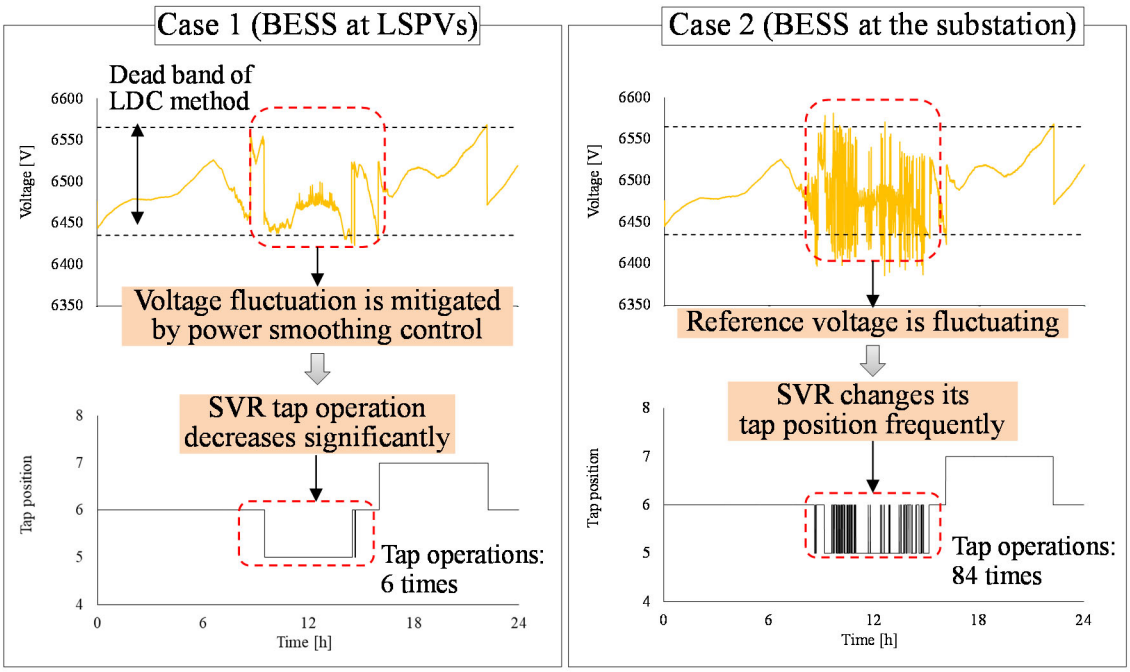

Fig. 4.16 Reference voltage and tap operation of the SVR (2007/1/4).

4.4.5 Suitable BESS site based on total cost

The analysis of the previous section showed that the BESS capacity minimization and reductions of SVR tap operations were in a trade-off relationship with the LSPV curtailment. Siting the BESS at the substation can minimize the BESS capacity, while the BESSs at LSPVs significantly decrease SVR tap operations and LSPV curtailment. The results indicate that determining the suitable BESS site is difficult owing to the trade-off relationship. The BESS capacity, SVR tap operations, and LSPV curtailment were converged to the initial and O&M cost [4-31], SVR replacement cost, and reduction of electricity sales to determine the suitable BESS site based on the cost calculation. However, calculating the total cost of the BESS installation is generally difficult because the defrayers of each cost are different. For instance, the power company bears the cost of the BESS installation and SVR replacement, while the LSPV curtailment decreases the benefit of the operators who possess LSPVs. Therefore, from the viewpoint of minimizing the social overhead cost, the total cost was calculated as follows. The BESS installation cost was calculated as described in Section 4.4.3. The cost of the LSPV curtailment was calculated based on the PV purchase price of the FIT, which is approximately 0.18 [$/kWh] [4-33]. The cost-benefit of SVR stress alleviation was calculated based on the replacement cost. Generally, the SVR is replaced when the number of tap operation reaches 200 000 times or 20 years, which is the rough standard of Japanese power companies. The simulation results showed that the BESS at the substation did not contribute to reducing the SVR tap operations, and the number of SVR tap operations reached 3707 in 345 days, implying 11 daily tap operations. Even if the same operation continues for 20 years, the number of tap operations will reach approximately 80300, which

is much less than 200 000. Therefore, the SVR replacement cost is the same regardless of the BESS installation site.

Based on the above results, the suitable BESS site was determined by the total cost of the BESS installation and the LSPV curtailment. In Case 1, the total cost is 9.29 M$, which is the BESS installation cost (9.46 M$) minus the benefit of the LSPV curtailment mitigation (0.17$). In Case 2, the total cost is 4.40 M$, which is the BESS installation cost. The cost of Case 2 is less than that of Case 1, and the substation is selected as the suitable site for BESS installation.

4.5 Summary of this chapter

In this chapter, I proposed the MCP scheme for BESSs in distribution networks. The MCP scheme determined the suitable BESS site and type based on three indices: 1) BESS capacity, 2) number of tap operations of OLTC and SVR, and 3) LSPV curtailment. In the simulation case study, BESSs were used for power smoothing of the substation/LSPVs and RPF prevention at the substation, reflecting the needs of Japanese power companies. The simulation results showed that the control of the MCP scheme achieved power smoothing, RPF prevention, and SoC adjustment without interaction between the controls. Regarding BESS planning, the results showed the following. (1) The substation is a suitable site for reducing the BESS capacity, but the BESS at the substation did not contribute to reducing the SVR tap operations and LSPV curtailment. By contrast, the BESSs at the LSPVs reduced the SVR tap operations and LSPV curtailment, but the BESS capacity increased large. (2) When the number of LSPVs was one or two, the suitable BESS type for reducing the BESS capacity was LiB, which has a high fixed P/E ratio of three. Conversely, RFB is the suitable BESS type when three LSPVs were installed. (3) The evaluation indexes—BESS capacity, SVR tap operations, and LSPV curtailment were converted into cost to identify the suitable site for BESS installation. The cost of the BESS installation at the LSPVs (9.29 M$) was higher than that at the substation (4.40 M$). Thus, the substation was selected as the suitable BESS site. The simulation results showed that the MCP scheme can effectively execute multipurpose control and determine the suitable BESS site and type.

References

[4-1] F. Zhang K. Meng, Z. Xu, Z. Dong, L. Zhang, C. Wan, and J. Liang, "Battery ESS Planning for Wind Smoothing via Variable-Interval Reference Modulation and Self-Adaptive SOC Control Strategy," *IEEE Trans. Sustain. Energy*, vol. 8, no. 2, pp. 695–707, Oct. 2016.

[4-2] H. Bitaraf, S. Rahman, and M. Pipattanasomporn, "Sizing Energy Storage to Mitigate Wind Power Forecast Error Impacts by Signal Processing Techniques," *IEEE Trans. Sustain. Energy*, vol. 6, no. 4, pp. 1457–1465, July 2015.

[4-3] S. De Torre, A. J. Sánchez-racero, J. A. Aguado, M. Reyes, and O. Martínez, "Optimal Sizing of Energy Storage for Regenerative Braking in Electric Railway Systems," *IEEE Trans. Power Sys.*, vol. 30, no. 3, pp. 1492–1500, May 2015.

[4-4] X. Ke, N. Lu, and C. Jin, "Control and Size Energy Storage Systems for Managing Energy Imbalance of Variable Generation Resources," *IEEE Trans. Sustain. Energy*, vol. 6, no. 1, pp. 70–78, Jan. 2015.

[4-5] B. Hartmann and A. Dán, "Methodologies for Storage Size Determination for the Integration of Wind Power," *IEEE Trans. Sustain. Energy*, vol. 5, no. 1, pp. 182–189, Jan. 2014.

[4-6] J. Dong, F. Gao, X. Guan, Q. Zhai, and J. Wu, "Storage-Reserve Sizing with Qualified Reliability for Connected High Renewable Penetration Micro-Grid," *IEEE Trans. Sustain. Energy*, vol. 7, no. 2, pp. 732–743, 2016.

[4-7] I. Miranda, N. Silva, and H. Leite, "A Holistic Approach to the Integration of Battery Energy Storage Systems in Island Electric Grids with High Wind Penetration," *IEEE Trans. Sustain. Energy*, vol. 7, no. 2, pp. 775–785, Apr. 2016.

[4-8] H. Zhao, M. Hong, W. Lin, and K. A. Loparo, "Voltage and Frequency Regulation of Microgrid with Battery Energy Storage Systems," *IEEE Trans. Smart Grid*, (in press).

[4-9] T. Yang, K. T. Mok, S.-C. Tan, C.-K. Lee, and S.-Y. R. Hui, "Electric Springs with Coordinated Battery Management for Reducing Voltage and Frequency Fluctuations in Microgrids," *IEEE Trans. Smart Grid*, vol. 9, no. 3, pp. 1943–1952, 2018.

[4-10] Z. Yi, W. Dong, and A. H. Etemadi, "A Unified Control and Power Management Scheme for PV-Battery-Based Hybrid Microgrids for Both Grid-connected and Islanded Modes," *IEEE Trans. Smart Grid*, (in press).

[4-11] C. Battistelli, Y. P. Agalgaonkar, and B. C. Pal, "Probabilistic Dispatch of Remote Hybrid Microgrids Including Battery Storage and Load Management," *IEEE Trans. Smart Grid*, vol. 8, no. 3, pp. 1305–1317, May 2017.

[4-12] A. Das and Z. Ni, "A Computationally Efficient Optimization Approach for Battery Systems in Islanded Microgrid," *IEEE Trans. Smart Grid*, (in press).

[4-13] A. Merabet, K. T. Ahmed, H. Ibrahim, R. Beguenane, and A. M. Y. M. Ghias, "Energy Management and Control System for Laboratory Scale Microgrid Based Wind-PV-Battery," *IEEE Trans. Sustain. Energy*, vol. 8, no. 1, pp. 145–154, Jan. 2017.

[4-14] T. A. Nguyen, M. L. Crow, and A. C. Elmore, "Optimal Sizing of a Vanadium Redox Battery System for Microgrid Systems," *IEEE Trans. Sustain. Energy*, vol. 6, no. 3, pp. 729–737, July 2015.

[4-15] Y. Liu, W. Du, L. Xiao, H. Wang, S. Bu, and J. Cao, "Sizing a Hybrid Energy Storage System for Maintaining Power Balance of an Isolated System with High Penetration of Wind Generation," *IEEE Trans. Power Syst.*, vol. 31, no. 4, pp. 3267–3275, 2015.

[4-16] Y. Yang, H. Li, A. Aichhorn, J. Zheng, and M. Greenleaf, "Sizing strategy of Distributed Battery Storage System with High Penetration of Photovoltaic for Voltage Regulation and Peak Load Shaving," *IEEE Trans. Smart Grid*, vol. 5, no. 2, pp. 982–991, Mar. 2014.

[4-17] S.-J. Lee, J.-H Kim, C.-H. Kim, S.-K. Kim, E.-S. Kim, D.-U. Kim, K.K. Mehmood, and S.U. Khan, "Coordinated Control Algorithm for Distributed Battery Energy Storage Systems for Mitigating Voltage and Frequency Deviations," *IEEE Trans. Smart Grid*, vol. 7, no. 3, pp. 1713–1722, May 2016.

[4-18] J. Tant, F. Geth, D. Six, P. Tant, and J. Driesen, "Multiobjective Battery Storage to Improve PV Integration in Residential Distribution Grids," *IEEE Trans. Sustain. Energy*, vol. 4, no. 1, pp. 182–191, Jan. 2013.

[4-19] Y. J. Zhang, C. Zhao, W. Tang, and S. H. Low, "Profit Maximizing Planning and Control of Battery Energy Storage Systems for Primary Frequency Control," *IEEE Trans. Smart Grid*, vol. 9, no. 2, pp. 712–723, Mar. 2018.

[4-20] J. Choi, I. Choi, G. An, and D. J. Won, "Advanced Power Sharing Method for Energy Efficiency Improvement of Multiple Battery Energy Storages System," *IEEE Trans. Smart Grid*, vol. 9, no. 2, pp. 1292–1300, Mar. 2018.

[4-21] S. K. Kollimalla, A. Ukil, H. B. Gooi, U. Manandhar, and N. R. Tummuru, "Optimization of Charge/Discharge Rates of a Battery Using a Two-Stage Rate-Limit Control," *IEEE Trans. Sustain. Energy*, vol. 8, no. 2, pp. 516–529, Apr. 2017.

[4-22] Y. Liu, W. Du, L. Xiao, H. Wang, and J. Cao, "A Method for Sizing Energy Storage System to Increase Wind Penetration as Limited by Grid Frequency Deviations," *IEEE Trans. Power Syst.*, vol. 31, no. 1, pp. 729–737, Jan. 2016.

[4-23] G. He, Q. Chen, C. Kang, P. Pinson, and Q. Xia, "Optimal Bidding Strategy of Battery Storage in Power Markets Considering Performance-Based Regulation and Battery Cycle Life," *IEEE Trans. Smart Grid*, vol. 7, no. 5, pp. 2359–2367, Sept. 2016.

[4-24] V. Knap, S. K. Chaudhary, D. Stroe, M. Swierczynski, B. Craciun, and R. Teodorescu, "Sizing of an Energy Storage System for Grid Inertial Response and Primary Frequency Reserve," *IEEE Trans. Power Syst.*, vol. pp. 3447 –3456, Sept. 2016.

[4-25] H. Pandžić, Y. Wang, T. Qiu, Y. Dvorkin, D. S. Kirschen, "Near-Optimal Method for Siting and Sizing of Distributed Storage in a Transmission Network," *IEEE Trans. Power Syst.*, vol. 30, no. 5, pp. 2288–2300, Sept. 2015.

[4-26] M. Pradeepkumar, "Frequency Regulation of Grid by Wind Turbine using Energy Storage System and SOC Feedback Control," presented at the *2015 Int. Conf. Innov. in Information, Embed. Commun. Syst.*, Aug. 2015.

[4-27] S. Akagi, R. Takahashi, A. Kaneko, M. Ito, J. Yoshinaga, Y. Hayashi, H.Asano, and H. Konda, "Upgrading Voltage Control Method Based on Photovoltaic Penetration Rate," *IEEE Trans. Smart Grid*, vol. 9, no. 5, pp.3994-4003, Sept. 2018.

[4-28] H. Matsukawa, T. Ohigashi, H. Yamaya, and K. Ogimoto, "Study on Photovoltaic System Installed Capacity in Japan," presented at the *36th Conf. Jpn. Soc. Energy Resour.*, pp.161-164, 2017.

[4-29] T. Shibata, T. Kumatomo, Y. Nagaoka, K. Kawase, and K. Yano, "Redox Flow Batteries for the Stable Supply of Renewable Energy," *SEI TECH. REV.*, 2013.

[4-30] Sumitomo Electric Industry Ltd., Press Release "Sumitomo Electric Supplies Redox Flow Battery to Taiwan Power Research Institute," Available: http://global-sei.com/company/press/2017/04/prs020.html.

[4-31] Pacific Northwest National Laboratory (PNNL), "National Assessment of Energy Storage for Grid Balancing and Arbitrage Phase II," pp. 6-7, 2013.

[4-32] J. Yoshinaga, S. Akagi, M. Ito, Y. Hayashi, and K. Ishibashi, "Cooperating Voltage Control Method Between Battery Energy Storage System and LRT and SVR for Purpose of Expansion of PV Introduction," *IEEJ Trans. Power Energy*, vol. 136, no. 3, pp.291-301, Mar. 2016, 10.1541/ieejpes.136.291 (in Japanese).

[4-33] Ministry of Economy Trade and Industry, (in Japanese). [Online]. Available: http://www.meti.go.jp/press/2017/03/20180323006/20180323006.html. [Accessed 3-Nov. 2018].

Chapter 5
Conclusion and Future Work

5.1 Conclusion

In this thesis, planning and control schemes for voltage control and BESS utilization were proposed.

In Chapter 2, a planning scheme was proposed to determine a suitable voltage control method, type of voltage control equipment, and timing for changing the voltage control method/installing new voltage control equipment. Using the proposed scheme, I realized a suitable voltage control method and determined the timing for upgrading the OLTC control; in addition, I achieved additional installation of the SVR or SVC based on the limit of the PVPR. The limit of the PVPR was calculated through numerical simulations and experiments with the ANSWER. The tendencies of the PVPR increase and distribution voltage profiles were consistent, validating the numerical simulation results.

The results of numerical simulation indicate that the limit of PVPR with OLTC is 55%, whereas the installation of SVR and SVC increased the rate to 95% and 100%, respectively. The SVR increases the PVPR more than the SVC while preventing violation of the 30-min averaged voltage. On the other hand, the SVC helped increase the PV penetration while preventing instantaneous voltage violation. Thus, this work demonstrated the necessity of controlling the SVR and SVC to increase PV penetration while preventing instantaneous voltage violation. The proposed method was used in a distribution network consisting of two feeders.

In Chapter 3, a scheme was proposed to determine the optimal control parameters and BESS capacity in order to ensure control performance. The control parameters were determined in the order of SPL and voltage control considering the mutual interaction of SPL and voltage control. Simulations of three days were performed to obtain the proper capacity combination based on a quantitative evaluation of the control performance. The simulation results showed that the proposed scheme could determine the optimal control parameters for SPL and voltage control, which prevent voltage violation and minimize SPL violation. The optimal capacity combination for the simulated system was determined as follows: energy, 1150 kWh; power, 1250 kW which is about 30 % of the LSPV capacity.

In chapter 4, a MCP scheme for BESSs in distribution networks was proposed. The MCP scheme determined the suitable BESS site and type based on three indices: 1) BESS capacity, 2) number of tap operations of the OLTC and SVR, and 3) LSPV curtailment. In the simulation case study, BESSs were used for power smoothing of the substation/LSPVs and RPF prevention at the substation, reflecting the needs of Japanese power companies. The simulation results showed that the control of the MCP scheme achieved power smoothing, RPF prevention, and SoC adjustment without interaction between controls. Regarding BESS planning, the results showed the following. (1) The substation is a suitable site for reducing the BESS capacity, but the BESS at the substation did not contribute to reducing the SVR tap

operations and LSPV curtailment. By contrast, the BESSs at LSPVs reduced the SVR tap operations and LSPV curtailment, but the BESS capacity increased. (2) When the number of LSPVs was one or two, the suitable BESS type for reducing the BESS capacity was LiB, which has a high fixed P/E ratio of three. Conversely, RFB is the suitable BESS type when three LSPVs were installed. (3) The evaluation indexes—BESS capacity, SVR tap operations, and LSPV curtailment—were converted into cost to identify the suitable site for BESS installation. The cost of BESS installation at the LSPVs (9.29 M$) was higher than that at the substation (4.40 M$). Thus, the substation was selected as the suitable BESS site. The simulation results showed that the MCP scheme can effectively execute multipurpose control and determine the suitable BESS site and type.

5.2 Future work

This thesis focused on a planning and control scheme for voltage controllers and BESSs to cope with various problems arising from a large amount of PV installation, namely, voltage rise, RPF at the substation, and PV fluctuation.

This thesis focused on using grid-side equipment because the utilization of those types of equipment can be considered rightly as a countermeasure for PV expansion. The conventional power network operated by using large-scale generators, such as hydroelectric/thermal power plants, will change to the new one that requires gird-/demand-side management according to the spread of PV, EV, BESS, and fuel cells for households. Recently, investigations and demonstration tests utilizing demand-side equipment have been under way. For instance, load reduction/load creation by the demand response at the time of tight supply/surplus power generation, and supply-demand balance adjustment by PV suppression can be cited. Virtual power plant demonstrations that integrate distributed power supplies by utilizing internet of things technology and utilize it for power network operation are also carried out. In addition, smart inverters with multiple control and communication functions are expected to improve the network operation flexibility. The integrated utilization of grid-/demand-side resources will become significant because it is considered that existing large-scale power supplies and DERs will coexist in future power networks. There are many technical challenges, but the following are given as examples: (1) Control of the EV group for avoiding excess capacity due to simultaneous charging of EV and preventing PV curtailment by charging surplus power, (2) Integrated control of large-scale BESS and PV curtailment for compatibility between control performance improvement and cost reduction, and (3) Establishment of a versatile and efficient voltage-management method with smart inverters and tap controllers.

Acknowledgment

I would like to extend my heartfelt gratitude to Prof. Yasuhiro Hayashi for his daily and invaluable advice, proposals, and encouragement. I would also like to extend my gratitude to Prof. Noboru Murata, Prof. Toru Asahi, and Prof. Hideo Ishii for their valuable comments, feedback, and advice on my thesis.

I am very grateful to Associate Prof. Masakazu Ito, Associate Prof. Yu Fujimoto, Dr. Jun Yoshinaga, Dr. Shinya Yoshizawa, Dr. Teru Miyazaki, Mr. Naoyuki Takahashi, Mr. Ryunosuke Miyoshi, Mr. Ryo Takahashi, Mr. Akihisa Kaneko, Prof. Hiroshi Asano, Mr. Hiromi Konda, Mr. Takashi Yano, Mr. Toshiya Hisada, Dr. Hideaki Nakahata, Mr. Katsuhisa Tawa, and Mr. Tran Xuan Mai.

I would also like to thank the graduates and Ph.D. students of Prof. Hayashi's laboratory, Dr. Shunsuke Kawano, Dr. Hiroshi Kikusato, Mr. Yuji Takenobu, and Mr. Kohei Murakami.

I am also grateful to the research collaborators and all the members of Prof. Hayashi's laboratory and the Leading Graduate Program in Science and Engineering, Waseda University, for their assistance.

Finally, I am grateful to my parents for their unwavering support.

February 2019

Satoru AKAGI

Figures and Tables

Research achievements

* indicate the directly related researches with this thesis

[Journals]

1. *Satoru Akagi, Ryo Takahashi, Akihisa Kaneko, Jun Yoshinaga, Masakazu Ito, Yasuhiro Hayashi, Hiroshi Asano, Hiromi Konda, "Upgrading Voltage Control Method Based on Photovoltaic Penetration Rate," IEEE Transactions on Smart Grid, vol. 9, no. 5, pp. 3994-4003, Sep. 2018
2. *Satoru Akagi, Shinya Yoshizawa, Jun Yoshinaga, Masakazu Ito, Yu Fujimoto, Yasuhiro Hayashi, Takashi Yano, Hideaki Nakahata, Toshiya Hisada, Xuan Mai Tran, "Capacity Determination of a Battery Energy Storage System Based on the Control Performance of Load Leveling and Voltage Control," Journal of International Council on Electrical Engineering, vol. 6, no. 1, pp. 94-101, Mar. 2016
3. Jun Yoshinaga, Satoru Akagi, Masakazu Ito, Yasuhiro Hayashi, Kazunari Ishibashi, Naoyuki Takahashi, "Voltage Fluctuation Issue on Distribution System at Time of Demand Response and Cooperating Voltage Control Method between Battery Energy Storage System and SVR," IEEJ Transactions on Power and Energy, vol. 136, no. 4, pp. 400-409. 2016. 4
4. Jun Yoshinaga, Satoru Akagi, Masakazu Ito, Yasuhiro Hayashi, Kazunari Ishibashi, "Cooperating Voltage Control Method between Battery Energy Storage System and LRT and SVR for Purpose of Expansion of PV Introduction," IEEJ Transactions on Power and Energy, vol. 136, no. 3, pp. 291-301, 2016. 3

[International Conference Proceedings]

1. Yuta Takasawa, Satoru Akagi, Shinya Yoshizawa, Hideo Ishii, Yasuhiro Hayashi, "Evaluation of Voltage Regulation Functions of Smart Inverters Based on Penetration Level and Curtailment in Photovoltaic Systems," Proceedings of 2018 IEEE PES Innovative Smart Grid Technologies Europe (ISGT- Europe), Oct. 2018
2. Yuji Takenobu, Satoru Akagi, Hideo Ishii, Yasuhiro Hayashi, Jens Boemer, Deepak Ramasubramanian, Parag Mitra, Anish Gaikwad, Ben York, "Evaluation of Dynamic Voltage Responses of Distributed Energy Resources in Distribution Systems," Proceedings of 2018 IEEE PES General Meeting (GM), Aug. 2018
3. Markus Kraiczy, Ben York, Mobolaji Bello, Davis Montenegro, Satoru Akagi, Martin Braun, "Coordinating Smart Inverters with Advanced Distribution Voltage Control Strategies," Proceedings of 2018 IEEE PES General Meeting (GM), Aug. 2018
4. Satoru Akagi, Ben York, Mobolaji Bello, Hideo Ishii, Yasuhiro Hayashi, "Configuration of Large-Scale Battery System with Volt-VAR Function in Distribution Network with Advanced Load Tap

Changer Control," Proceedings of 7th World Conference on Photovoltaic Energy Conversion (WCPEC), Jun. 2018

5. Yuta Takasawa, Satoru Akagi, Shinya Yoshizawa, Hideo Ishii, Yasuhiro Hayashi, "Effectiveness of Updating the Parameters of the Volt-VAR Control Depending on the PV Penetration Rate and Weather Conditions," Proceedings of Innovative Smart Grid Technologies Asia (ISGT-Asia), Dec. 2017
6. Jun Yoshinaga, Satoru Akagi, Wataru Hirohashi, Hideo Ishii, Yasuhiro Hayashi, "Demonstrations of Communication Standards for Automated Demand Response and Smart Gird," Proceedings of International Council on Large Electric Systems (CIGRE), Aug. 2016
7. Akihisa Kaneko, Ryo Takahashi, Satoru Akagi, Masakazu Ito, Yasuhiro Hayashi, "Determination Method of Optimal Dead Band Width under Centralized Voltage Control Using IT Switches Data in Three Sectionalized Three Connected Distribution Networks," Proceedings of International Conference on Electrical Engineering (ICEE), Jul. 2016
8. Satoru Akagi, Shinya Yoshizawa, Masakazu Ito, Yu Fujimoto, Jun Yoshinaga, Yasuhiro Hayashi, Takashi Yano, Hideaki Nakahata, Toshiya Hisada, "Capacity Evaluation of a Battery Energy Storage System for Multipurpose Utilization," Proceedings of International Conference on Electrical Engineering (ICEE), Jul. 2016
9. Satoru Akagi, Ryo Takahashi, Akihisa Kaneko, Masakazu Ito, Jun Yoshinaga, Yasuhiro Hayashi, Hiromi Konda, "Determination of the Most Suitable Voltage Control Method Depending on Photovoltaic Installation Rate," Proceedings of 2015 IEEE PES Asia-Pacific Power and Energy Engineering Conference, Nov. 2015
10. Satoru Akagi, Shinya Yoshizawa, Jun Yoshinaga, Masakazu Ito, Yu Fujimoto, Yasuhiro Hayashi, Takashi Yano, Hideaki Nakahata, Toshiya Hisada, Xuan Mai Tran, "Basic Study of Grid-Connected Battery Energy Storage System Capacity Determination for Load Leveling and Voltage Control," Proceedings of International Conference on Electrical Engineering (ICEE), Jul. 2015
11. Satoru Akagi, Jun Yoshinaga, Naoyuki Takahashi, Shunsuke Kawano, Ryunosuke Miyoshi, Yasuhiro Hayashi, "Voltage Control Method with the Amount of Demand Response Reduction," Proceedings of 6th World Conference on Photovoltaic Energy Conversion (WCPEC), Nov. 2014
12. Jun Yoshinaga, Satoru Akagi, Yasuhiro Hayashi, Mikihiko Wada, Yasuhito Isoe, "Multi-Objective Control Method of Battery Energy Storage System for Distribution System," Proceedings of International Conference on Electricity Distribution (CIRED) Workshop 2014, Jun. 2014

[Domestic Conference Proceedings (in Japanese)]

1. 高澤佑太，赤木覚，芳澤信哉，石井英雄，林泰弘，「PV 発電状態分類に基づく Volt-VAR 制御時と定力率制御時の電力損失に関する評価」，平成 30 年電気学会電力・エネルギー部門大会, 徳島，2018 年 9 月

2. 赤木覚，芳澤信哉，吉永淳，伊藤雅一，藤本悠，林泰弘，矢野孝，久田俊哉，田和克久，「配電系統における PV のならし効果を考慮した系統用蓄電池の容量設計に関する基礎検討」，平成 30 年電気学会全国大会，福岡，2018 年 3 月
3. 高澤佑太，赤木覚，芳澤信哉，石井英雄，林泰弘，「スマートインバータの Volt-VAR 制御パラメータによる配電系統への影響評価に関する一検討」，平成 30 年電気学会全国大会，福岡，2018 年 3 月
4. Yuji Takenobu, Satoru Akagi, Hideo Ishii, Yasuhiro Hayashi, Hantao Cui, Kevin Tomsovic, "Transient Stability Analysis Considering Reactive Power Support of Smart Inverters in Distribution Networks," 平成 29 年電気学会電力・エネルギー部門大会, 中野，2017 年 9 月
5. 高澤佑太，赤木覚，芳澤信哉，石井英雄，林泰弘，「スマートインバータ Volt-VAR 機能パラメータ変更の配電損失最小化観点からの評価」, 平成 29 年電気学会電力・エネルギー部門大会, 中野，2017 年 9 月
6. 赤木覚，芳澤信哉，吉永淳，伊藤雅一，藤本悠，林泰弘，矢野孝，中幡英章，久田俊哉，「系統用蓄電池による変動緩和と余剰吸収の多目的制御に関する基礎検討」，平成 29 年電気学会全国大会，富山，2017 年 3 月
7. 高澤佑太，赤木覚，芳澤信哉，石井英雄，林泰弘，「スマートインバータの Volt-VAR 機能の制御パラメータ変更による無効電力出力量への影響評価」，平成 29 年電気学会全国大会，富山，2017 年 3 月
8. 赤木覚，芳澤信哉，吉永淳，伊藤雅一，藤本悠，林泰弘，矢野孝，中幡英章，久田俊哉，「多目的を想定した系統用蓄電池の容量設計に関する基礎検討」，平成 28 年電気学会全国大会，仙台，2016 年 3 月
9. 金子曜久，赤木覚，高橋諒，吉永淳，林泰弘，「三分割三連系センサ開閉器計測データを用いた集中電圧制御での不感帯幅の影響評価」，平成 28 年電気学会全国大会，仙台，2016 年 3 月
10. 吉永淳，赤木覚，林泰弘，石橋一成，「PV 導入拡大に対応した SVR と蓄電池との協調電圧制御手法の検討」，平成 27 年電気学会電力・エネルギー部門大会，名古屋，2015 年 8 月
11. 赤木覚，芳澤信哉，吉永淳，伊藤雅一，藤本悠，林泰弘，矢野孝，中幡英章，久田俊哉，チャンスンマイ，「負荷平準化と電圧制御を目的とした系統用蓄電池システムの容量決定に関する基礎検討」，平成 27 年電気学会全国大会，東京，2015 年 3 月
12. 赤木覚，吉永淳，高橋尚之，三好龍之介，林泰弘，「デマンドレスポンスによる負荷の削減量を用いた電圧制御手法の基礎検討」，平成 26 年電気学会電力・エネルギー部門

大会，京田辺，2014 年 9 月

13. 吉永淳，赤木覚，林泰弘，「PV 導入限界量拡大を目的とした蓄電池による有効・無効電力制御法の検討」，平成 26 年電気学会全国大会，松山，2014 年 3 月

[Award]

1. *平成 26 年電気学会電力・エネルギー部門大会，Young engineer Poster Competition (YPC) 奨励賞，2014.9.11
2. *IEEE Power & Energy Society Japan Joint Chapter，IEEE PES Japan Joint Chapter 学生優秀論文賞，2018.1.12